BAŞKENT UNIVERSITY
INSTITUTE OF SCIENCE AND ENGINEERING
DEPARTMENT OF ELECTRICAL-ELECTRONICS ENGINEERING DOCTOR OF PHILOSOPHY IN ELECTRICAL-ELECTRONICS ENGINEERING

ULTRA-WIDEBAND BUTLER MATRIX DESIGN

BY

SÜLEYMAN MELİKŞAH YAYAN

PHD THESIS

ANKARA - 2021

BAŞKENT UNIVERSITY
INSTITUTE OF SCIENCE AND ENGINEERING
DEPARTMENT OF ELECTRICAL-ELECTRONICS
ENGINEERING DOCTOR OF PHILOSOPHY IN
ELECTRICAL-ELECTRONICS ENGINEERING

ULTRA-WIDEBAND BUTLER MATRIX DESIGN

BY

SÜLEYMAN MELİKŞAH YAYAN

PHD THESIS

ADVISOR

ASST. PROF. DR. ALPARSLAN ÇAĞRI YAPICI

ANKARA - 2021

BAŞKENT UNIVERSITY
INSTITUTE OF SCIENCE AND ENGINEERING

This study, which was prepared by Süleyman Melikşah Yayan, for the program of PHD, has been approved in partial fulfillment of the requirements for the degree of DOCTOR OF PHILOSOPHY in Electrical and Electronics Engineering Department by the following committee.

Date of Thesis Defense: 16 / 12 / 2021

Thesis Title: Ultra-Wideband Butler Matrix Design

Examining Committee Members	**Signature**
Prof. Dr. Asım Egemen YILMAZ	
Asst. Prof. Dr. Alparslan Çağrı YAPICI	
Prof. Dr. Sedat NAZLIBİLEK	
Asst. Prof. Dr. Murat ÜÇÜNCÜ	
Asst. Prof. Dr. Çağlar ARPALİ	

APPROVAL

……………...………..

Director, Institute of Science and Engineering

Date: … / … / ………

BAŞKENT ÜNİVERSİTESİ

FEN BİLİMLERİ ENSTİTÜSÜ

DOKTORA TEZ ÇALIŞMASI ORİJİNALLİK RAPORU

Tarih: … / … / ……..

Öğrencinin Adı, Soyadı: Süleyman Melikşah Yayan

Öğrencinin Numarası: 21410169

Anabilim Dalı: Elektrik ve Elektronik Mühendisliği

Programı: Doktora

Danışmanın Unvanı/Adı, Soyadı: Asst. Prof. Dr. Alpaslan Çağrı Yapıcı

Tez Başlığı: Ultra-Wideband Butler Matrix Design

Yukarıda başlığı belirtilen Doktora tez çalışmamın; Giriş, Ana Bölümler ve Sonuç Bölümünden oluşan, toplam .... sayfalık kısmına ilişkin, … / … / …….. tarihinde şahsım/tez danışmanım tarafından ………………… adlı intihal tespit programından aşağıda belirtilen filtrelemeler uygulanarak alınmış olan orijinallik raporuna göre, tezimin benzerlik oranı % ……….’dır. Uygulanan filtrelemeler:

1. Kaynakça hariç

2. Alıntılar hariç

3. Beş (5) kelimeden daha az örtüşme içeren metin kısımları hariç

“Başkent Üniversitesi Enstitüleri Tez Çalışması Orijinallik Raporu Alınması ve Kullanılması Usul ve Esaslarını” inceledim ve bu uygulama esaslarında belirtilen azami benzerlik oranlarına tez çalışmamın herhangi bir intihal içermediğini; aksinin tespit edileceği muhtemel durumda doğabilecek her türlü hukuki sorumluluğu kabul ettiğimi ve yukarıda vermiş olduğum bilgilerin doğru olduğunu beyan ederim.

Öğrenci İmzası:………………….

ONAY

Tarih: … / … / ……..

Öğrenci Danışmanı Unvan, Ad, Soyadı, İmza:

Asst. Prof. Dr. Alpaslan Çağrı Yapıcı

To my loving wife and family.

ACKNOWLEDGEMENT

I would like to express my gratitude to Dr. Alparslan Çağrı Yapıcı and the members of my jury, for their guidance and contributions.

I would like to thank to my company, Aselsan Inc.

Finally, I would also like to give special thanks to my wife and family for their support and patience.

ÖZET

Süleyman Melikşah Yayan
ULTRA-WIDEBAND BUTLER MATRIX DESIGN
Başkent Üniversitesi Fen Bilimleri Enstitüsü
Elektrik ve Elektronik Mühendisliği Bölümü
2021

Bu çalışmada, Ku frekans bandının altında çalışan geniş bantlı 4x4 Butler matris tasarımı önerilmiştir. Önerilen 4x4 Butler matrisi 3GHz ila 12 GHz arasında çalışmaktadır. Geniş bant performansı elde etmek için, Butler matrisinde kullanılan kuplörler ve faz kaydırıcılar da geniş bantta çalışacak şekilde tasarlanmıştır. Yapılan çalışmaları doğrulamak için tasarlanan Butler matris üretilmiştir. Ölçüm sonuçları değerlendirildiğinde özellikle Butler matrisinin çıkış portları arasındaki ardışık faz farklarının, benzetim sonuçlarına çok yakın olduğu görülmüştür. Butler matrisi ile birleştirmek için 4x1'lik mikroşerit anten dizisi tasarlanmıştır. 4x1 anten dizisini 4x4 Butler matrisinin çıkış portlarına bağlanarak yapılan benzetimlerde önerilen yapının anten dizisinin ışınım örüntülerini 4 farklı yöne başarıyla yönlendirebildiği gözlenmiştir. 4x4 Butler matrisin huzme eğme yeteneklerini doğrulayabilmek için 4x1 mikroşerit anten dizisi üretilmiştir ve üretilen bu anten dizisi Butler matris ile birleştirilmiştir. Butler matrisinin her bir giriş portunun uyarılmasıyla oluşturulan uzak alan ışınım örüntüleri, yankısız odada ölçülmüştür. Ölçüm sonuçları, tasarlanan 4x4 Butler matrisinin anten dizisini huzmelerini istenilen yönlere başarılı bir şekilde eğebildiğini göstermiştir.

ANAHTAR KELİMELER: Butler Matrix, Ultra-Wideband, Yönlü Kuplör, Faz Kaydırıcı.

ABSTRACT

Süleyman Melikşah Yayan
ULTRA-WIDEBAND BUTLER MATRIX DESIGN
Başkent University Institute of Science
Department of Electrical-Electronics Engineering
2021

In this study, a wideband 4x4 Butler matrix design operating below Ku-band is proposed. The proposed 4x4 Butler matrix operates between 3GHz to 12 GHz. So as to achieve wideband performance, couplers and phase shifters that are used in the Butler matrix are also designed to perform within wideband. The designed Butler matrix has been manufactured to verify its operation. It has been seen that the measured results especially the consecutive phase differences between the output ports of the Butler matrix were very close to the simulated results. A 4x1 patch antenna array is designed to be used with Butler matrix. In the simulation environment, the 4x4 Butler matrix is connected to the designed 4x1 microstrip antenna array, in order to see if it would be able tilt the beam of the designed antenna array to the desired directions. The simulation results of the 4x4 Butler matrix combined with the 4x1 antenna array have shown that the 4x4 Butler matrix is able to tilt the antenna beam successfully to the 4 different directions. So as to verify the beam tilting capabilities of the 4x4 Butler matrix, the designed 4x1 patch antenna array is manufactured and combined with the Butler matrix. The farfield patterns created by exciting each input port of the Butler matrix is measured in the anechoic chamber. The measurement results yield that the designed 4x4 Butler matrix is able to tilt the antenna array pattern successfully to the desired directions.

KEYWORDS: Butler Matrix, Ultra-Wideband, Directional Coupler, Phase Shifter.

CONTENTS

LIST OF TABLES

Page

LIST OF FIGURES

Page

Chapter 1

Introduction

Generally, single element antenna's radiation pattern is wide and therefore has low values of directivity. In radar applications, to be able to satisfy the demand for long distance communications, electrical size of the antenna is needed to be increased. In order to increase electrical size and directivity of the antenna, an array of elements (usually identical) are brought together in an electrical and geometrical configuration [1]. By assembling an antenna array that consists of multiple antenna elements, more directive beam can be formed at a specified angular direction.

In early radar applications, mechanically steered antenna or antenna arrays were used for tracking targets. As technology progressed, electrically steered antennas that utilizes from beam-forming networks i.e phased array antennas became more attractive due to their flexibility in pattern steering [2]. Drastic decrease in steering time (from seconds to miliseconds) and capability to steer antenna beams more accurately made antenna arrays with beam-forming networks more desirable for radar applications. These beam-forming networks can be either passive or active.

The Butler matrix is a passive beam-forming network. It has multiple output ports, the number of which is equal to the number of input ports. When one of the input ports of the Butler matrix is excited while the other input port are terminated with 50 ohm matched load, the input power is split equally between output ports while having progressive phase difference in between output ports. When combined with the radiating antenna elements, depending on its number of input ports, a Butler matrix can generate multiple beams in different directions on a single plane. A Butler matrix consists of two main components. These are hybrid couplers and phase shifters. In order obtain a wideband Butler matrix or any other wideband microwave system, components within the system must have even wider bandwidth. Therefore, each component that will be designed to form a Butler matrix need to have higher bandwidth performance.

One of the main components of the Butler matrix is quadrature hybrid couplers. Quadrature hybrid couplers are the most common directional couplers that are used in microwave systems. Quadrature hybrid couplers are the special case of directional couplers. They have four ports and transfer input power to the through and coupled ports equally with 90°phase difference while providing isolation between input ports. There are plenty of quadrature hybrid coupler topologies such as coupled line couplers, lange couplers, Schwinger reversed phase couplers, Riblet short-slot couplers, couplers with apertures in planar lines [3].

There are several studies made on wideband quadrature hybrid couplers. In order to acquire wideband performance, cascaded branch line topologies are used and the performance of the branch line couplers is enhanced significantly at the expense of larger area of implementation [4]-[6]. In some studies [8]-[9], substrate integrated waveguide (siw) based hybrid couplers are used. However, siw based structure has a challenging manufacturing process and may be more disadvantageous in Ka-band compared to other topologies. Patch resonators with cross-slots are also utilized to acquire wideband characteristics [10] - [11].

The second component of the Butler matrix is phase shifters.Depending on the application they can be either passive or active. Compared to active phase shifters, passive ones are easy to fabricate, cost effective and more invulnerable to temperature and their environment. Nowadays most of the microwave systems are required to operate in wider bandwidths due to to compatibility with wide-range of application hence the need for wide-band phase shifters arises and especially passive ones are preferred for advantages on active phase shifters.

Phase shifter topology in [12] is based on a substrate-integrated-waveguide (SIW) technology. By adding additional metallic posts, fair bandwidth is acquired. However, neither the bandwidth acquired with this topology is wide enough nor SIW based phase shifter is easy to fabricate especially for high frequencies. In order to have broadband performance, coupled lines and L-shaped network are used in [13] and considerably higher fractional bandwidth is achieved from L-band to C-band. However, even for L band coupling space between coupled lines seem to be very tight.It may not be a good candidate for Ka frequency band in terms of realization. One of the innovative ways to acquire a broadband phase shifter is proposed by [14]. Instead of using coupled lines, lange coupler is used. However this topology still has the same problem as coupled lines which is small gaps within lange coupler. Since coupled line topologies has small gap problems which would be very problematic in high frequencies what is proposed in [15] seems to be a good candidate since no coupled lines are involved. The proposed structure utilizes from the coupling of the resonators located at the top and the bottom of the structure. As an resonator elliptical microstrip patches are chosen to be coupled through elliptical aperture that are etched to the ground plane in the middle of the structure.

There are also variety of studies about Butler matrices. The Butler matrix topologies that are based on a substrate-integrated-waveguide (SIW) technology are proposed in [17], [18]. SIW technology proposed in these papers seems to have limited bandwidth capability which is increased up to 24%. Patch based Butler matrices are proposed in [19] and [11].In order to increase bandwidth cross-slot are etched on patch resonators and return loss bandwidth is increased up to %38. Multi-section branch-line couplers are utilized in papers [20] and [21] to achieve wideband 4x4 Butler matrices. Frequency bandwidth is increased up to 40%. However, phase shift errors achieved with such topologies are extermely high. Most wide-band performance with moderate phase shift errors is achieved with the topology that utilizes from slot coupling between resonators located at different layers of the multi-layer structure in [22]-[23]. Main problem with this topology is manual alignment of the layers either via screws or tapes. However, manual alignment method to acquire multi-layer structure causes formation of unwanted standing waves and results in performance dips at several frequency location along the frequency of operation.

In this work, an improved manufacturing method is proposed in order to get better multi-layer wide-band performance with Butler matrix topologies. The layers of the multi-layer structure is aligned and combined to each other via prepreg material during production process. Prepreg materials are one of the main materials that are used in multi-layer pcb topologies. They are used to bond pcb layers to each other under temperature and pressure. In order to achieve wide-band performance with Butler matrix, hybrid couplers and phase shifters that are to be used during assemby of the Butler matrix needs to achieve wide-band performance. Therefore, in chapter 2, a multi-layer wideband quadrature hyrid coupler topology is presented. Proposed topology uses prepreg material to bond top and bottom pcb cards. It has been observed that insertion of a prepreg material in between top and bottom pcb cards had caused a discontinuity in between ground planes of the top and bottom pcb cards where aperture coupling happens. This discontinuity causes unwanted surface waves on prepreg material and performance of the coupler degrades at several frequencies. This issue is solved by specially adjusted vias shielding around the microstrip lines and resonators. The resulting manufactured structure operates within 3 GHz to 12 GHz where return loss is less than -18 dB within whole frequency range. Equal power division and 90°phase difference between output ports are achieved. In the next chapter, a multi-layer wide-band phase shifter design utilizing the same topology is presented. The proposed topology also operates from 3 GHz to 12 GHz. The measurement results shows that insertion loss of the proposed phase shifter is less than 1.35 dB within the whole frequency band while achieving 45°phase shift. Finally, a multi-layer Butler matrix design that is the assembly of the proposed quadrature hybrid coupler and phase shifter is presented. The proposed Butler matrix achieves maximum of -12 dB return loss at each input port within 3 GHz to 12 GHz. Measurement results of the proposed Butler matrix also indicates equal power division within output ports of the Butler matrix while providing desired phase difference between them depending on the excited input port of the Butler matrix. Moreover, in order to verify beam tilting ability of the proposed structure, Butler matrix is combined with a 4x1 microstrip antenna array. It has been seen that proposed structure tilts the beam of the 4x1 antenna array to four different directions at azimuth plane successfully.

Chapter 2

Quadrature Hybrid Couplers

Quadrature hybrid couplers are the most common directional couplers that are used in microwave components such as dividers, combiners, mixers, feeding networks, amplifiers. Quadrature hybrid couplers are the special case of directional couplers. They have four ports and transfer input power to the through and coupled ports of the coupler equally with 90° phase difference while providing isolation between the input ports. There are plenty of quadrature hybrid coupler topologies such as coupled line couplers, lange couplers, Schwinger reversed phase couplers, Riblet short-slot couplers, couplers with apertures in planar lines [3]. One of the main performance indicators of couplers is phase imbalance between output ports of the couplers. Phase imbalance has a significant role where hybrid couplers are utilized as a part of a beamforming network. In beamforming networks, multiple hybrid coupler are connected to each other so that a specific phase distribution can be acquired at output ports of the beamforming network. In such topologies, phase imbalances of the couplers have a cumulative effect on phase distribution at output ports of the beamforming network. Therefore, in order to have a broadband performance in beamforming networks, couplers used in such networks should have wideband performance with very low phase imbalance values.

In this work, main focus has been solely on multi-layer quadrature hybrid couplers. As a coupling mechanism, aperture coupling has been preferred. Aperture coupling is utilized in a manner such that the resonators at the top and the bottom substrates of the couplers are coupled to each other through an aperture. Quadrature hybrid couplers that operate at both Ka-band and below Ku-band is studied.

2.1 Quadrature Hybrid Coupler Studies at Ka-Band

In this section, a compact and wideband multi-layer quadrature hybrid couplers are studied. The proposed structures will aim to operate within the wide frequency range (24GHz to 34GHz) in Ka-Band while having a minimal amplitude and phase imbalance within the whole frequency band.

2.1.1 Coupler Designs with the Elliptical and Butterfly Shaped Resonators

Multi-layer microstrip slot coupled wide-band quadrature hybrid coupler structure is designed in CST Microwave Studio environment. The geometry and the perspective view of the proposed structure is shown in Fig. 2.1. The proposed structure has four ports and it is consisted of two equally thick microstrip layers. Microstrip layers are combined back to back. The input port-1 and through output port-3 lays on one layer while coupled output port-2 and isolated port-4 lays on the other layer. Coupling is accomplished by coupling of the elliptically shaped resonators through the elliptically etched apertures on ground planes the microstrip layers.

Microstrip lines are etched on a substrates with ε_r=2.2, tanδ=0.0009 and thickness of 5 mils. Initial design dimensions for width of the elliptically shaped resonators and slots are determined by using the static approach mentioned in [24]. Even and odd mode impedances (Zoe and Zoo) of the structure is calculated using equations 2.1 and 2.2.

$$Zoe = \frac{60\pi}{\sqrt{\varepsilon_r}} \frac{K(k_1)}{K'(k_1)} \tag{2.1}$$

$$Zoo = \frac{60\pi}{\sqrt{\varepsilon_r}} \frac{K'(k_2)}{K(k_2)} \tag{2.2}$$

where

$$k1 = \sqrt{\frac{sinh^2(\pi G/4h)}{sinh^2(\pi G/4h) + cosh^2(\pi W/4h)}} \tag{2.3}$$

$$k2 = tanh\,(\pi W/4h) \tag{2.4}$$

The ratio $\frac{K(k_1)}{K'(k_1)}$ in equations 2.1 and 2.2 are calculated by using Hilberg formulas as follows:

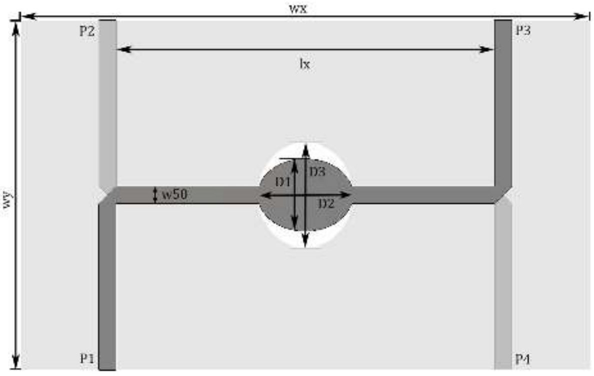

(a)

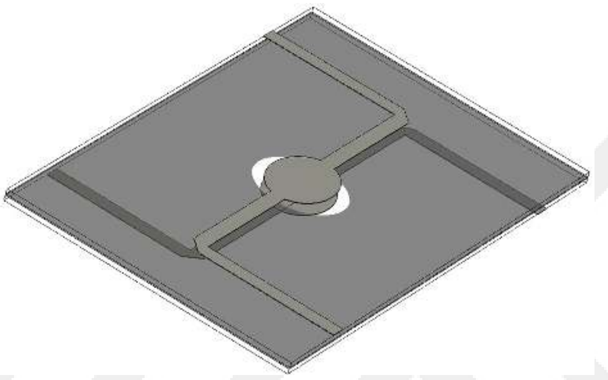

(b)

Figure 2.1: (a)The geometry of the proposed quadrature hybrid coupler. (b)Perspective view of the quadrature hybrid coupler.

$$\frac{K(k_1)}{K'(k_1)} = \begin{cases} \frac{2}{\pi} ln\left(2\sqrt{\frac{1+k}{1-k}}\right) & 0.5 \leq k^2 \leq 1 \\ \\ \frac{\pi}{2ln\left(2\sqrt{\frac{1+\sqrt{1-k^2}}{1+\sqrt{1+k^2}}}\right)} & 0 \leq k^2 \leq 0.5 \end{cases} \tag{2.5}$$

By using equations (2.6) to (2.10) W and G has been calculated while couplers length L is taken to be quarter of effective wavelength. In order to find elliptical dimensions of the coupler, elliptical approximations in [15] are used. Initial elliptical dimension are $D_1 = 1.60$, $D_2 = 1.58$ and $D_3 = 2.01$ has been calculated. After initial dimensions are found, final results are acquired by further parametric study using electromagnetic simulation tool CST Microwave Studio. The final dimensions of the designed quadrature hybrid coupler are given in Table 2.1.

Fig. 2.2 shows the s-parameters of the simulated quadrature hybrid coupler. It is seen from Fig. 2.2 that return loss of the hybrid coupler is above 18 dB within the whole frequency band. According to 2.2, isolation between input port and isolated port seems to be close to

Table 2.1: The final dimensions of the designed quadrature hybrid coupler.

Parameter	Value (mm)
wx	12.23
wy	7.51
lx	8.12
$w50$	0.37
$D1$	1.55
$D2$	2.05
$D3$	2.267

-20 dB while coupled power to the output ports port-2 and port-3 seems to be -3 dB.

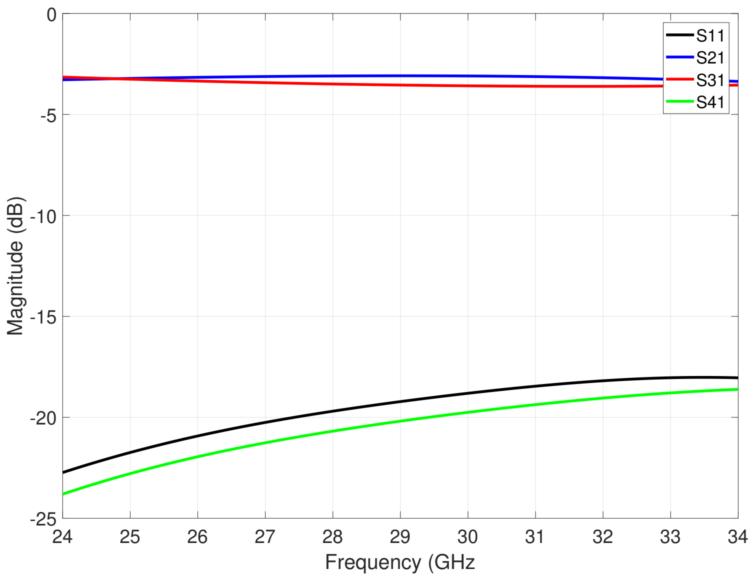

Figure 2.2: S-parameters of the simulated quadrature hybrid coupler.

Fig. 2.3 indicates the amplitude difference between coupled and through ports of the directional quadrature hybrid coupler. It is seen from the Fig. 2.3 that input power coupled to the through port and coupled port of the quadrature hybrid coupler is split equally. Amplitude difference between coupled powers of through and coupled ports is less than 0.5 dB which can be considered to have achieved wideband equal power split along whole operating band. In order to have wideband quadrature hybrid coupler performance, one must create 90 degree phase difference between coupled and through ports in addition to the equal power split along whole operating band. In Fig. 2.4, phase difference between power transferred to the coupled and through ports is shown. Results indicates that expected 90 degree phase difference is also achieved with approximately 2 degrees phase error along whole operating band.

The multi-layer topology given in Fig. 2.1 isn‘t easy to manufacture. In order to combine separate layers without interfering with the aperture coupling mechanism, substrate materials have to be brought together by screws. Since in Ka-band microstrip lines and resonators

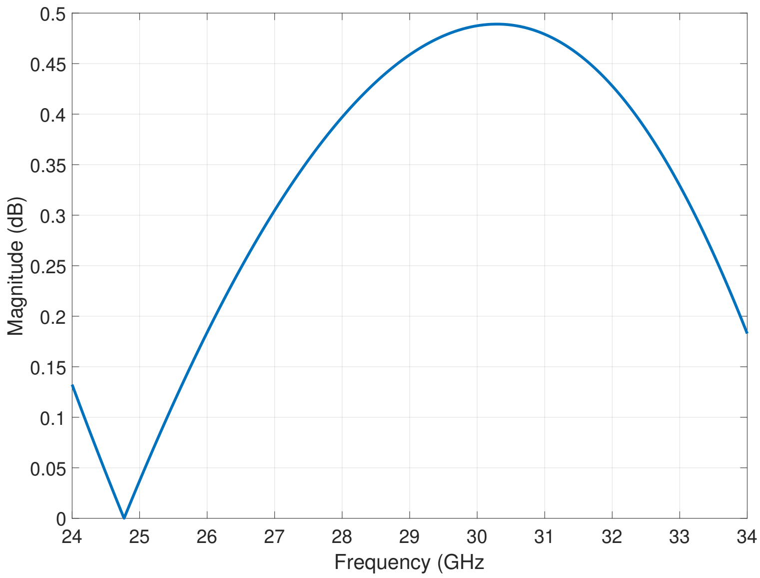

Figure 2.3: Amplitude difference between the output ports.

are very small, the screws shall be as small as possible and their placement should be done carefully. If the screws are not placed at an adequate distance from the structure, they may degrade the performance of the structure. Moreover, if layers isn't be combined as closely as possible especially around the cavity, performance of the structure would suffer significantly.

As a second topology, resonators of the coupler are changed into the butterfly shaped resonators. However, there is a major difference between the first and second topology. In the second topology, 0.1 mm thick bonding material is inserted in between the layers. Although, it is expected to cause an extra loss and create gap between ground planes of the layers, manufacturing errors of this topology will be less compared to the first topology. Instead of using elliptically shaped resonators, the butterfly shaped resonators are used to overcome the losses and the performance degradation due to inserted bonding material. 0.127mm thick substrate material with $\varepsilon_r = 2.94$ is used for this coupler. The geometry of the coupler is given in Fig. 2.5. The simulated s-parameter results of the second topology and phase difference between output ports are is given in Fig. 2.6 and Fig. 2.7. It is seen from the Fig. 2.6 - Fig. 2.7 that the new coupler with butterfly shaped resonators has very wide operating bandwidth in terms of return loss and phase difference between the output ports. Fig. 2.8 shows that 90° phase difference with less than 1.5° phase imbalance is achieved between the output ports while return loss is above 22dB within the whole frequency band.

Comparison of the insertion losses of the both couplers is given in Fig. 2.8. The insertion loss results given in Fig. 2.2 - Fig. 2.8 shows that although there is an approximately 0.3 dB loss due to the added bonding material, equal power split is achieved. It is safe to say that this topology is better than 1st topology in terms of return loss and phase difference between

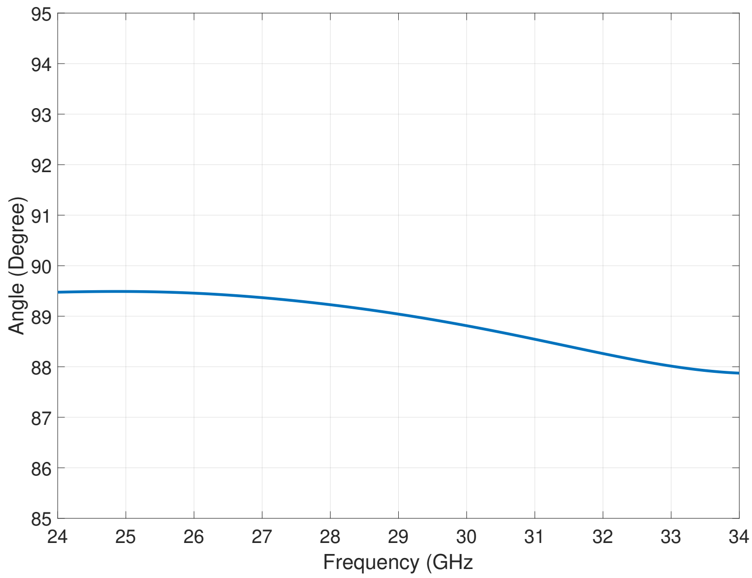

Figure 2.4: Phase difference between the output ports.

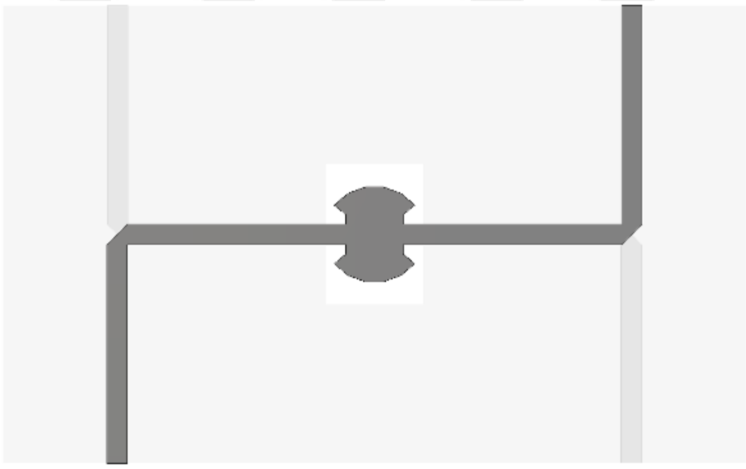

Figure 2.5: The geometry of the multi-layer coupler topology with the butterfly shaped resonators.

the output ports while slight loss introduced to the structure due to the bonding material.

2.1.2 Measurement Results

Two different manufacturing methods have been implemented in order to decide which method is going to provide the closest s-parameters results compared to the s-parameter results of the simulated models. Ideally, in order to acquire best possible coupling, spacing between layers should be as close to zero as possible so that insertion losses are kept at minimum.

First method was to mechanically combine the PCB layers with screws and nuts. In order

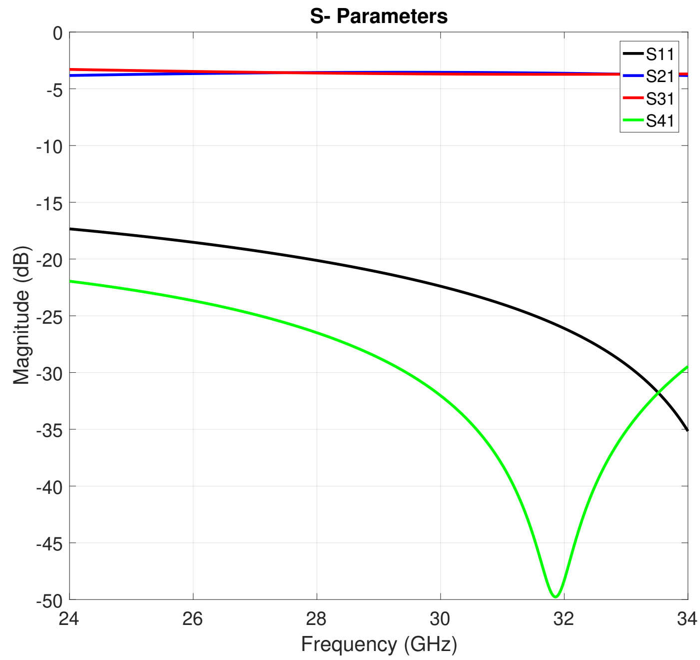

Figure 2.6: S-parameters of the simulated coupler with the butterfly shaped resonators.

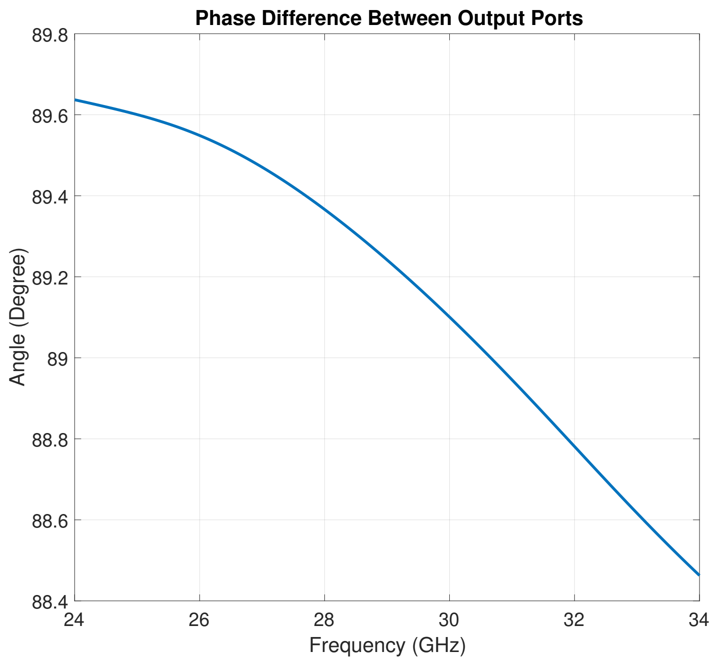

Figure 2.7: The simulated phase difference between the output ports of the coupler with the butterfly shaped resonators.

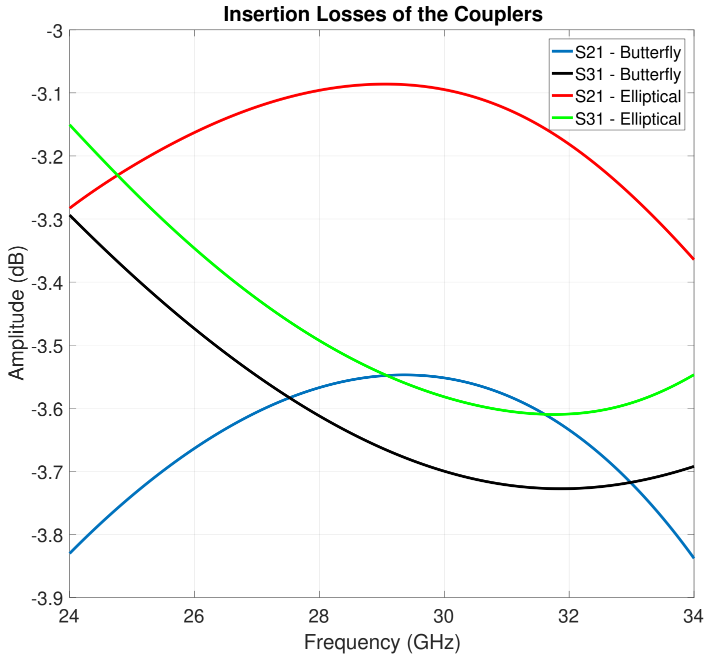

Figure 2.8: Comparison of the insertion losses of the both couplers.

to implement this method, coupler with the elliptical resonators was chosen. In Fig. 2.9, the simulated geometry of the coupler along with the e-field on the surface of the coupler is presented. In order to acquire more accurate results, connectors to be used, screws and nuts are also added to the simulations. As can be seen from Fig. 2.9, multiple screws are used around the resonators. In order not to effect the performance of the resonators, screws are kept at a carefully chosen distance where they don't interfere with the e-field distribution of the resonators.

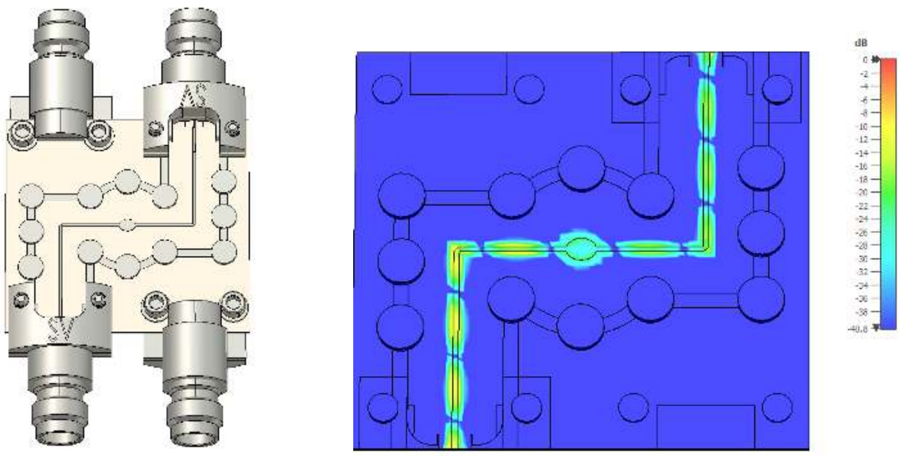

(a) (b)

Figure 2.9: (a) The simulation geometry of the coupler with the connectors and screws. (b) The e-field distribution on the surface of the coupler.

In Fig. 2.10, the geometry of the manufactured coupler with elliptical resonators is given. In order to acquire wideband performance, coupler was designed using a 0.127mm thick substrate material with $\varepsilon_r = 2.2$. However, since the PCB layers are not thick enough, multi-layer coupler structure could not be kept planar due to the weight of rf connectors and measurement results were far away from the expected results.

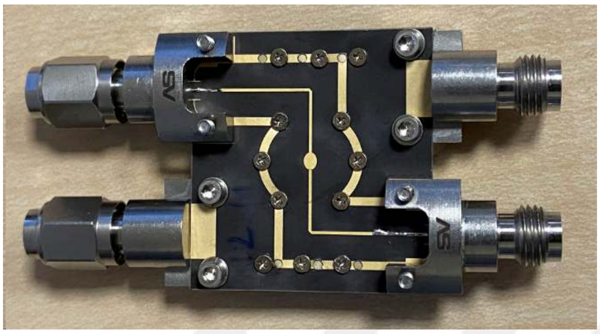

(a)

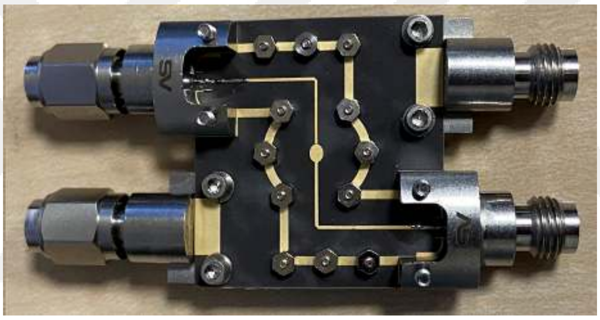

(b)

(c)

Figure 2.10: (a) Front view of the coupler with the elliptical resonators .(b) Back view of the coupler with the elliptical resonators. (c) Side view of the coupler with the elliptical resonators.

The second topology is utilizing from a manufacturing method that comprise of combining the PCB materials with a bonding material. In order to avoid bending problem, tougher material with $\varepsilon_r = 2.94$ and thickness of 0.127mm is used during manufacturing process. In between ground planes of the substrate materials, 0.1mm thick bonding material is inserted. In Fig. 2.11, the geometry of manufactured coupler with the butterfly shaped resonators is given.

Compared to the first topology bending problem is overcome and mechanically more

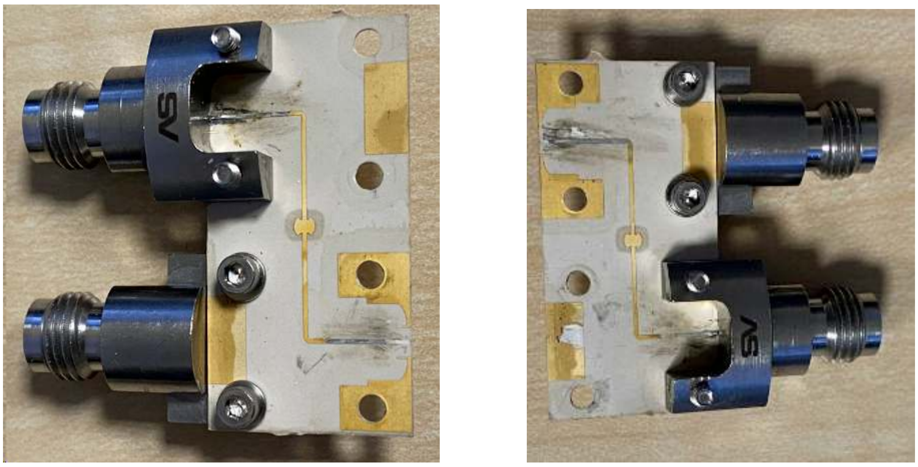

(a) (b)

Figure 2.11: (a) Front view of the coupler with butterfly shaped resonators. (b) Back view of the coupler with butterfly shaped resonators.

reliable end product is acquired. This is accomplished by the use of tougher substrate and a bonding material. Use of bonding material has two apparent advantages. These are increased total thickness of the whole structure and rigidness due to the mechanical properties of the bonding material. Despite of the mechanically enhanced structure, the measurement results of this coupler was also unsatisfactory. This problem is assumed to be due to unpredictable electrical nature of the bonding material at high frequencies.

2.2 Quadrature Hybrid Coupler Studies Below Ku-Band

2.2.1 Coupler with the Elliptically Shaped Resonators

The productions tolerances plays a very significant role on the measurements results at Ka-band. The dimensions of the microstrip lines and the radiators need to be as small as 0.37mm. Therefore the production and the assembly of the components in a multi-layer topology needs to have tolerances at micron levels. In addition to these, every component that is used in this topology has significantly higher insertion loss values when operating at Ka-band. All of these reasons make debugging problematic during the measurement process. Hence, in order to examine whether this topology is suitable for a production or not, it has been decided to design and measure the similar topologies at lower frequencies.

As an initial point, the quadrature hybrid coupler in [15] is chosen. The geometry of this design is seen in Figure 2.12. This design consists of two PCB cards with ε_r = 3.55 and tanδ=0.027 and the PCB cards have thickness of 0.508mm. Dimensions of the geometry is given according to the 2.1 at Table 2.3.

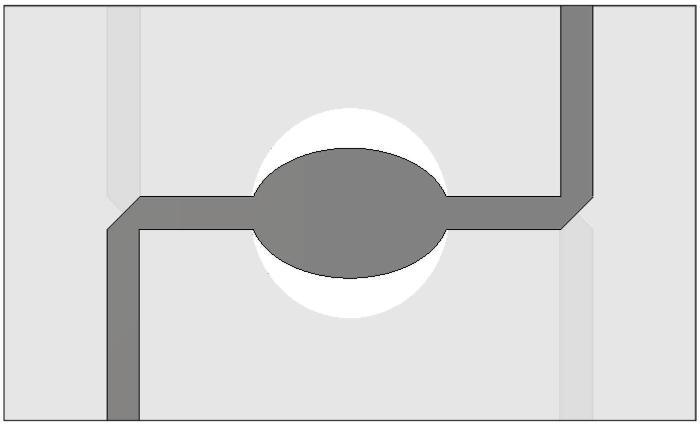

Figure 2.12: The geometry of the reference design

Table 2.2: Dimensions of the designed quadrature hybrid coupler.

Parameter	Value (mm)
wx	25
wy	15
lx	15.2
$w50$	1.18
$D1$	4.7
$D2$	7.6
$D3$	7.2

Fig. 2.13 shows the s-parameters of the simulated quadrature hybrid coupler. It is seen

from Fig. 2.13 that return loss of the hybrid coupler is above 22 dB within the whole frequency band. According to 2.13, isolation between input port and isolated port is less than -23 dB while coupled power to the output ports, port-2 and port-3, seems to be around -3 dB.

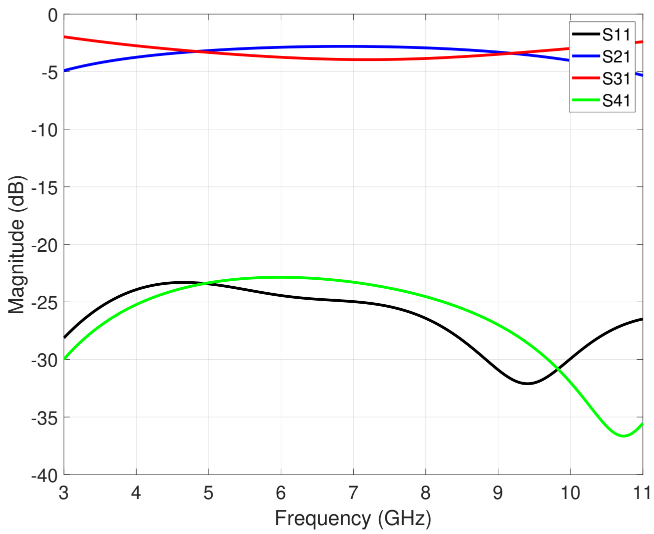

Figure 2.13: S-parameters of the simulated quadrature hybrid coupler

In Fig. 2.14, amplitude difference between output ports of the directional quadrature hybrid coupler is indicated. It is seen from the Fig. 2.14 that input power coupled to the output port most equally in the middle of the frequency band. Amplitude difference between coupled powers of through and coupled ports increases up to 3 dB.

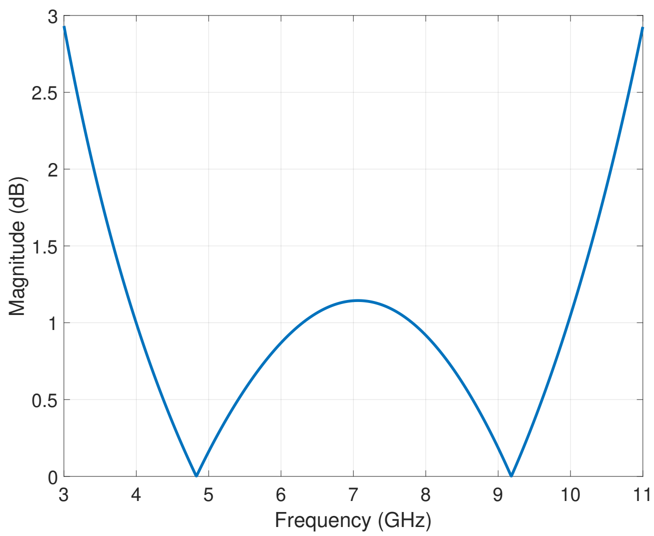

Figure 2.14: Amplitude difference between the output ports

In Fig. 2.15, phase difference between the output ports is shown. It is seen from the results that phase difference fluctuates around 90 degree with 2 degree phase error.

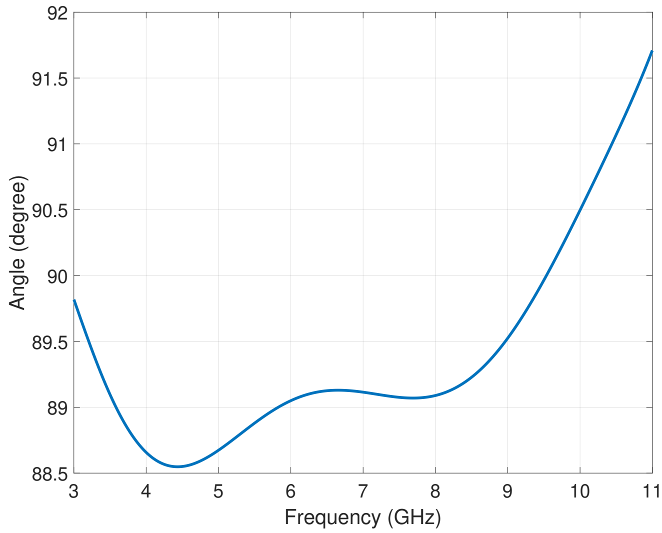

Figure 2.15: Phase difference between the output ports.

In order to manufacture this topology without any external bonding agent(screw), there has to be a internal bonding agent for combining the PCB cards. As an internal bonding agent, 0.09mm thick pre-preg material with $\varepsilon_r = 3.5$ and tanδ=0.004 is inserted in between the PCB cards. In Fig. 2.16 the PCB layout with and without the pre-preg material is presented.

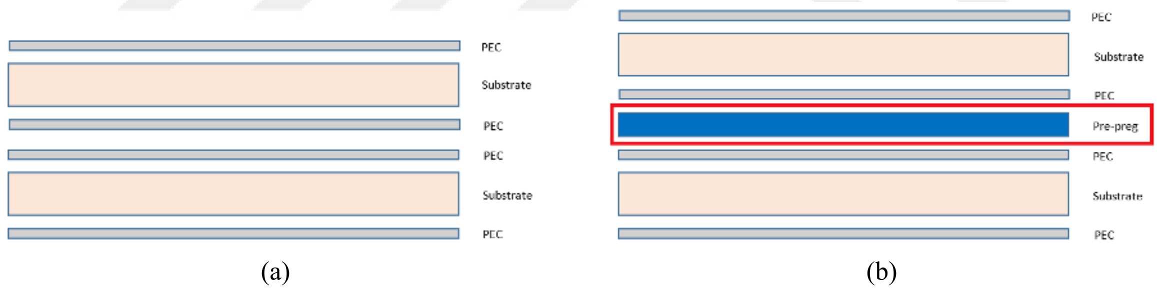

Figure 2.16: (a) The PCB layout without any bonding agent. (b) The PCB layout with the pre-preg material.

In Fig. 2.17, s-parameters of the new design with the pre-preg material in between the PCB cards is shown. It is seen from the results that there are undesired performance dips at several frequencies. Further look at these dips yield that standing waves are formed on the prepreg material due to the gap between ground planes of the PCB cards. In Fig. 2.18, the e-field distribution at a plane in between the PCB cards when there is no bonding agent and a pre-preg material is given at 6.94 GHz where the first dip occurs.

It is seen from Fig. 2.18 that at there is a serious standing wave problem that needs to be fixed at frequencies where there are unwanted performance dips. So as to fix this problem

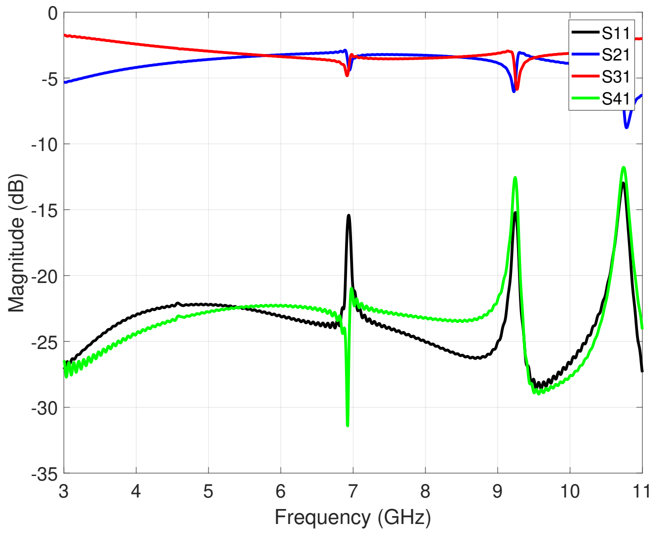

Figure 2.17: S-parameters of the simulated quadrature hybrid coupler with pre-preg material in between PCB cards.

and avoid unwanted electric fields on the surface of the PCB cards, it has been decided to cage these electric fields around the microstrip lines with vias. Vias' lengths are chosen such that vias connect top layer conductor of the upper PCB card to bottom layer conductor of the lower PCB. While inserting microstrip lines, distance between vias to the microstrip lines are chosen such that inserted vias doesn't effect existing electric field distribution of the microstrip lines. The geometry of the new design with vias is given in Fig 2.19.

Fig. 2.20 shows the s-parameters of the simulated quadrature hybrid coupler. It is seen from Fig. 2.13 that return loss and isolation between input port and isolated port of the hybrid coupler is above 18 dB within the whole frequency band. Compared to the design without any vias and bonding material, these results seems to be satisfactory.

In Fig. 2.21, amplitude difference between output ports of the directional quadrature hybrid coupler is shown. Fig. 2.21 shows that at the middle of the frequency band, amplitude difference is around 0.75 dB which is 0.5 dB better than original design whereas at the lower edge of the frequency band amplitude difference increases up to 3.5 dB.

Fig. 2.22 indicates the phase difference between the output ports. It is seen from the results that phase difference fluctuations increases up to 12 degrees around 90 degrees which seems to be the downfall of the via cage around the microstrip lines. These phase imbalance could be decreased by further optimization of the coupler dimensions and distance between vias and microstrip lines. However, for the purpose of this study which is to see if it is possible to manufacture this topology with internal bonding agent, this desing is manufactured with these results.

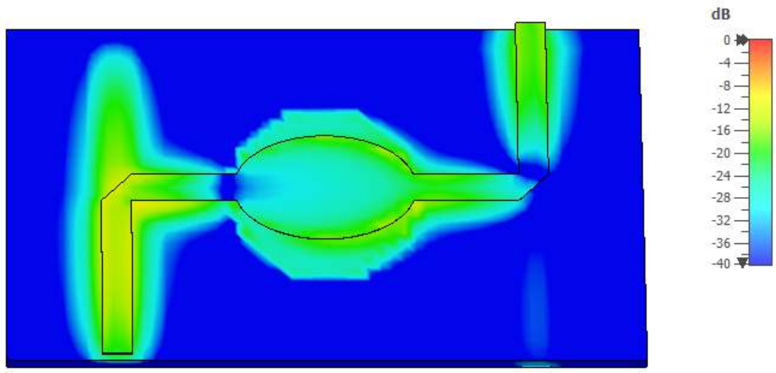

(a)

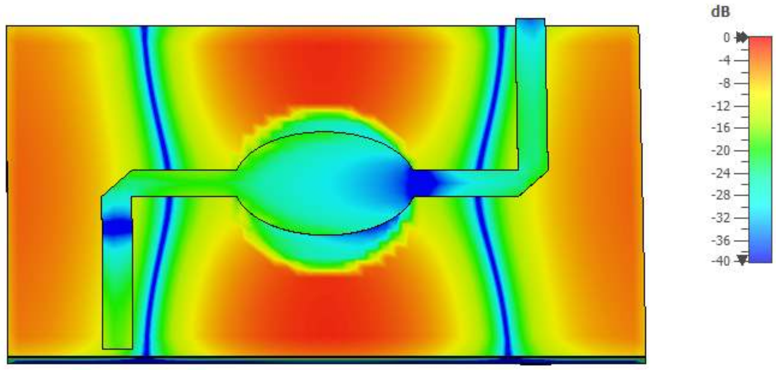

(b)

Figure 2.18: (a) The e-field distribution at a plane in between PCB cards when there is no bonding agent. (b) The e-field distribution at a plane in between PCB cards when there is a pre-preg material in between PCB cards.

2.2.2 Measurement Results of the Coupler with the Elliptically Shaped Resonators

The geometry of the manufactured quadrature hybrid coupler is shown in Fig.2.23. Port numbers for the measurement results are marked on the manufactured geometry shown in Fig. 2.23. Multiple 2-port measurements are performed on 2-port network analyzer to measure the full performance of the coupler.During 2-port measurements, the connectors that are not connected to the network analyzer are terminated with 50 ohm terminations.

Fig. 2.24 shows the s-parameters of the simulated and measured quadrature hybrid coupler results. It is seen from Fig. 2.24 that measured return loss and isolation results are approximately 5 dB worse than expected whereas the measured and simulated insertion loss results seems to agree with each other.

In Fig. 2.25, the simulated and measured amplitude difference between output ports of the directional quadrature hybrid coupler are shown. Along the most of the frequency band

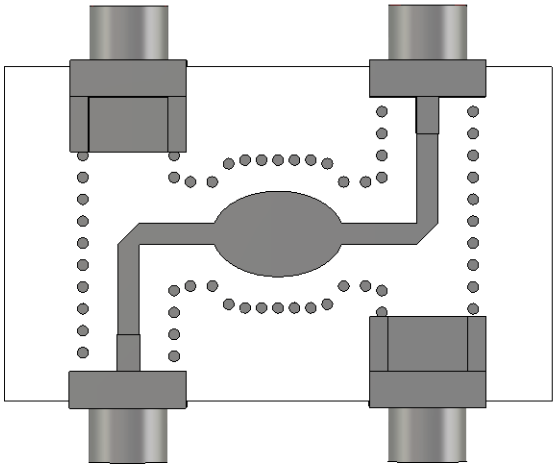

Figure 2.19: The geometry of the new design with the vias

the measured and simulated amplitude differences seem to be close to each other except at the end of the frequency band.

Fig. 2.26 indicates the simulated and measured phase difference results between the output ports. It is seen from Fig. 2.26 that the manufactured quadrature hybrid coupler performed better than the simulation. Instead of 12° phase imbalance, the manufactured quadrature hybrid coupler only has 4° phase imbalance.

2.2.3 Coupler with the Butterfly Shaped Resonators

The results of the manufactured multi-layer quadrature hybrid coupler with an internal bonding agent seems to be promising. Therefore a novel quadrature hybrid coupler using the new found method will be designed and proposed. New quadrature hybrid coupler utilizes from the same multi-layer microstrip structure while having butterfly shaped resonators and apertures instead of elliptically shaped geometries. Design of the new coupler was initialized without any vias to examine if previous standing wave issues would still cause any problems.

The geometry of the proposed structure is shown in Fig. 2.27. As it can be seen from the Fig. 2.27, bottom PCB card is mirrored version of the top PCB card as in previous designs. Coupling in this structure is accomplished by coupling of butterfly shaped resonators. Apertures used for coupling also has butterfly shaped and they are etched to the ground planes of the top and bottom PCB cards.

The electrical and physical properties of the PCB cards that are used in this multi-layer structure are ε_r = 3, tanδ=0.017 and PCB cards thickness = 0.508mm. In order to design a multi-layer aperture coupled coupler and acquire initial design dimensions for butterfly

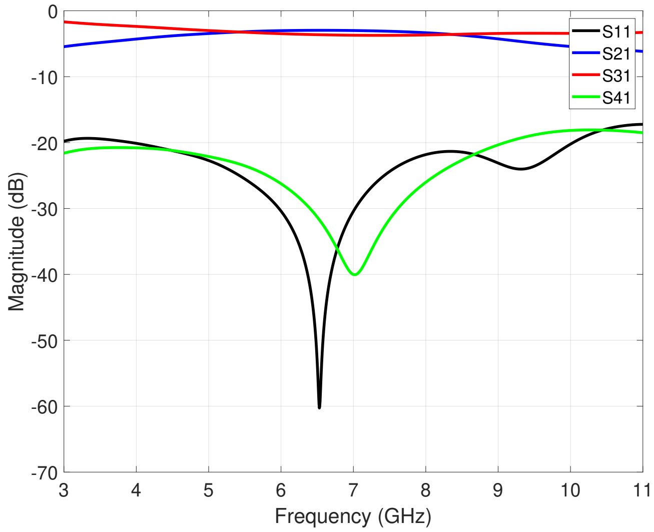

Figure 2.20: S-parameters of the simulated quadrature hybrid coupler

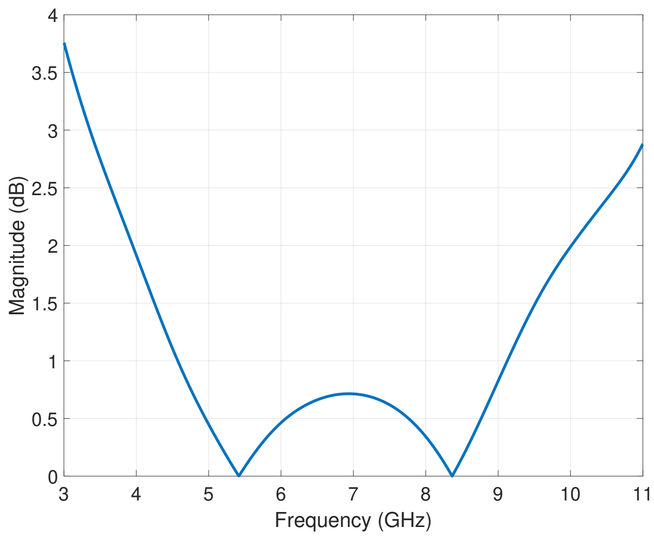

Figure 2.21: Amplitude difference between the output ports

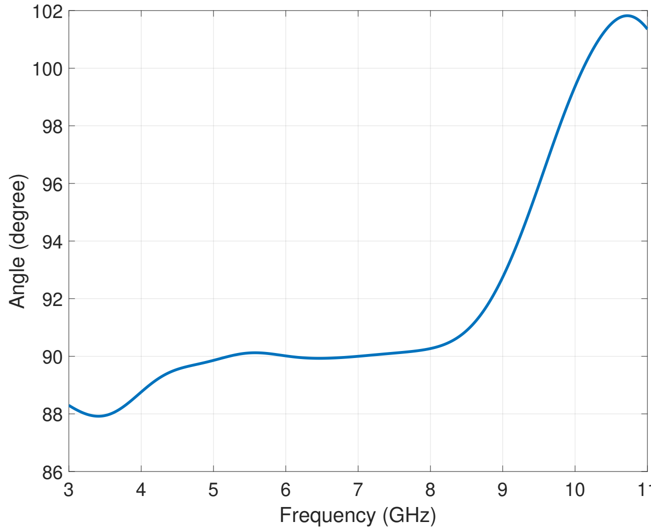

Figure 2.22: Phase difference between the output ports.

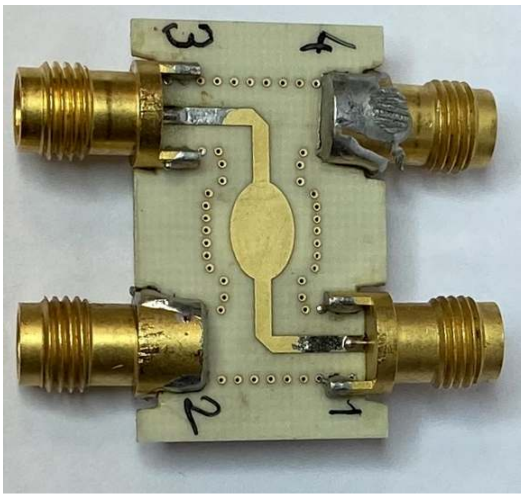

Figure 2.23: The geometry of the manufactured quadrature hybrid coupler.

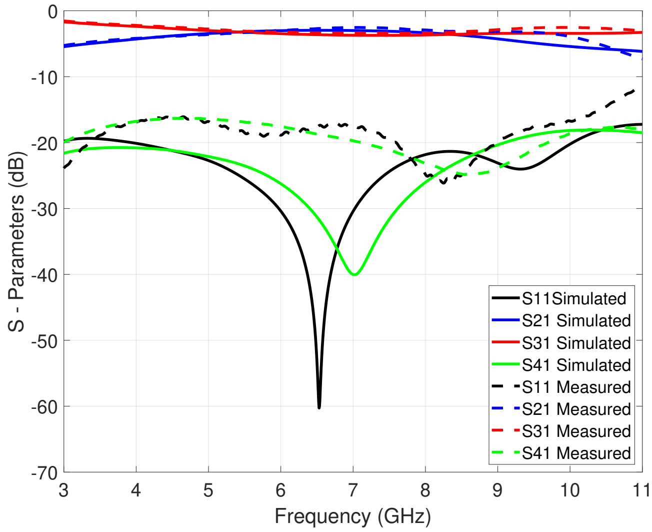

Figure 2.24: S-parameters of the simulated and measured quadrature hybrid coupler.

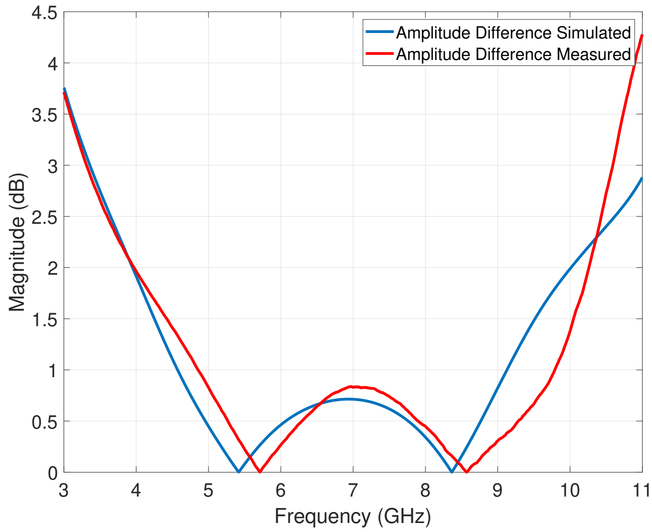

Figure 2.25: The simulated and measured amplitude difference between the output ports.

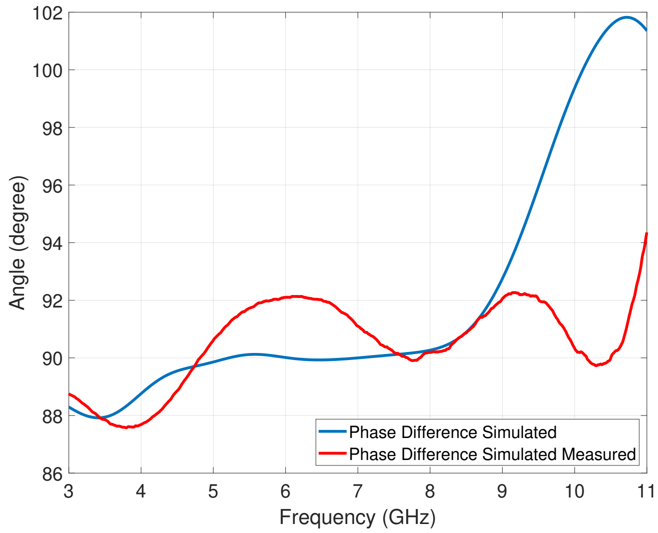

Figure 2.26: The simulated and measured phase difference between the output ports.

shaped resonators, the static approach mentioned in [24] is utilized. In Fig. 2.28, the coupler model used for the quasi-static analysis in [24] is presented. As can be seen from Fig. 2.28, the resonators and aperture in [24] are both rectangularly shaped. In this work to be able to acquire the initial design parameters for the butterfly shaped resonators, the area equivalent rectangular resonators and aperture is used. First of all, even and odd mode impedances (Zoe and Zoo) of equivalent rectangular structures is calculated using equations Eq.2.6 and Eq.2.7.

$$Zoe = \frac{60\pi}{\sqrt{\varepsilon_r}} \frac{K(k_1)}{K'(k_1)} \tag{2.6}$$

$$Zoo = \frac{60\pi}{\sqrt{\varepsilon_r}} \frac{K'(k_2)}{K(k_2)} \tag{2.7}$$

where,

$$k1 = \sqrt{\frac{sinh^2(\pi G/4h)}{sinh^2(\pi G/4h) + cosh^2(\pi W/4h)}} \tag{2.8}$$

$$k2 = tanh(\pi W/4h) \tag{2.9}$$

The ratio $K(k_1)/K'(k_1)$ in equations (2.6) and (2.7) are calculated by using Hilberg formulas [26] as follows:

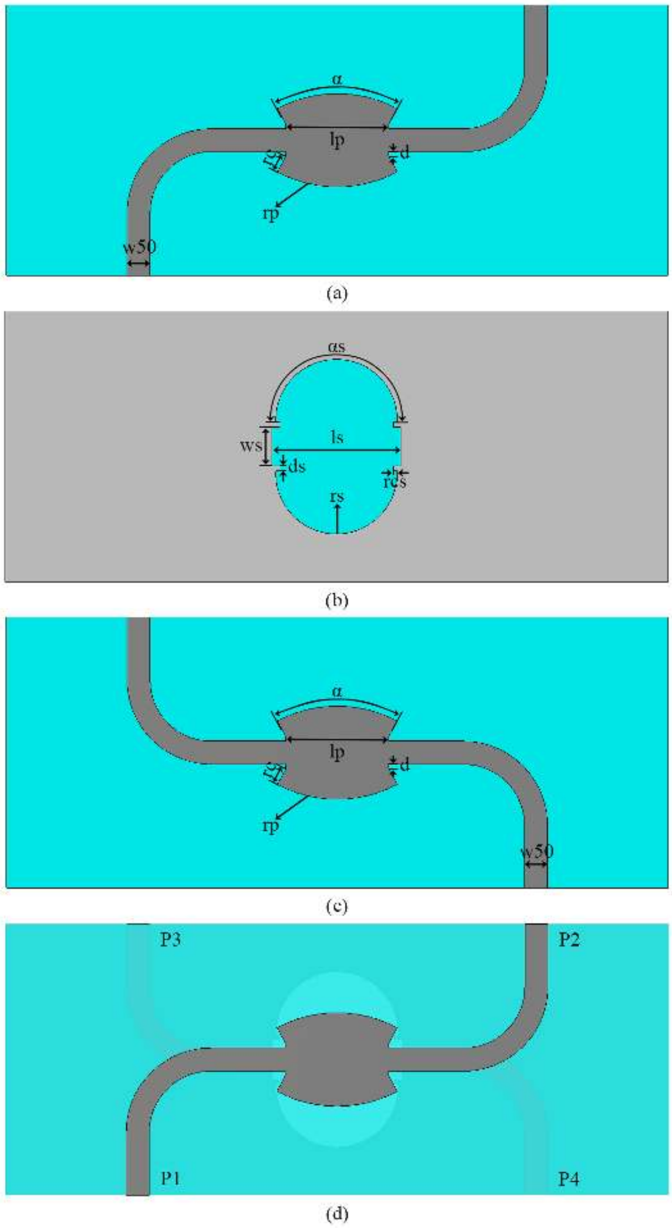

Figure 2.27: (a) Front view of the top PCB card of the coupler. (b) Ground plane of both top and bottom PCB cards of the coupler. (c) Front view of the bottom PCB card of the coupler. (d) Transparent view of the coupler.

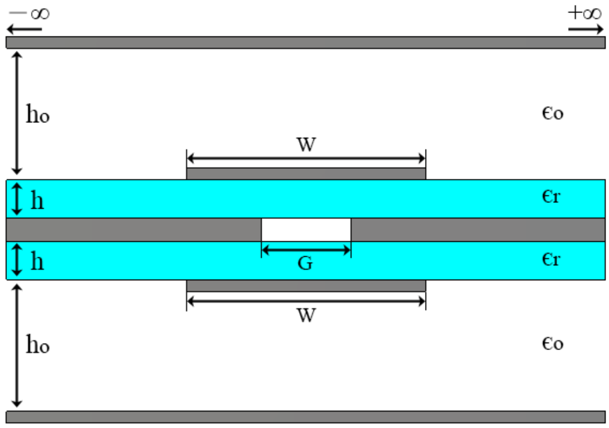

Figure 2.28: The coupler model used for the quasi-static analysis in [24]

$$\frac{K(k_1)}{K'(k_1)} = \begin{cases} \frac{1}{2\pi}\ln\left[2\frac{\sqrt{1+k}+\sqrt[4]{4k}}{\sqrt{1+k}-\sqrt[4]{4k}}\right] \\ for\ 1 \leq \frac{K}{K'} \leq \infty\ and\ \frac{1}{\sqrt{2}} \leq k \leq 1 \\ 2\pi/\ln\left[2\frac{\sqrt{1+k'}+\sqrt[4]{4k}}{\sqrt{1+k'}-\sqrt[4]{4k}}\right] \\ for\ 0 \leq \frac{K}{K'} \leq 1\ and\ 0 \leq k \leq \frac{1}{\sqrt{2}} \end{cases} \tag{2.10}$$

$$k^2 + k'^2 = 1 \tag{2.11}$$

In order to design a hybrid quadrature coupler, the magnitude of the coupling between the output ports should be 3dB which means the coupling coefficient C must be equal to 0.5. In Eq.2.12 and Eq.2.13, relationship between the coupling coefficient C and even/odd mode impedances Z_{oe}/Z_{oo} are given.

$$C = -20log\left(\frac{Z_{oe} - Z_{oo}}{Z_{oe} + Z_{oo}}\right) \tag{2.12}$$

$$Zo = \sqrt{Z_{oe}Z_{oo}} \tag{2.13}$$

Using Eq.2.12 and Eq.2.13, it has been found that Z_{oe}=120.9 ohm and Z_{oo}=20.7 ohm for Z_o=50 ohm for all the input and the output ports. Initially, length of the resonator lp and length of the aperture ls is equal to each other as they are quarter of the effective wavelength, λ_{eff}. Hence 90° phase difference will be acquired between output ports of the coupler. Using Eq. 2.14, initial lp and ls values are found to be 5.31mm.

$$\lambda_{eff} = \frac{c}{f\sqrt{\varepsilon_r}} \tag{2.14}$$

By using equations (2.6) to (2.11) the width of the equivalent rectangular resonator W and the width of the equivalent rectangular aperture G has been also calculated analytically. The dimensions ofthe W and G are found to be 4.47mm and 4.74mm consecutively. In order to find dimensions of resonators and aperture of the proposed design. It is assumed that area of butterfly shaped resonators and slots should be equal to their rectangularly projected counterparts. Area (A) of the butterfly shaped resonators and slots are calculated using same Eq. 2.15.

$$A = \left(r_c + \frac{l_p}{2sin(\frac{\alpha}{2})}\right)^2 \alpha - \frac{l_p^2}{2}cot(\frac{\alpha}{2})) + 2l_p(d + \frac{w_{50}}{2}) \tag{2.15}$$

When Eq. 2.15 is solved analytically, as an initial point radial edge of the resonator rc is found to be 0.9mm while angle of the arc of the butterfly shaped resonator α is found to be as 52.6 degrees. Following the same methodology, using Eg. 2.15 where resonator dimensions are replaced with the aperture dimensions, radial edge of the aperture rcs is found to be 0.2mm and angle of the arc of the butterfly shaped aperture eα_s is found to be 135.9mm. The radius of arc of the resonator rp is equal to $(rc + lp/(2sin(\alpha_s/2))$ and radius of arc of the aperture rs is equal to the $(rcs + ls/(2sin(\alpha_s/2))$. The remaining parameters that determines distance between radial edges and straight section of the shapes d and d_s are taken to be 0.25mm for ease of manufacturing. These results are not suitable to be able to operate with a wide-band performance since static approach is only solved at the center frequency of operation. Therefore, using the initial values acquired by analytical methods, further electromagnetic simulations are performed to get optimal results for wideband performance.

All simulations in this work are performed in the CST Microwave Studio environment. In Fig. 2.29, the optimal s-parameters of the simulated quadrature hybrid coupler are presented. It is seen from Fig. 2.29 that return loss of the hybrid coupler is above 18 dB within the whole frequency band. According to 2.29, isolation between input port and isolated port is less than -18 dB while coupled power to the output ports, port-2 and port-3, seems to be around -3 dB.

The proposed wideband topology requires that top substrate material has to be combined with the bottom substrate material along with their conductive layers. These layers has to be combined such that there is no alignment error within the layers. Existence of any alignment

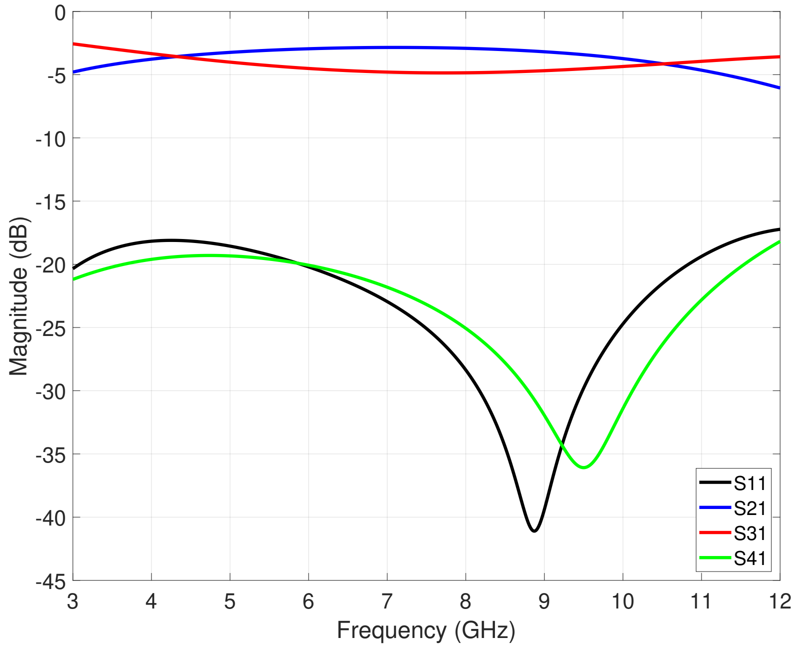

Figure 2.29: S-parameters of the simulated quadrature hybrid coupler.

errors would result in drastic performance changes in wideband response of the structure since coupling between the output ports are accomplished through the apertures etched to the ground plane of the PCB cards. Another source of an error would be the space between substrate materials. Space between the layers has to be kept homogeneous especially at the aperture region so that aperture coupling isn't effected due to any unwanted losses and disturbances. In order to manufacture this topology without effecting the wideband performance either an external bonding agent such as screw or internal bonding agents such as tapes or pre-preg materials must be used. In this study, in order to get best possible result, bonding of substrate materials with an internal bonding agent is preferred. By using an internal bonding agent, the space between the layers can be controlled more homogeneously within the whole area of the structure whereas an external bonding agent would only provide local homogeneity and it would be limited to the areas outside of the transmission line in order not to break transmission.

In this work, instead of combining the PCB cards manually with a tape after production process, it has been decided to combine them with a pre-preg material during the production process. Pre-preg materials are the main components that are used to manufacture multi-layer PCB structures. They are manufactured in a controlled environment where the fiber cloths are impregnated with a resin material so that their electrical and physical properties are more reliable compared to the tapes. They are not only used as a bonding material but also used as an insulating material between the PCB cards. In the proposed topology, a pre-preg material is used as a bonding material. During the manufacturing process, it has been placed in between the top and bottom PCB cards and all layers are merged under pressure and heat. There are three main advantages to using a pre-preg material instead of tapes. First one is that the electrical properties of the pre-preg materials are known and reliable. To be able design a broadband microwave component with multi-layer stackup, it is of paramount importance to model all the substrate materials with the correct electrical properties. The second advantage of the pre-preg materials is that the alignment errors are minimized in a controlled manufacturing environment where automated optical inspection and metrology equipments are used during the production process. Final advantage is that the thickness inhomogenieties are minimized due to the merging process which is performed under pressure and temperature. Compared to any manual bonding process, use of the pre-preg materials to realize multi-layer PCB stackup is more reliable, repeatable and more stable.

As an internal bonding agent, 0.092mm thick pre-preg material with ϵ_r = 2.91 and tanδ=0.0018 is inserted in between PCB cards. In Fig. 2.30 PCB layout with and without pre-preg material is indicated.

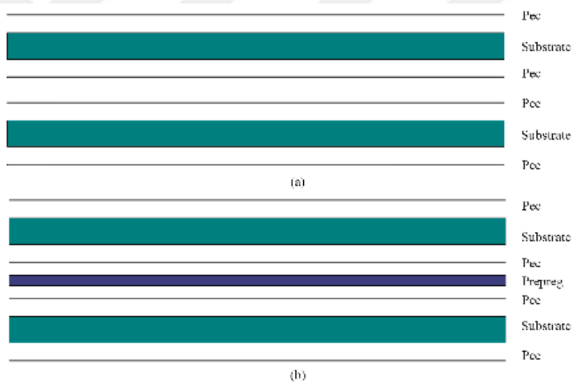

Figure 2.30: (a) The PCB stack-up without any bonding agent. (b) The PCB stack-up with the pre-preg material.

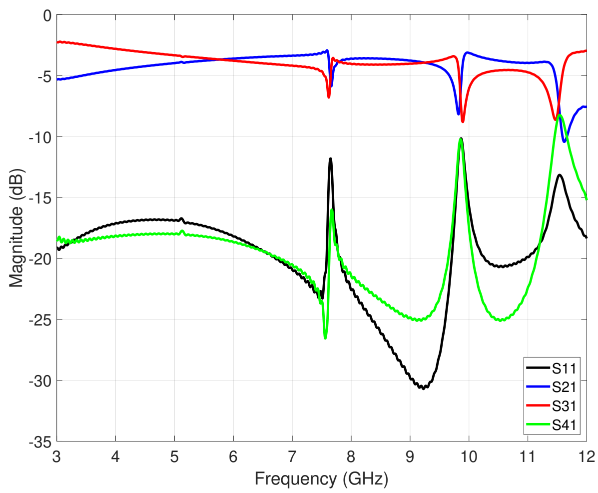

Figure 2.31: S-parameters of the simulated quadrature hybrid coupler with the pre-preg material in between the PCB cards.

In Fig. 2.31, s-parameters of the new design with the pre-preg material in between the PCB cards are shown. It is seen from the results that there are undesired performance dips at several frequencies. Further look at those dips yield that the standing waves are formed on the pre-preg material due to the gap between ground layers of the PCB cards. In Fig. 2.32, the e-field distribution at a plane in between the PCB cards when there is no bonding agent and a pre-preg material is given at 7.56 GHz where first dip occurs.

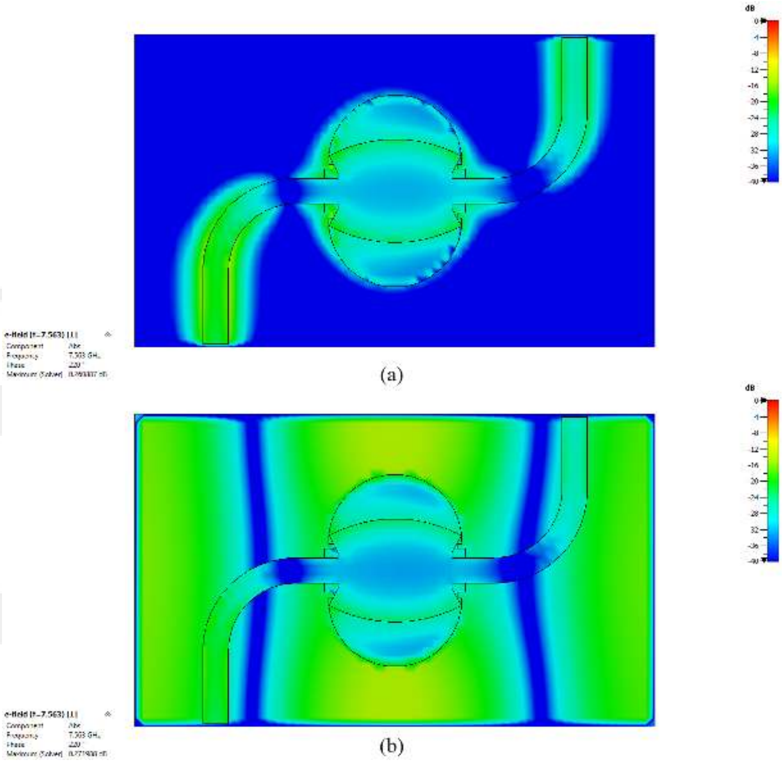

Figure 2.32: (a) The e-field distribution at a plane in between the PCB cards when there is no bonding agent. (b) The e-field distribution at a plane in between the PCB cards when there is a pre-preg material in between the PCB cards.

It is seen from Fig. 2.32 that there is a serious standing wave problem due to the unwanted surface waves on prepreg materials at frequencies where there are unwanted performance dips. So as to fix this problem and avoid unwanted electric fields on the surface of the PCB cards, it has been decided to cage these electric fields around the microstrip lines with the vias. To be able to effectively shield the electric fields, vias' lengths are chosen such that vias connect the top layer conductor of the upper PCB card to the bottom layer conductor of the lower PCB. In order to avoid an unwanted surface wave on the prepreg material, not only the length of the via but also placement of the vias on the PCB cards are significant. Therefore, while inserting shielding vias, distance between vias and the microstrip lines are chosen carefully by using simulations so that inserted vias don't effect the existing electric field distribution of the microstrip line.

The geometry of the new design with vias is given in Fig 2.33. In Fig. 2.34, the e-field distribution at a plane in between the PCB cards after the insertion of the shielding vias is given. It is seen from the Fig. 2.34 that insertion of the vias prevents formation of the standing waves on the prepreg material.

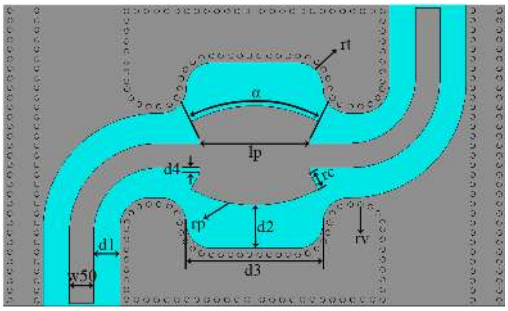

(a)

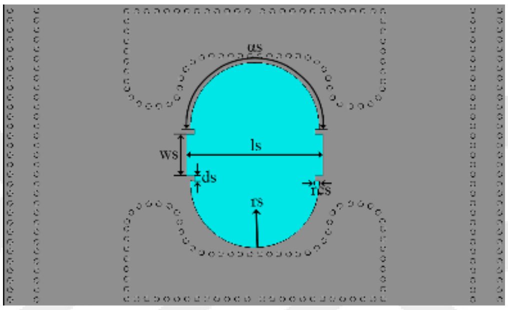

(b)

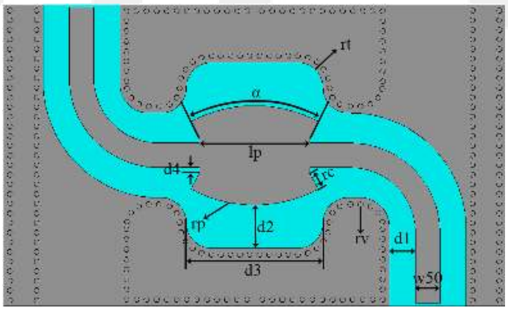

(c)

Figure 2.33: (a) Front view of the top PCB card of the proposed quadrature hybrid coupler. (b) Ground plane of the both top and bottom PCB cards of the proposed quadrature hybrid coupler. (c) Front view of the bottom PCB card of the proposed quadrature hybrid coupler.

After insertion of the vias, further optimization is performed on the structure to acquire better results. The optimal dimensions of the designed quadrature hybrid coupler are given at Table 2.3.

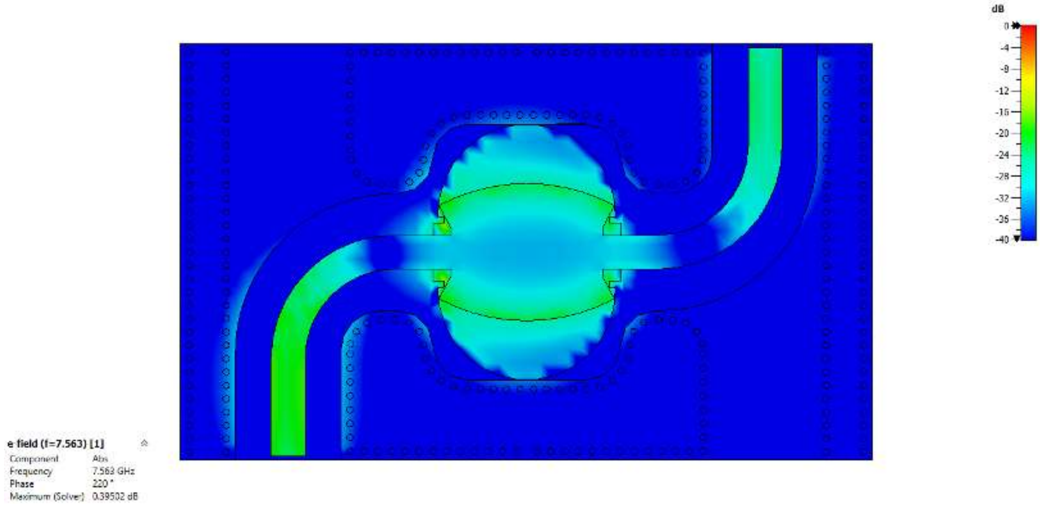

Figure 2.34: The e-field distribution at a plane in between the PCB cards after insertion of the shielding vias.

Table 2.3: The optimal dimensions of the designed quadrature hybrid coupler.

Parameter	Value (mm)
α	56.08
lp	5.46
$w50$	1.22
rp	6.74
rc	0.93
rv	0.3
rt	1.25
$d1$	1.3
$d2$	2.14
$d3$	6.79
$d4$	0.25
αs	184.8
ls	6.78
ws	2.08
rs	3.2
rcs	0.2
ds	0.25

2.2.4 Measurement Results of the Coupler with the Butterfly Shaped Resonators

The manufactured quadrature hybrid coupler is shown in Fig.2.23. Size of the manufactured design is 35mm x 17mm. Port numbers for the measurement results are marked on the manufactured geometry shown in Fig. 2.35. In order to measure the whole performance of the coupler, two-port pna network analyzer is utilized. Connectors that are not used during two ports measurements are terminated with 50 ohm terminations.

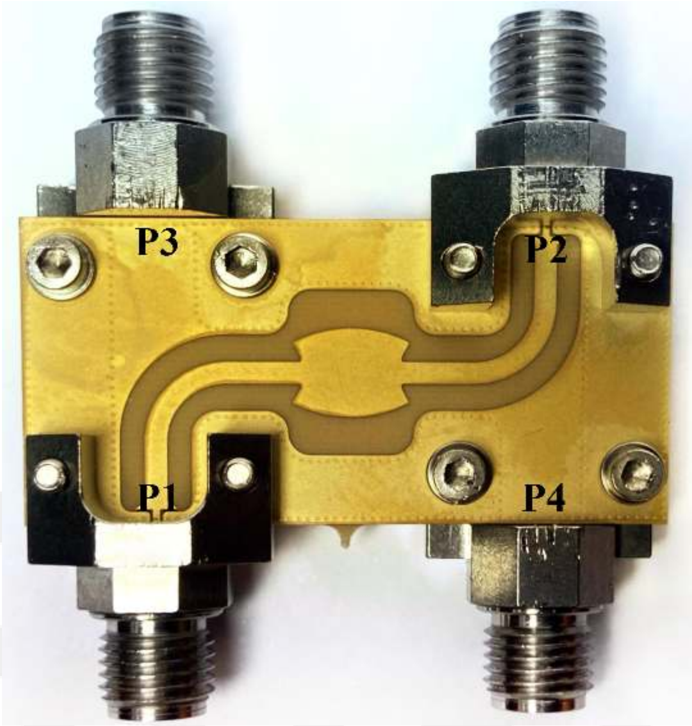

Figure 2.35: The manufactured quadrature hybrid coupler.

Fig. 2.36 shows the s-parameter results of the simulated and measured quadrature hybrid coupler. It is seen from Fig. 2.36 that the measured return loss and the isolation results are agree well with each other. The isolation of the coupler seems to have a narrow band notch at around 11 GHz, although it does not effect the performance of the coupler,

In Fig. 2.37, the simulated and measured amplitude imbalance between the output ports of the directional quadrature hybrid coupler are shown. Along the most of the frequency band, the measured and simulated amplitude imbalance seem to be very consistent with each other. It is seen that difference between the measured and simulated amplitude imbalance is less than 0.2 dB within whole frequency range.

Fig. 2.38 indicates the simulated and measured phase difference results between the output ports. It is seen from Fig. 2.38 that the manufactured quadrature hybrid coupler has also good results in terms of the phase response. The phase imbalance of the manufactured structure is less than $\pm 2.5^{\circ}$ within 3GHz to 12 GHz. It is seen that the difference between the measured and simulated phase imbalance is less than 1.3° within the whole frequency range.

The performance comparison of the quadrature hybrid couplers that are mentioned in the literature and the proposed design are presented at the Table 2.4. When performance of the all structures in the Table 2.4 are compared in terms of the operating bandwidth, the proposed

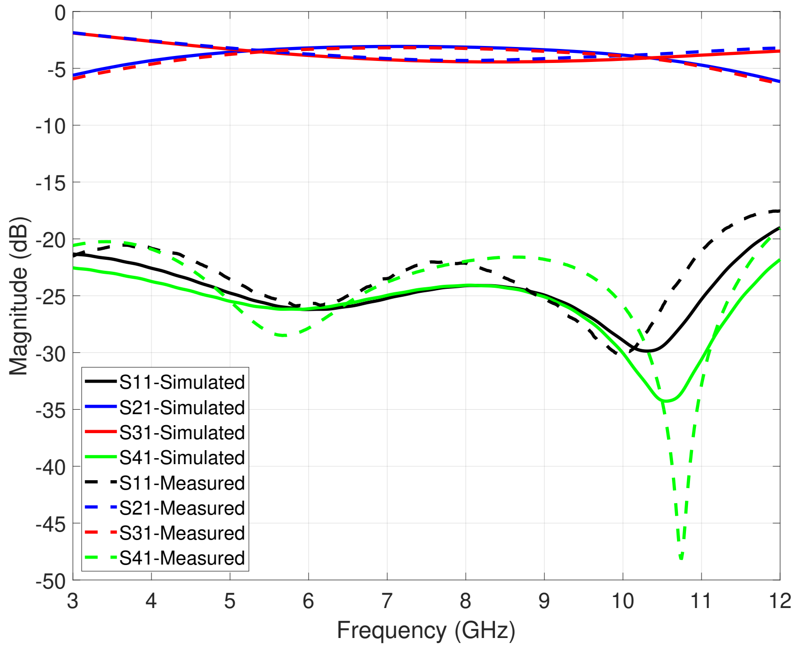

Figure 2.36: S-parameters results of the simulated and measured quadrature hybrid coupler.

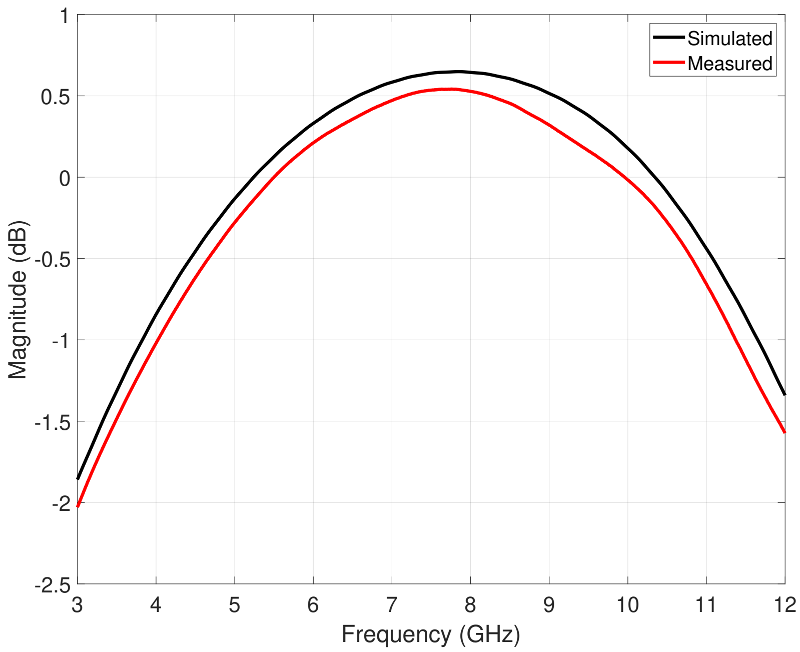

Figure 2.37: The simulated and measured amplitude imbalance between the output ports.

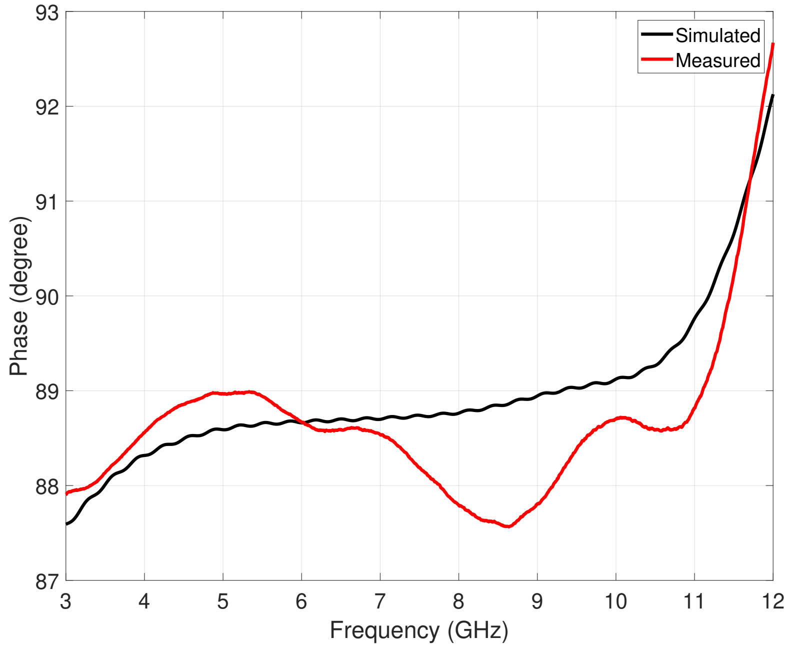

Figure 2.38: The simulated and measured phase difference between the output ports.

structure seems to have the widest frequency bandwidth by far except [15]. Although some of the papers didn't include any phase imbalance data of the manufactured designs including [15] which has closest operating bandwidth to the proposed design, it is safe to say that the proposed design has the lowest phase imbalance within the widest frequency range compared to the other studies. In addition to that, in terms of sizes of the designs in Table 2.4, the proposed design is fairly compact considering its operating frequency band.

Table 2.4: The performance comparison of the quadrature hybrid couplers that are mentioned in the literature and the proposed design.

References	Frequency (GHz)	Phase Imbalance (deg)	Size (cm)
[4]	1.75-2.75	-	3.55x3.50
[5]	1.50-2.60	3.0	3.70x2.90
[6]	1.65-2.60	3.0	7.50x11.0
[7]	1.39-2.45	3.2	7.89x3.94
[8]	22.0-26.0	6	-
[9]	10.7-14.2	8	-
[9]	23.0-27.0	10	-
[10]	2.27-3.12	2	-
[15]	3.10-10.6	-	2.50x1.50
Proposed Structure	3.00-12.0	2.5	3.50x1.70

Chapter 3

Phase Shifter

Aside from the couplers, the phase shifters are also one of the most frequently used microwave components. Depending on the application, they can be either passive or active. Compared to the active phase shifters, the passive ones are easier to design and fabricate. In addition to those benefits, they are also cost effective and more invulnerable to the temperature and their environment. Nowadays, most of the microwave systems are required to operate in a wider bandwidths for compatibility with wide-range of application hence the need for wide-band phase shifters arises and especially the passive ones are preferred for their advantages on the active phase shifters.

Major performance parameters of an phase shifters are insertion loss between the input and output ports and phase imbalance of the phase difference acquired between the output ports of the phase shifter. Main focus of this chapter will be on design of the -45° phase shifters.

3.1 Phase Shifter Studies at Ka-Band

In this section, studies have been focused on the compact and wideband multi-layer phase shifter topologies. These topologies aim to operate within Ka-Band and have a minimal phase imbalance along the whole operating frequency band.

3.1.1 Design Results

Most of the proposed microstrip based phase shifters including [15], doesn‘t operate above X-band. In this study, the operating frequency band has been chosen to be Ka-band. It has been seen that as the frequency of the operation increases dielectric losses become more critical for a multi-layer microstrip structures. As an initial point, a substrate with ε_r = 2.2, tanδ = 0.0009 and thickness of 62 mils has been chosen. However, it has been seen that it was not even possible to achieve close to stable phase shifting over a moderately wide bandwidth of frequency. In order to reduce the dielectric losses, thickness of the substrate has been decreased to 20 mils. It has been realized that, better results were possible as the substrates get thinner. Therefore, it has been decided to use a substrate with 5 mils of thickness.

In order to find best topology with highest performance, multiple phase shifters have been designed. All of the phase shifters have been designed in CST Microwave Studio environment. Same multi-layer topology mentioned in the previous chapter has been used for the phase shifter designs. Other than shapes of resonators and coupling slots, stack-up of the designs have been left the same. The microstrip lines are etched on a substrate with ε_r = 2.2, tanδ = 0.0009 and thickness of 5 mils. The static approach used in previous section is utilized. In order to find an initial design parameters for the phase shifters, area equivalent rectangular resonators and apertures are used. First of all, even and odd mode impedances (Zoe and Zoo) of the equivalent rectangular structures are calculated using equations Eq.2.6 and Eq.2.7. It has been found that Z_{oe}=132.3 ohm and Z_{oo}=18.9 ohm for Z_o=50 ohm for all input and output ports. To be able to design 45° phase shifter, the coupling coefficient in Eq. 2.12 is taken to be 0.75 and coupling length ψ is taken to be 90° according to the [25]. Definition of the coupling length (ψ) is given in Eq. 3.1.

$$\psi = \beta_{eff} l_c \tag{3.1}$$

β_{eff} in Eq. 3.1 is the effective propagation constant while l_c is the physical length of the coupling structure. Eq. 3.2 shows formula for the effective propagation constant. Parameter l_c is found using Eq. 3.1 and Eq. 3.2. As an initial point, length of the resonators and aperture is taken to be equal to l_c = 1.74mm.

$$\beta_{eff} = \frac{360\varepsilon_r}{\lambda} \tag{3.2}$$

By using equations (2.6) to (2.11), width of the equivalent rectangular resonator W and width of the equivalent rectangular aperture G has been also calculated analytically. The dimensions of the W and G are found to be 1.59mm and 1.61mm consecutively. In order to find dimensions of the resonators and aperture of the proposed designs. It is assumed that the area of resonators and slots used should be equal to their rectangularly projected counterparts. For the butterfly shaped resonators and slots Eq. 2.15 has been utilized. In order to calculate dimensions of the elliptical resonators and aperture, the diameter dimensions which are along the propagation direction is taken to be equal to l_c as an initial point and other dimension are calculated using area of the equivalent ellipse.

In the first structure, the butterfly shaped resonators have been used at each layer. Butterfly shape of the resonators have been acquired by combining two identical arcs back to back from the center of the arcs. The coupling in this structure is accomplished by a rectangular slot that is etched to the ground plane in between the layers. The initial parameters are found to be rc=0.3mm, α=87.3° where parameter d=0 and $w50$=0.37mm. In order to get optimal performance, dimensions of the 1st structure is optimized in CST Design Studio. The acquired optimal dimensions are rc=0.89mm, α=84.2°, ls=1.61mm, ws=3mm, lst=0.93mm. The perspective view and the geometry of layers of the optimized 1st structure can be found in Fig. 3.1.

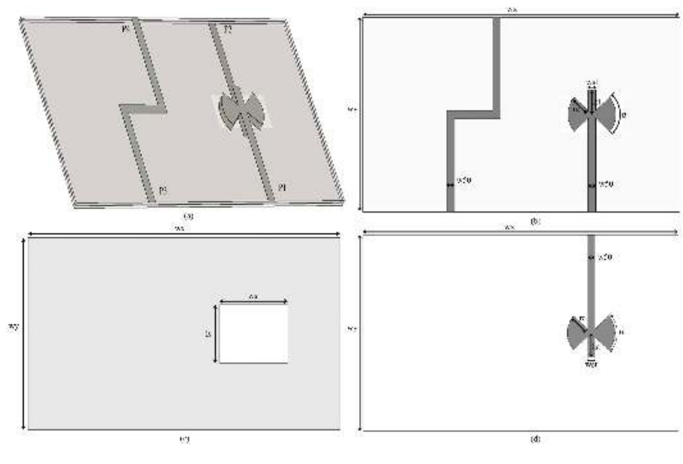

Figure 3.1: (a) Perspective view of the optimized structure. (b) Top layer of the phase shifter. (c) Mid layer of the phase shifter. (d) Bottom layer of the phase shifter.

The second structure uses elliptically shaped resonators. However, the coupling in the second shapes is still accomplished through rectangular slot etched to the ground plane that both of the elliptical resonators share with each other. The initial design dimensions are found to be $D1$=1.01mm, $D2$=1.74mm. In order to get the optimal performance, dimensions of the 2nd structure is optimized in CST Design Studio. The optimal dimensions are $D1$=3.68mm, $D2$=1.48mm, ls=1.46mm, ws3.53mm. The perspective view and geometry of layers of the second structure can be found in Fig. 3.2.

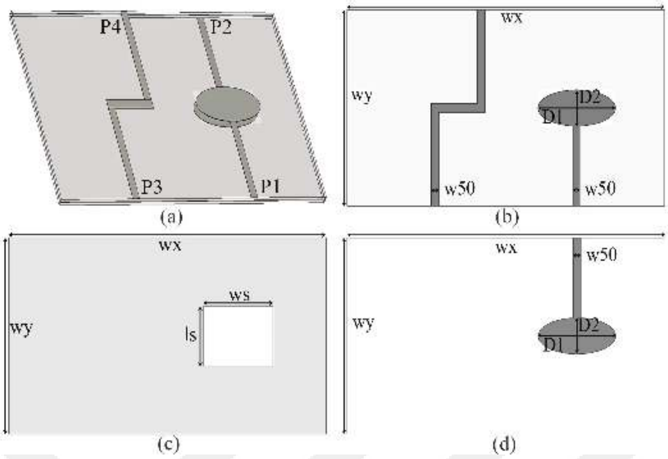

Figure 3.2: (a) Perspective view of the structure. (b) Top layer of the phase shifter. (c) Mid layer of the phase shifter. (d) Bottom layer of the phase shifter.

The third multi-layer structure not only uses rectangular resonators but also uses rectangular slot to make sure the coupling happens between the resonators on the top layer and bottom layer. CST Design Studio is utilized to find the optimal results. The optimal dimensions are found to be wp=3.39mm, ls=2.68mm and ws=3.3mm. Perspective view and geometry of the layers of the third structure can be found in Fig. 3.3.

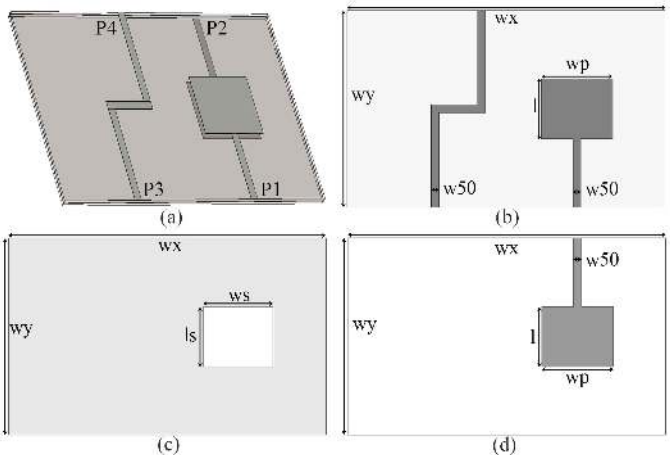

Figure 3.3: (a) Perspective view of the structure. (b) Top layer of the phase shifter. (c) Mid layer of the phase shifter. (d) Bottom layer of the phase shifter.

The final multi-layer phase shifter structure has elliptically shaped resonators and the coupling is accomplished through the elliptically shaped slot, etched to the ground plane. The slotted ground plane is shared by both of the elliptically shaped patch elements. The initial dimensions for the structure is found to be $D1$=1.01mm, $D2$=1.74mm, $D3$=1.03mm. The final dimensions of the structure after further optimization process made in CST Design Studio are found to be $D1$=4.46mm, $D2$=2.26mm, $D3$=4.36mm. The perspective view and geometry of the layers of the last proposed structure is shown in Fig. 3.4.

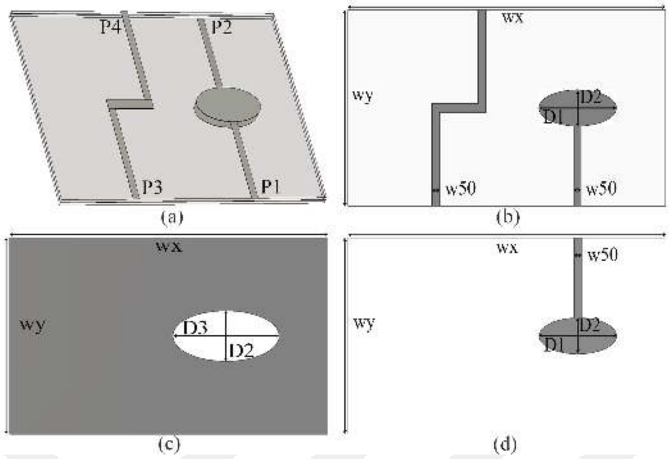

Figure 3.4: (a) Perspective view of the structure. (b) Top layer of the phase shifter. (c) Mid layer of the phase shifter. (d) Bottom layer of the phase shifter.

Fig. 3.5 shows the S-parameters of the simulated phase shifters. It is seen from Fig. 3.5 that return loss results of the all phase shifters are below -12 dB. Return loss of the structure4 seems to be worst of them. Especially after 28 GHz, the performance of the structure4 decreases drastically. When Fig. 3.5 is examined closely, it is also seen that structure2 and structure3 seem to exhibit similar performances while structure1 which is the multi-layer phase shifter with the butterfly shaped resonators, seems to perform better than all of the other structures. Return loss of the structure4 is approximately above 20 dB within the frequency band of 24 GHz - 34 Ghz. When these return loss results are considered, using the butterfly shaped resonators seems to provide more favorable results. However, one must also consider insertion loss and phase difference along the whole frequency band before deciding which structure is the best one.

Fig. 3.6 presents insertion loss results of the proposed phase shifters. As it is seen from the Fig. 3.6 that structure4 again performs below the other topologies. Insertion loss of the phase shifter with both elliptical resonators and elliptical slot is below 1.2 dB within the whole frequency band. Although structure2 and structure3 have similar return loss results, structure3 seems to perform better when insertion loss results are compared. It is also seen from the Fig. 3.6 that phase shifter with the butterfly shaped resonators again perform better than other phase shifters. Insertion loss results of structure1 changes from 0.6 dB to 1.35 dB along the whole frequency band.

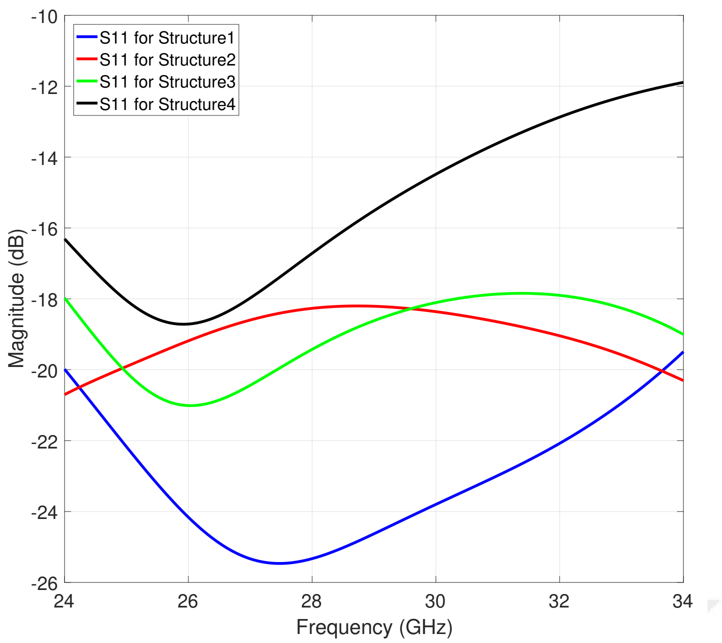

Figure 3.5: Return loss of the simulated phase shifters.

Fig. 3.7 indicates phase difference of the simulated phase shifters. The phase difference is calculated between proposed topologies and 50 ohm microstrip straight lines. The straight lines are all kept same for all of the proposed topologies. It is seen from Fig. 3.7 that phase difference imbalance of the phase shifters around 45° are about $\pm 6°$ for structure3 and structure4 while it increases up to $\pm 7°$ for the rest of the structure. Although return loss and insertion loss results of the proposed topologies are fluctuating, this fluctuation does not seem to reflect on to the phase difference values.

In this section, 4 different wideband phase shifter topologies that employs different coupled patch elements through etched slots in between the ground planes of the patches has been studied. All of the designed phase shifters have achieved constant 45° phase shift with the maximum phase imbalance of $\pm 7°$ within the operating band (24GHz to 34GHz). However, not all of them performed as well as each other in terms of the insertion loss and return loss. Especially the phase shifter with the elliptical patches and elliptical slot etched to the ground plane performed worst while phase shifter with the butterfly shaped patch resonators was the best of them. Its return loss results were better than 20 dB across the whole operating band while its insertion loss changed from 0.6 dB to 1.35 dB along the whole frequency band.

3.1.2 Measurement Results

The geometry of the manufactured phase shifters is seen in Fig. 3.8. These phase shifters have been manufactured to be mechanically combined with screws and nuts. However, same

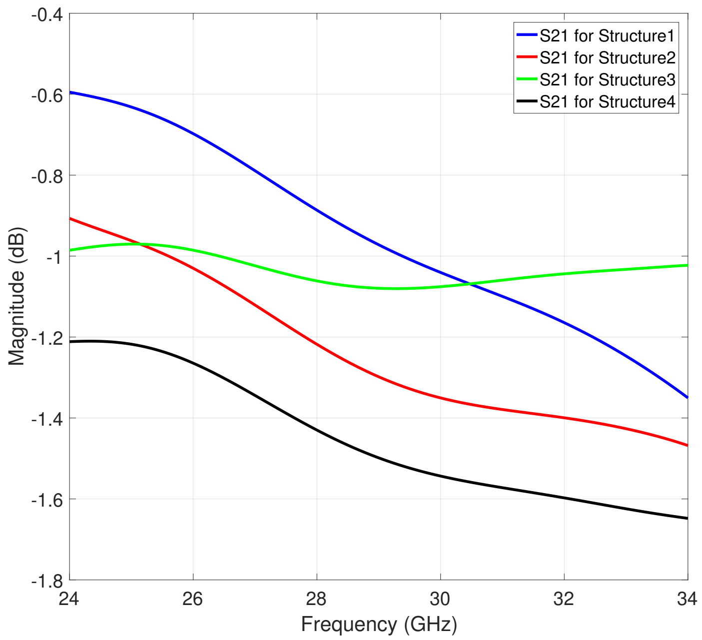

Figure 3.6: Insertion loss of the simulated phase shifters.

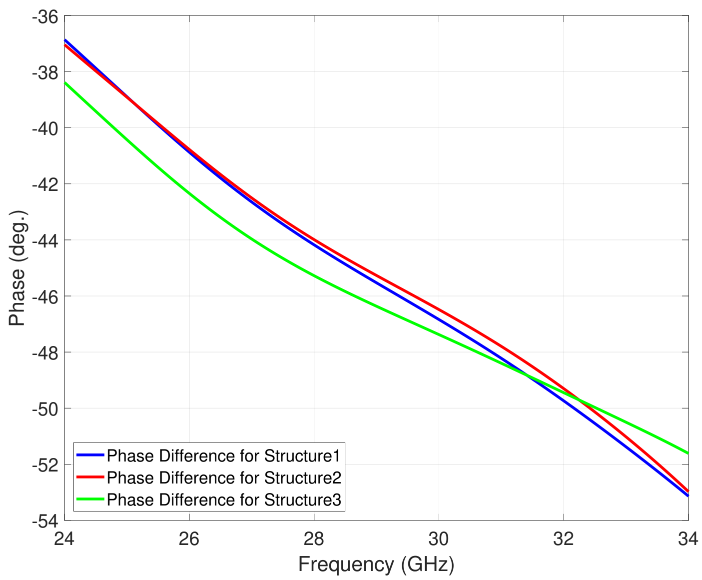

Figure 3.7: Phase difference of the simulated phase shifters.

manufacturing problems mentioned in previous section have been seen for these designs too. 0.127mm thick substrates were not strong enough to hold the rf connectors. In addition to existing problems, during manufacturing, layers had been processed incorrectly which had also lead to some mis-alignment problems.

(a) (b)

Figure 3.8: (a) Front view of the coupler with the butterfly shaped resonators. (b) Back view of the coupler with the butterfly shaped resonators.

3.2 Phase Shifter Studies Below Ku-Band

In this section, in order to get better manufactured results, frequency band of the phase shifter studies have been performed below Ku-Band. Specifically, focus of the studies in this section is to design a phase shifter that will operate within 3-12 GHz and has a minimal phase imbalance along the whole operating frequency band.

3.2.1 Phase Shifter with the Butterfly Shaped Resonators

In this section, as an initial design, a phase shifter with the butterfly shaped resonators has been studied since all of the previous studies have shown that aperture coupling mechanism between the resonators performed better when resonators are shaped like a butterfly. In order to achieve the best possible results, not only the resonators but also aperture that is utilized for the coupling is chosen to be shaped like a butterfly. Initial design dimensions are found to be rc=0.3mm, rcs=0.6mm, α=144.6°, α_s=126.2°, lp=ls=5.31mm where parameter d=0.25 and $w50$=1.22mm. Further optimization has been carried out in CST Design Studio. In order to prevent the standing wave formation explained in previous chapter, the shielding vias are added to the multi-layer phase shifter at the first stages of the phase shifter design. The same PCB stack-up as in section 2.2.3 have utilized to design the phase shifters. In Fig. 3.9, the geometry of the optimized phase shifter is given. The design dimensions are given in Table 3.1.

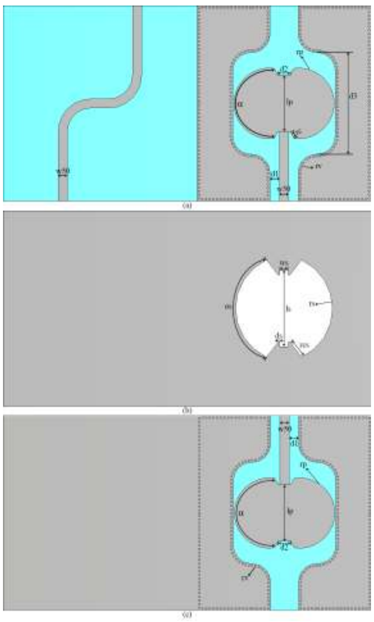

Figure 3.9: (a) Front view of the top PCB card of the phase shifter. (b) Ground plane of the both top and bottom PCB cards of the phase shifter. (c) Front view of the bottom PCB card of the phase shifter.

Table 3.1: Dimensions of the designed phase shifter.

Parameter	Value (mm)
α	195.9
lp	7.67
$w50$	1.22
rp	4.79
rc	1.03
rv	0.25
$d1$	1.30
$d2$	1.72
$d3$	13.79
αs	129.9
ls	10.35
ws	1.14
rs	7.28
rcs	2.55
ds	0.25

In Fig. 3.10, return loss of the simulated phase shifter is presented. It is seen from the Fig. 3.10 that the magnitude of the return loss is above 10 dB until 11.2 GHz. In order for an microwave component to be accepted as working within a frequency range, it is supposed to have at least -10 dB return within specified frequency band. Therefore, in terms of return loss, acquired results are not acceptable.

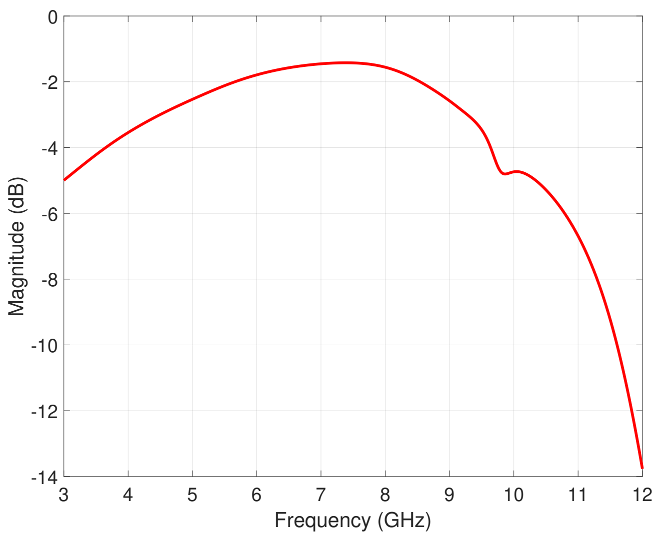

Figure 3.10: Return loss of the simulated phase shifter.

Fig. 3.11 shows insertion loss of the simulated phase shifter. Result presented in Fig. 3.11 indicate that the designed phase shifter is a very lossy microwave component. Especially, at the middle of the frequency band, insertion loss reaches to 7.4 dB. Such insertion loss levels are not acceptable for an phase shifter. This much of unwanted loss causes phase shifter to act as an attenuator which is not a desirable property for a phase shifter.

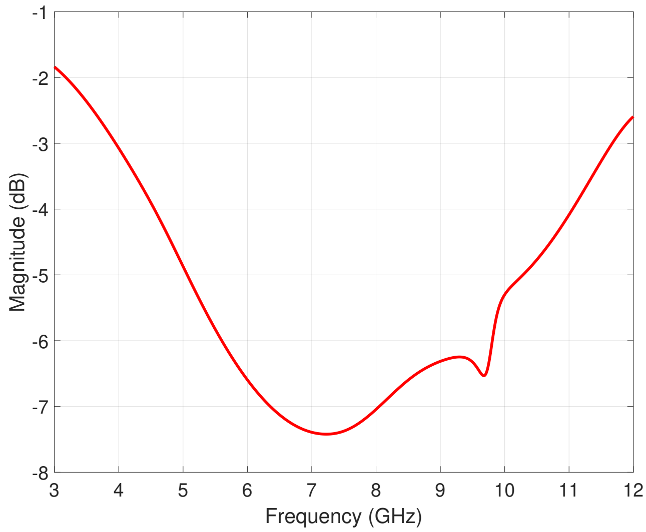

Figure 3.11: Insertion loss of the simulated phase shifter.

In Fig. 3.12 phase difference of the simulated phase shifter is given. Result in Fig. 3.12 depicts that -45° phase shift has been achieved in a very narrow band width. The phase imbalance seems to be around 25°. Lower phase imbalance values has to be achieved since the designed phase shifter will be utilized in a Butler matrix and phase imbalance of the phase shifters will have cumulative effect on phase imbalance at the output ports of the Butler matrix. Therefore better results has to be achieved on the phase shifters.

3.2.2 Phase Shifter with the Rectangular Resonators

The phase shifter with the butterfly shaped resonators and the aperture couldn't achieve acceptable results. Although the butterfly shaped resonators and coupling aperture yielded good results as an quadrature hybrid coupler, they have been seen to be not suitable as an -45° phase shifter. Therefore the phase shifter design has been changed such that the resonators and the aperture to be used for providing coupling between resonators have been turned into rectangular shapes. The initial design dimensions are found to be as wp=5.4mm, ws=5.68mm, lp=ls=5.31mm. However, as it was seen in the previous section, structure is needed to be optimized in order to get the optimal results. In order to achieve better matching throughout the operating frequency band, rectangular open ended stubs have been also added

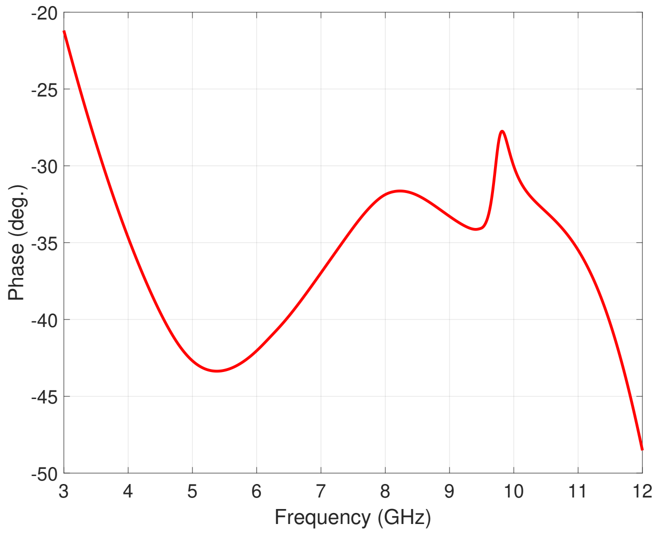

Figure 3.12: Phase difference of the simulated phase shifters..

to the resonators during optimization process. The same PCB stack-up as in the previous section has been utilized in this design. The geometry of the optimized phase shifter with rectangular resonators is given in Fig. 3.13.

In order to get better understanding of the phase shifter with the rectangular resonators and stubs. Parametric studies have been performed. As an initial parameter, width of the rectangular resonators wp has been studied. In Fig. 3.14, effect of the parameter on the phase difference has been provided. It seen from the Fig. 3.14 that parameter wp doesn't effect phase difference much until mid frequency band. However, after 7.5 GHz, it is seen that changing wp has a drastic effect on phase difference. As wp changes from 2.5mm to 5.5mm phase difference at the end of the frequency band changes from -10° to -100°.

Fig. 3.15 demonstrates effect of change in the parameter wp on the return loss. It seen from the Fig. 3.15 that the parameter wp has significant impact on the return loss of the phase shifter along the whole frequency band. Minimum magnitude of the return loss decreases to 8 dB as wp is 2.5mm while it increases up to 15 dB as wp is 5.5mm.

In Fig. 3.16, effect of the change in the parameter lp on the phase difference is indicated. Fig. 3.16 shows that lp has larger effect after mid frequency band. As lp changes from 3mm to 6mm, the phase difference at the end of the frequency band changes from -10° to -60°.

Fig. 3.17 demonstrates effect of the change in parameter lp on the return loss. It is seen from the Fig. 3.17 that the parameter lp also effects the magnitude of the return loss considerably. Maximum of the magnitude of the return loss decreases to 10 dB as lp is 2.5mm while it reaches to 15 dB as lp is 6mm.

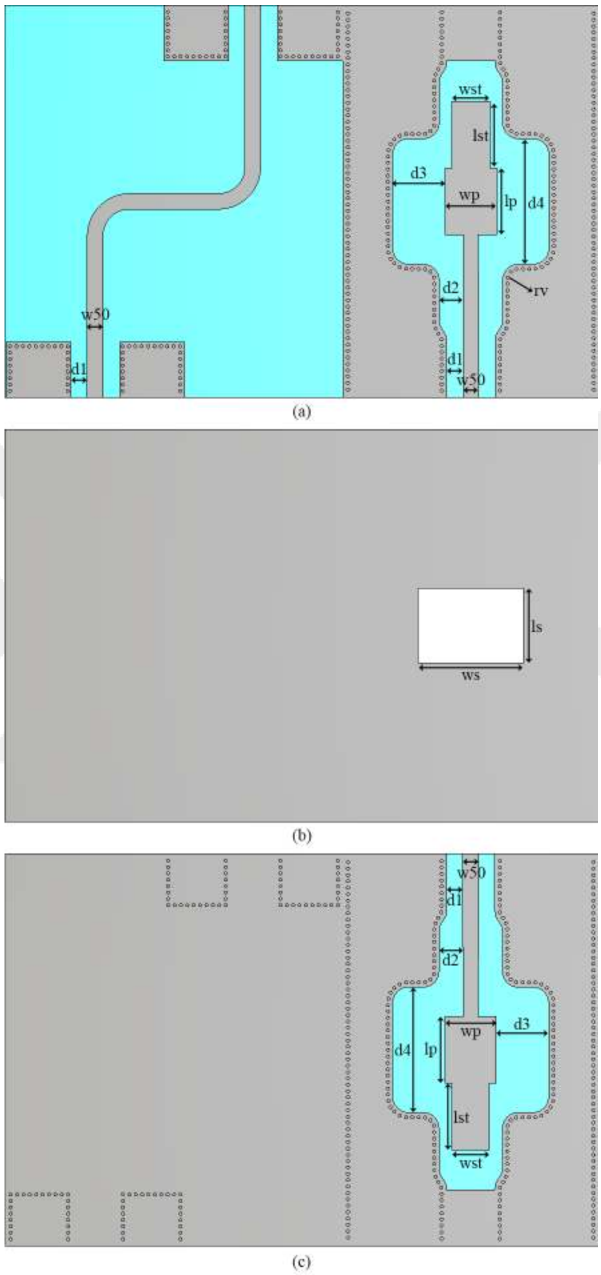

Figure 3.13: (a) Front view of the top PCB card of the phase shifter. (b) Ground plane of the both top and bottom PCB cards of the phase shifter. (c) Front view of the bottom PCB card of the coupler.

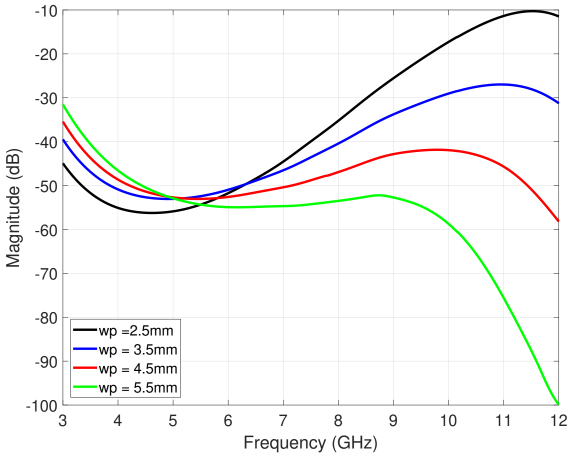

Figure 3.14: Effect of the change in the parameter wp on the phase difference.

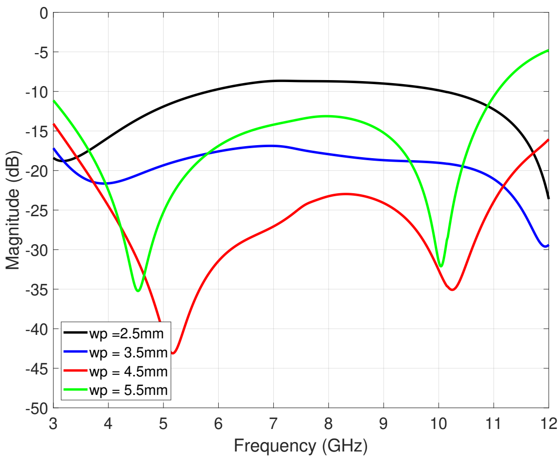

Figure 3.15: Effect of the change in the parameter wp on the return loss.

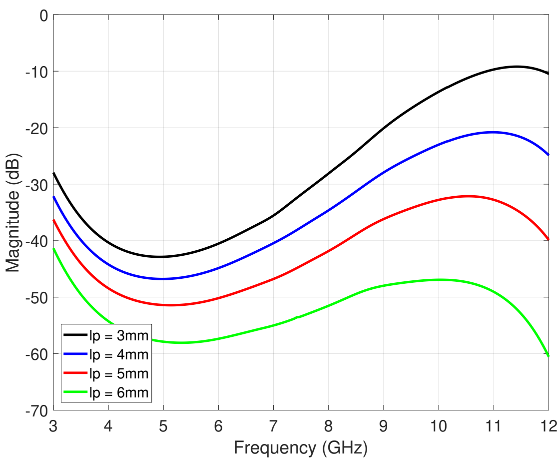

Figure 3.16: Effect of the change in the parameter lp on the phase difference.

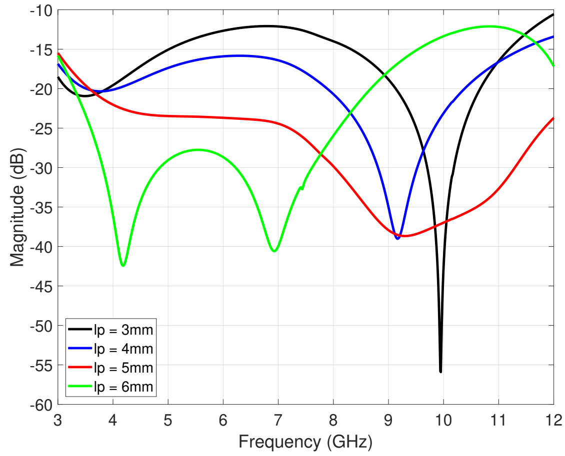

Figure 3.17: Effect of the change in the parameter lp on the return loss.

In Fig. 3.18, effect of the change in the parameter ws on the phase difference is shown. Fig. 3.18 shows that ws does not effect the phase difference as much as wp and lp. The effect of ws on the phase difference is mostly seen at the beginning of the frequency band. As ws changes from 6mm to 9mm, the phase difference at the beginning of the band changes from approximately -20° to -40°.

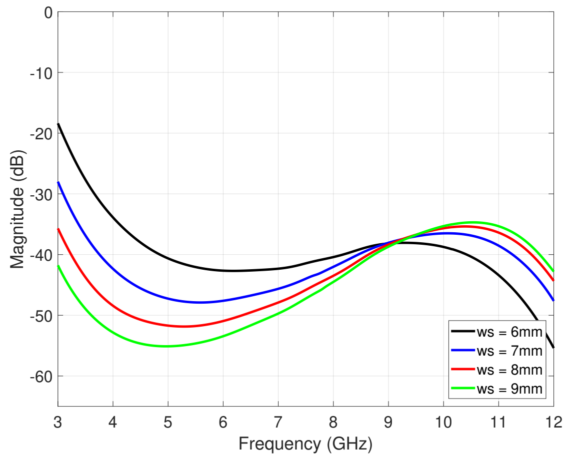

Figure 3.18: Effect of the change in the parameter ws on the phase difference.

Fig. 3.19 demonstrates effect of the change in the parameter ws on the return loss. It is seen from 3.19 that compared wp and lp, ws has more dramatic effect on magnitude of the return loss. As ws changes from 6mm to 9mm, the maximum magnitude of the return loss increases from 5 dB to 20dB.

Fig. 3.20 shows effect of the change in the parameter ls on the phase difference. Results in Fig. 3.20 indicates that ls also has an effect on the phase difference at the end of the frequency band. It is also seen from Fig. 3.20 that changing ls even 1mm can cause some

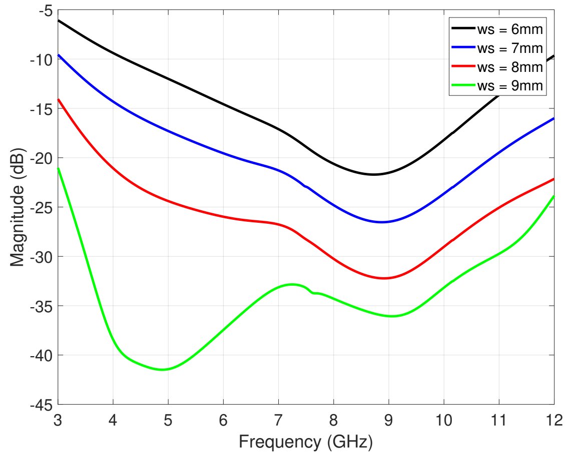

Figure 3.19: Effect of the change in the parameter *ws* on the return loss.

sudden changes on the phase difference. Therefore *ls* has to be changed cautiously.

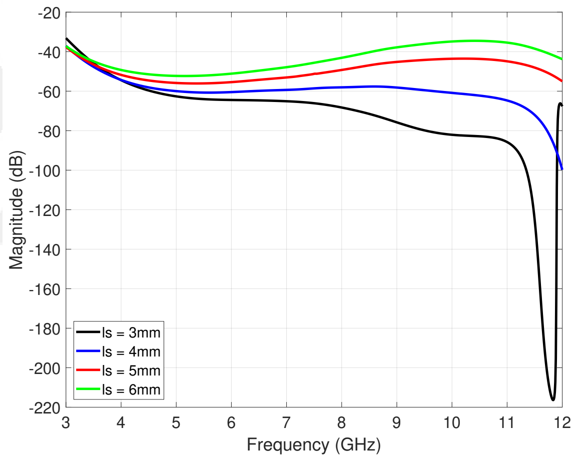

Figure 3.20: Effect of the change in the parameter *ls* on the phase difference.

In Fig. 3.21, effect of change in the parameter *ls* on the return loss is presented. Fig. 3.21 shows that *ls* also has some impact on the magnitude of the return loss. However, it may not be the most critical parameter in terms of return loss.

Fig. 3.22 depicts effect of change in the parameter *wst* on the phase difference. It is clear from the Fig. 3.22 that the parameter *wst* does not effect the phase difference much. However, it is seen that even a 1mm change in the parameter *wst* may cause some sudden shifts in the frequency.

Fig. 3.23 indicates effect of the change in the parameter *wst* on the return loss. It is seen from Fig. 3.23 that as *wst* changes from 2mm to 5mm, maximum of the magnitude return loss changes from 6dB to 14dB.

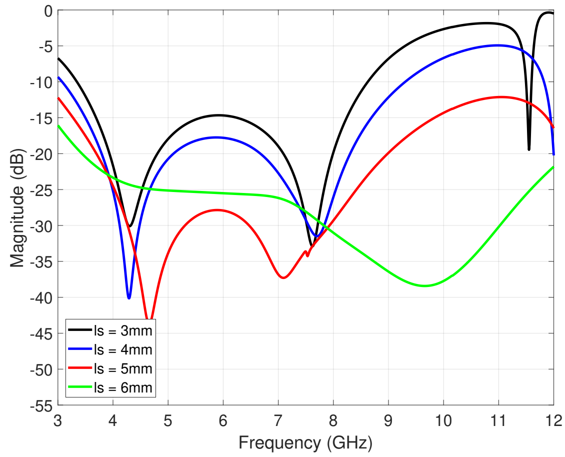

Figure 3.21: Effect of the change in the parameter *ls* on the return loss.

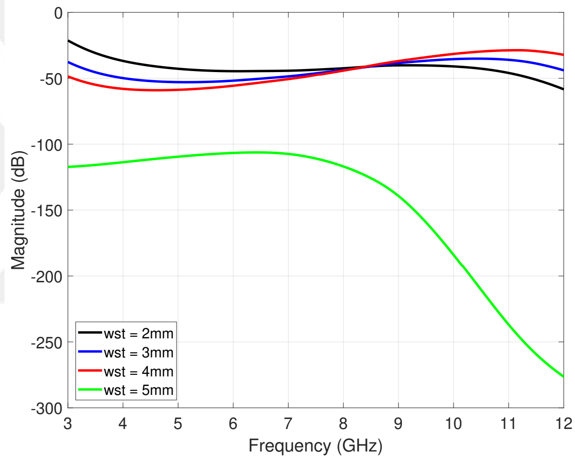

Figure 3.22: Effect of the change in the parameter *wst* on the phase difference.

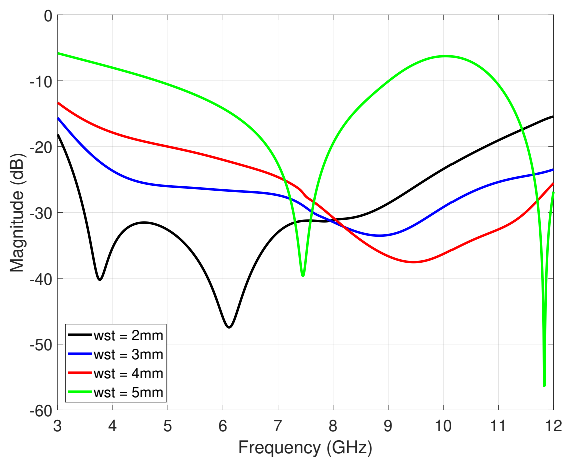

Figure 3.23: Effect of the change in the parameter *wst* on the return loss.

In Fig. 3.24, effect of the change in the parameter lst on the phase difference is indicated. Results in Fig. 3.24 shows that lst plays a very crucial roll in adjusting phase difference. As it changes from 2mm to 8mm, the phase difference changes from -40 to -240°.

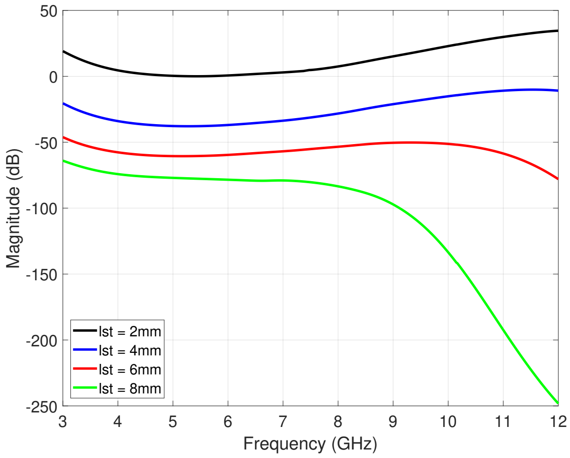

Figure 3.24: Effect of the change in the parameter lst on the phase difference.

Fig. 3.25 demonstrates effect of the change in the parameter lst on the return loss. When results shown in Fig. 3.25 examined, it is seen that as parameter lst changes from 2mm to 8mm, maximum magnitude of the return loss changes from -8 dB to -15dB.

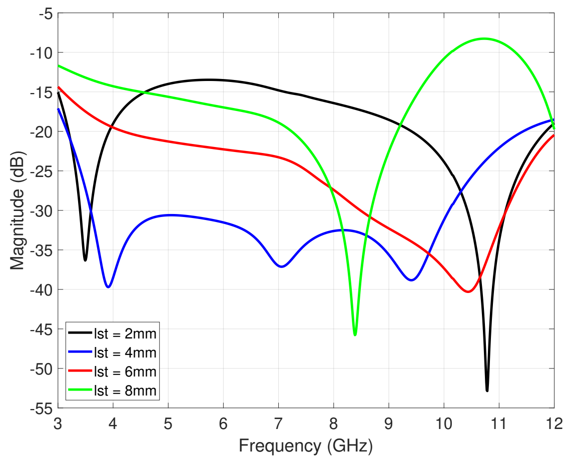

Figure 3.25: Effect of the change in the parameter lst on the return loss.

As it is seen from the results Fig. 3.14 to Fig. 3.25, effect of the parameters on the phase difference and the return loss are intertwined with each other. In order to find the parameters that will yield the best results, an optimization is needed to be performed. The optimal dimensions of the phase shifter are given in Table 3.2.

Table 3.2: The optimal dimensions of the designed phase shifter.

Parameter	Value (mm)
wst	2.98
lst	5.22
wp	4.02
lp	5.24
$w50$	1.22
$d1$	1.30
$d2$	1.90
$d3$	4.11
$d4$	9.85
ws	8.24
ls	5.85

Fig. 3.26 indicates return loss of the simulated phase shifter. It is seen from Fig. 3.26 that the return loss is below -15 dB within the whole frequency band. After 4 GHz, the return loss results seem to get better as they are below -20 dB within the frequency range 4GHz - 12GHz.

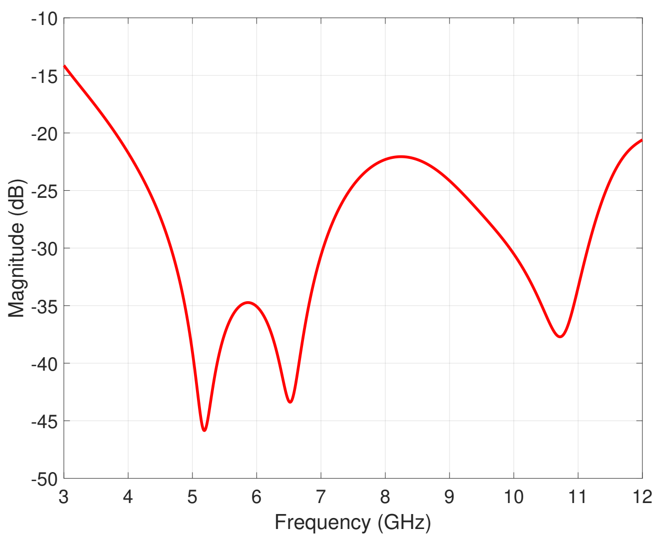

Figure 3.26: Return loss of the simulated phase shifter.

In Fig. 3.27, insertion loss of the simulated phase shifter is presented. Fig. 3.27 demonstrates that the insertion loss is less than 0.5 dB until 11 GHz whereas it increases up to 1.1 dB after the 11 GHz threshold through the end of the frequency band. Compared to the phase shifter design in the previous section, the new structure is a very low loss component.

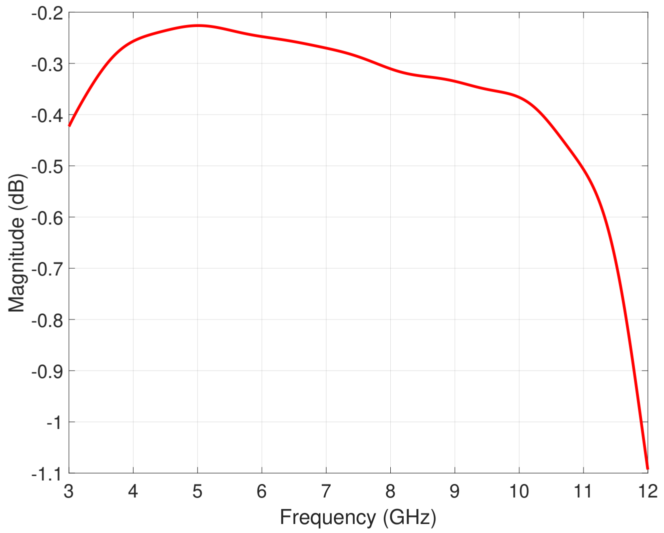

Figure 3.27: Insertion loss of the simulated phase shifter.

Fig. 3.28 show the phase difference of the simulated phase shifter. It is seen from Fig. 3.28 that -45° phase difference is achieved along the whole frequency band. The phase imbalance acquired with this new structure seems to have dropped to 8° which will lead to considerably lesser phase imbalance at the output ports of the Butler matrix compared to the previous structure.

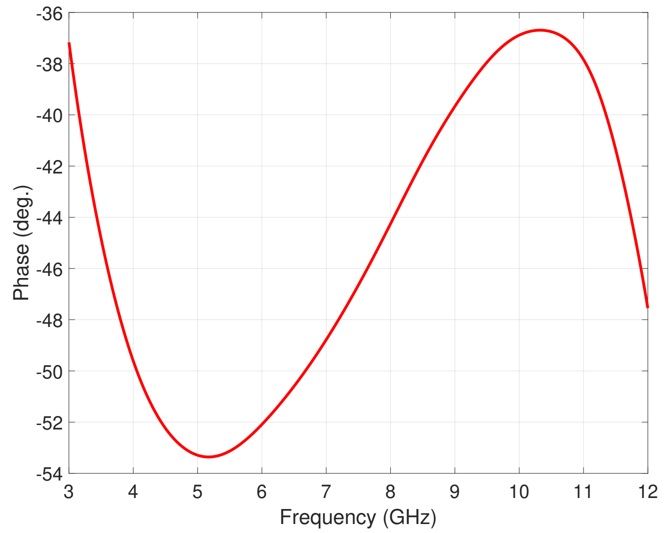

Figure 3.28: Phase difference of the simulated phase shifter.

3.2.3 Measurement Results of the Phase Shifter with the Rectangular Resonators

The geometry of the manufactured phase shifter is shown in Fig.3.29. Size of the manufactured design is 46.5mm x 33.5mm. The port numbers for the measurement results are marked on the manufactured geometry shown in Fig. 3.29. In order to measure the whole performance of the coupler, two-port pna network analyzer has been utilized.

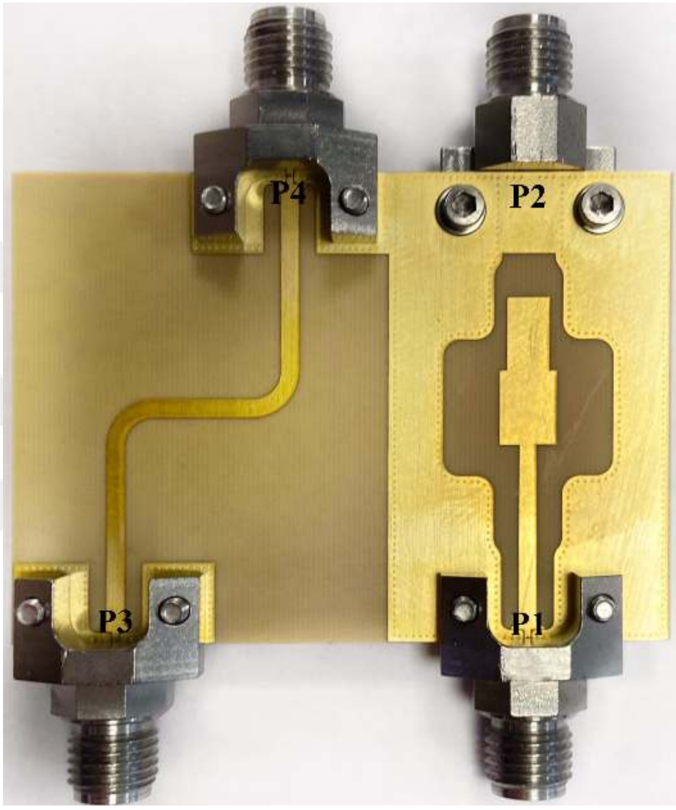

Figure 3.29: The geometry of the manufactured phase shifter.

Fig. 3.30 shows the simulated and measured return loss results of the phase shifter. It is seen from the Fig. 3.30 that although the general behavior of the simulated and measured results agree with each other, the measured return loss result seems to have shifted about 800 Mhz towards end of the frequency band. In addition to the shift in frequency, degradation in the magnitude of the return loss is also seen. Especially, after 8.5 GHz, return loss falls below -15dB threshold.

Fig. 3.31 indicates the simulated and measured insertion loss results of the phase shifter. It is seen from the 3.31 that the measured results are close to the simulated results. However, some unexpected fluctuations are seen around 7.5 GHz and 8.7 GHz. In addition to these fluctuations, the measured insertion loss results show 0.2 dB extra loss at the end and the beginning of the frequency band.

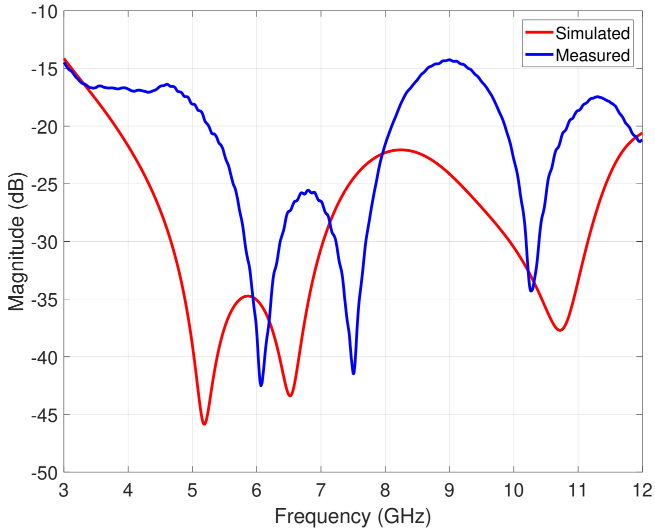

Figure 3.30: The simulated and measured return loss results of the phase shifter.

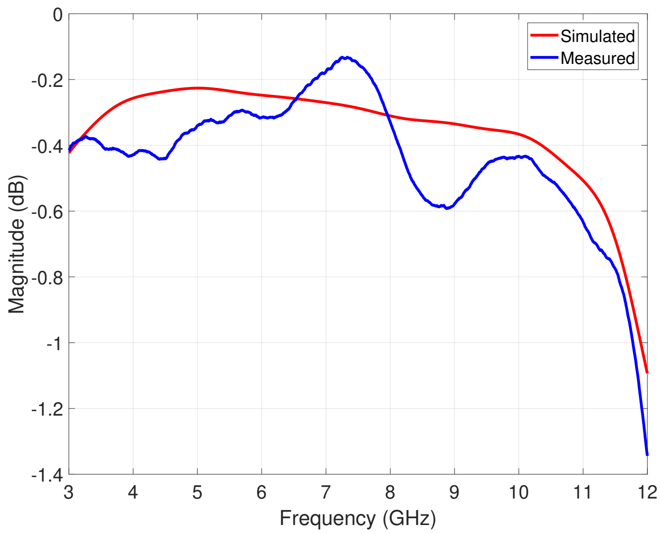

Figure 3.31: The simulated and measured insertion loss results of the phase shifter.

In Fig. 3.32, the simulated and measured phase difference acquired by the phase shifter is provided. The results in Fig. 3.32 shows that agreement between the simulated and measured phase differences lessens after 7 GHz and disagreement reaches to its maximum at 12 GHz. At the end of the frequency band 14° of phase difference is observed between the simulated and measured results. The disagreement between the simulated and measured s-parameter results in Fig. 3.30 and Fig. 3.31 seems to have effected the expected phase difference between the output ports of the structure.

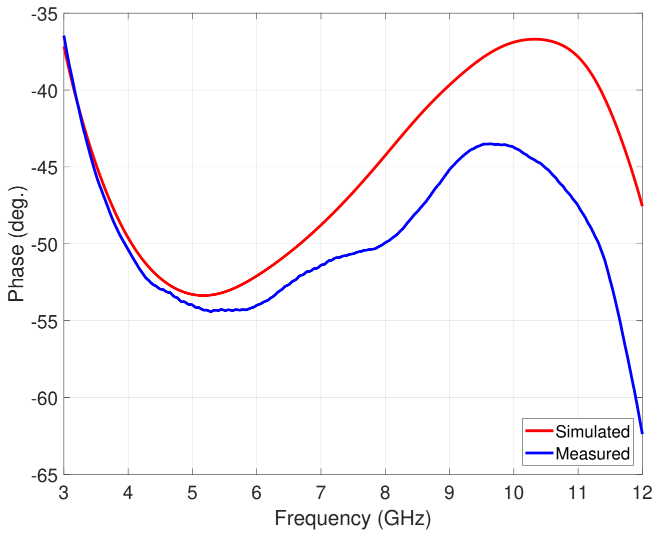

Figure 3.32: The simulated and measured phase difference acquired by the phase shifter.

Chapter 4

Butler Matrix

The Butler matrix is a type of passive beam-forming network. It can be used as a feed network for the phased array antennas. Depending on which input is excited, there exist a fixed phase difference between the output ports of the Butler matrix. Hence, when this network is integrated with an antenna array, the antenna beam is steered to the specific directions in one plane.

Typical Butler matrix consists of n input ports and n output ports. At a single frequency, it has a capability to form multiple beams if all of the input ports are excited separately. The number of beams that can be formed by a Butler matrix is equal to the number of input ports of the Butler matrix.

A Butler matrix consists of two main components. These are quadrature hybrid couplers and phase shifters. In order to achieve a wideband performance with a Butler matrix, the couplers and phase shifters that are used to create Butler matrix have to also have a wide band performance.

In this work, Butler matrix with 4 input ports and 4 output ports has been studied. Simple schematic representation of the 4×4 Butler matrix is given Fig. 4.1.

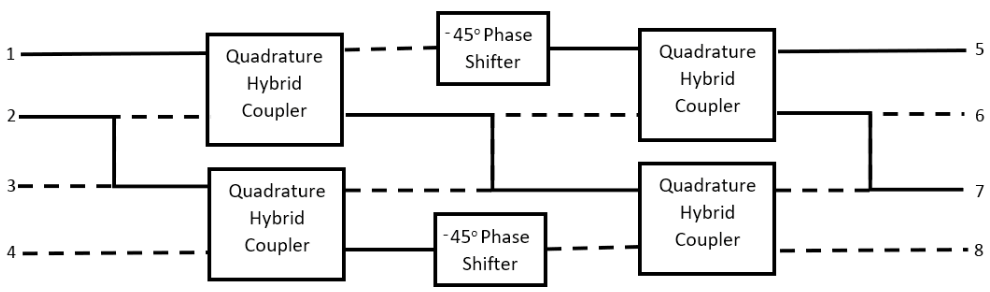

Figure 4.1: Schematic representation of the 4×4 Butler matrix.

4.1 4×4 Butler Matrix

In this section, 4×4 Butler matrix that has 4 input and 4 output port operating below Ku-band is presented. This Butler matrix is consisted of four quadrature hybrid couplers and two phase shifters. The quadrature hybrid couplers and phase shifters that are utilized to form the Butler matrix are the ones presented in the previous chapters. As an quadrature hybrid coupler, coupler with the butterfly shaped resonator as well as the butterfly shaped coupling aperture has been utilized. As an phase shifter, phase shifter with the rectangular resonator and rectangular coupling aperture is used. The electrical and physical properties of the PCB cards that are used in this multi-layer structure are $\varepsilon_r = 3$, tanδ=0.017 and PCB cards thickness = 0.508mm which is also same as manufactured quadrature hybrid couplers and phase shifters. The geometry of the simulated 4×4 Butler matrix is given in Fig. 4.2. Distance between input and output ports have been adjusted to be 15mm.

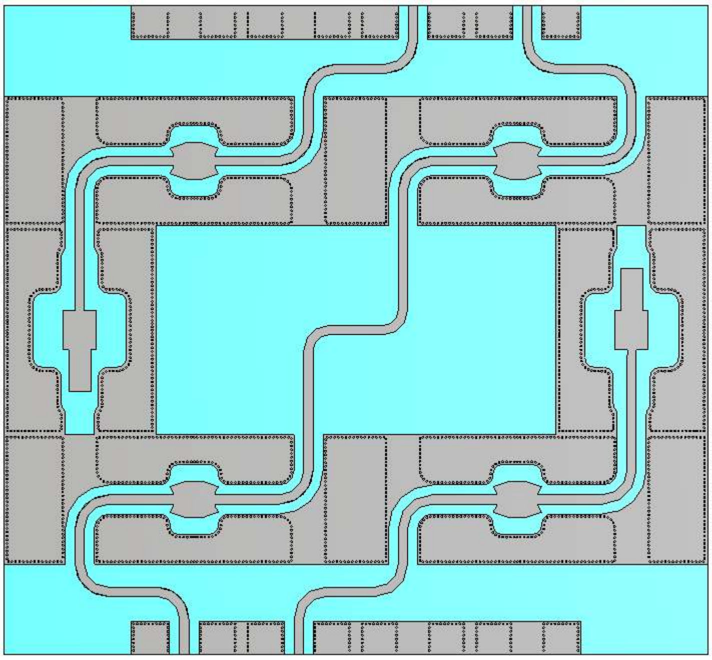

Figure 4.2: The geometry of the simulated 4×4 Butler matrix.

In Fig.4.3 - Fig.4.6, the e-field distribution of the 4×4 Butler matrix when all input ports are excited one by one is given. The amplitude and phase distribution at the output ports of the Butler matrix can be observed from the figures. It is also seen from the figures that close to -20dB isolation is seen between the input ports.

Fig. 4.7 shows the simulated return loss results of the 4×4 Butler matrix. It is seen from Fig. 4.7 that, magnitude of all the return losses are below 15 dB within the frequency range of 3GHz-12GHz. It is also observed from the Fig. 4.7 that S11 and S44 are equal to each other while S22 and S33 are equal to other.

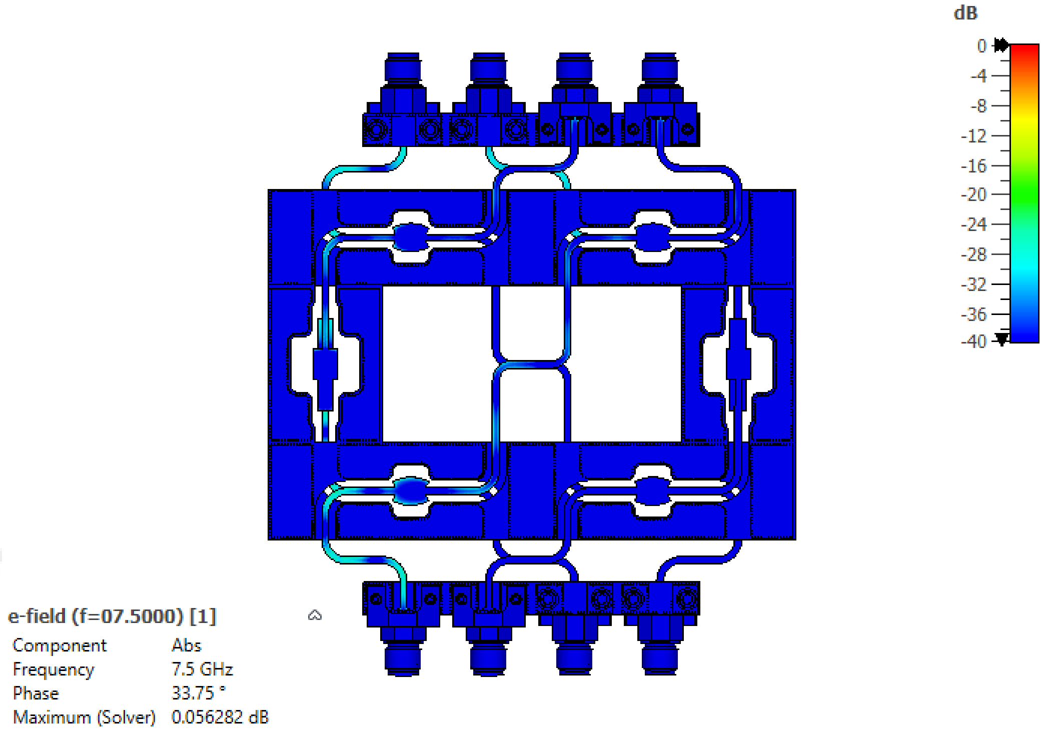

Figure 4.3: The e-field distribution of the 4×4 Butler matrix when port-1 is excited.

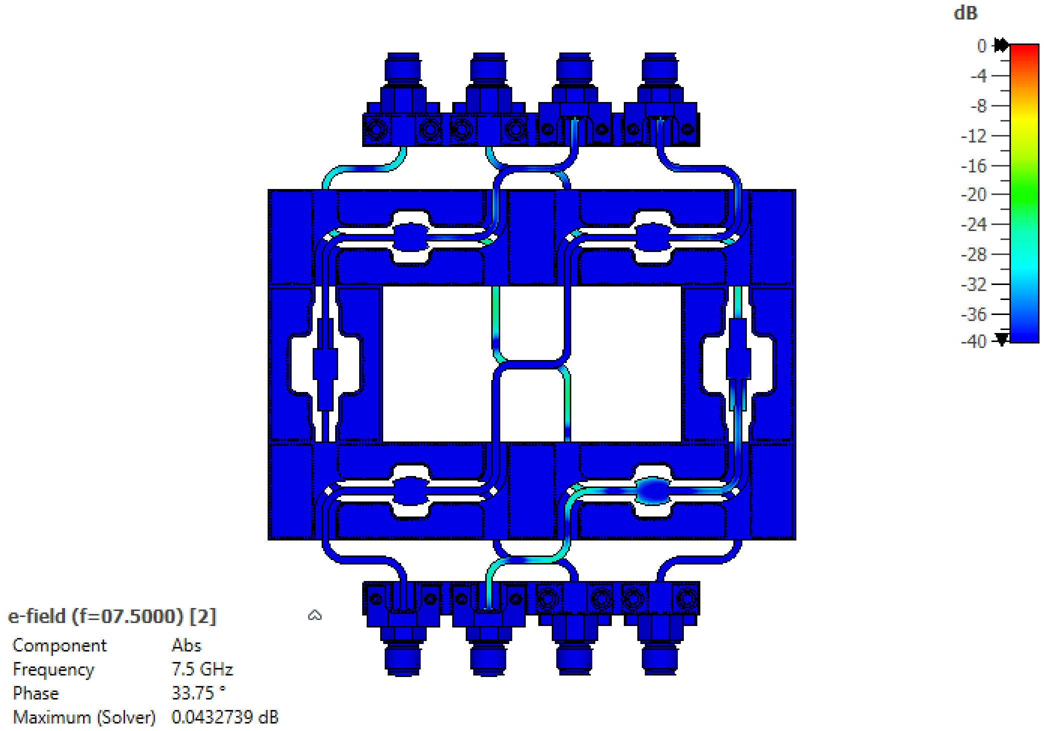

Figure 4.4: The e-field distribution of the 4×4 Butler matrix when port-2 is excited.

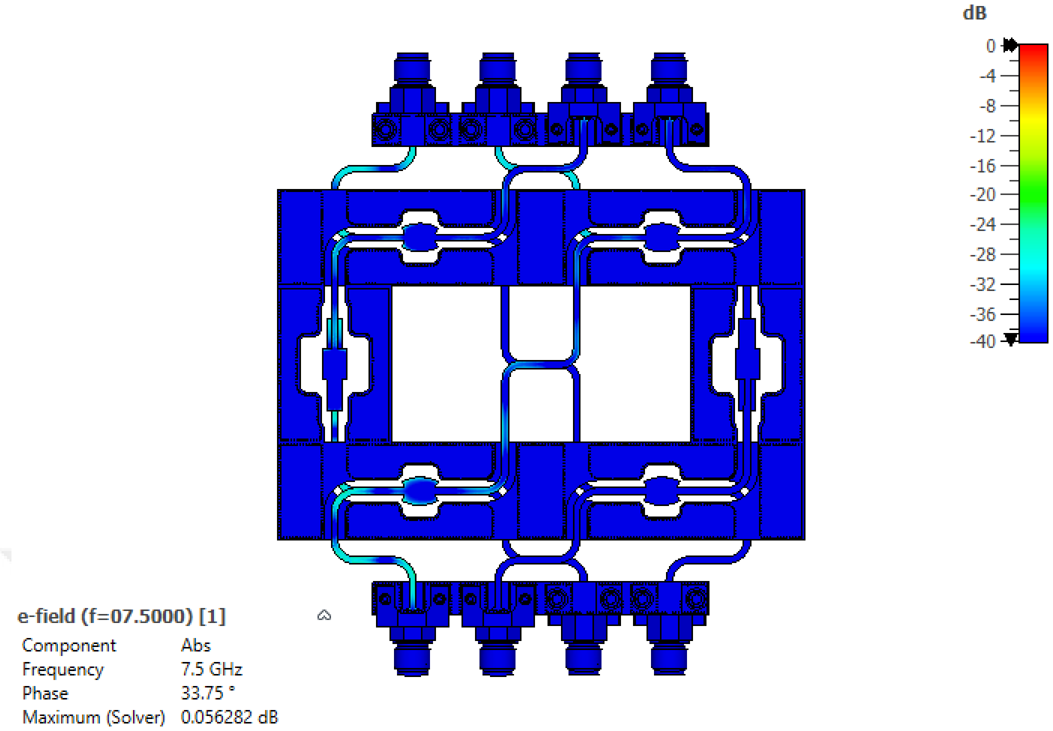

Figure 4.5: The e-field distribution of the 4×4 Butler matrix when port-3 is excited.

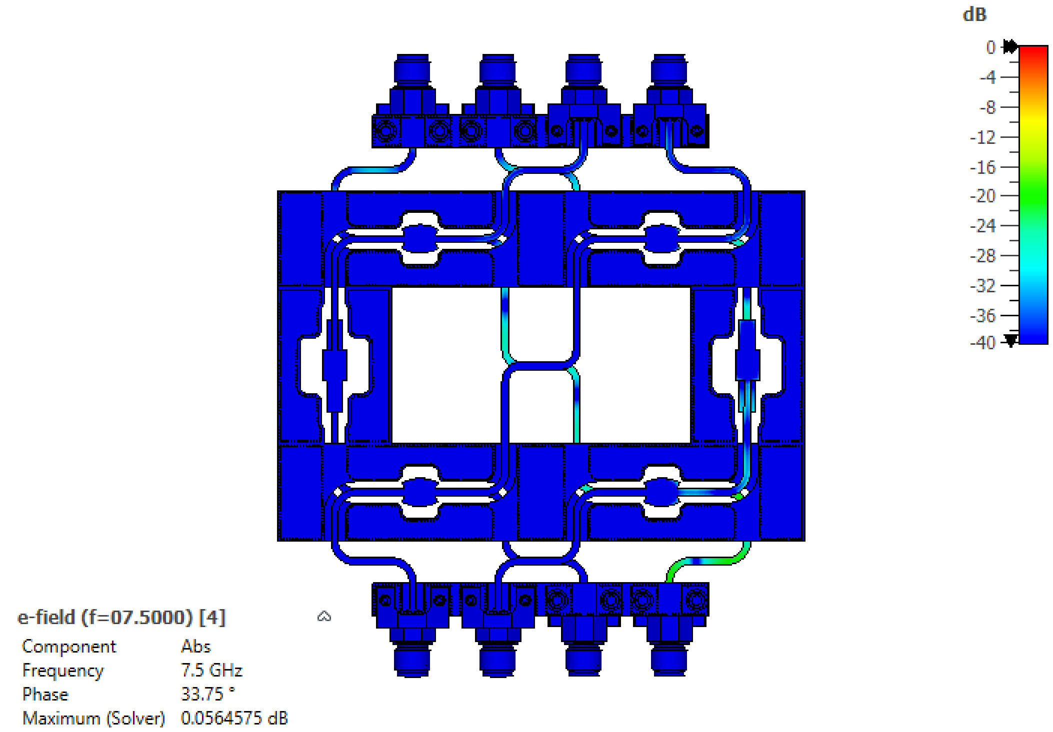

Figure 4.6: The e-field distribution of the 4×4 Butler matrix when port-4 is excited.

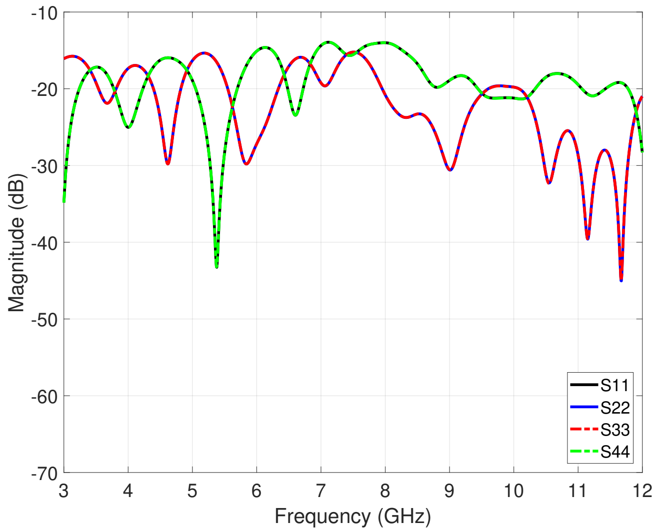

Figure 4.7: The simulated return loss results of the 4×4 Butler matrix.

In Fig. 4.8, the simulated insertion loss results of the 4×4 Butler matrix when port-1 is excited are presented. Fig. 4.8 shows that equal power division is achieved when port-1 of the Butler matrix is excited. Amplitude imbalance between the output ports increases at the beginning and end of the frequency band. Maximum amplitude imbalance between the output ports is 3.5 dB.

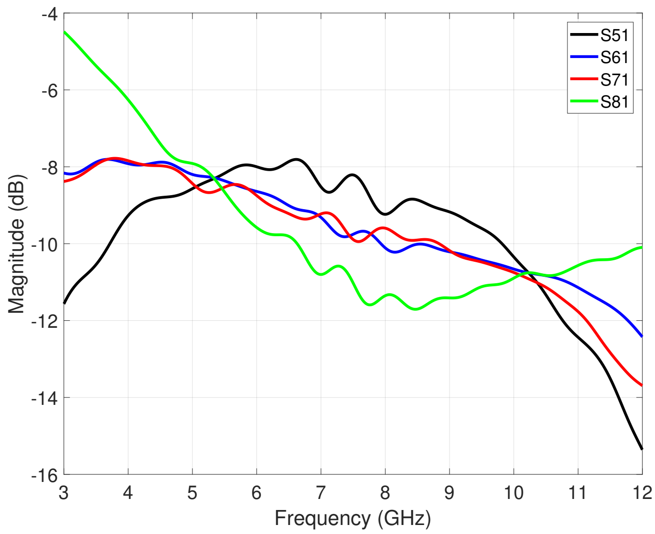

Figure 4.8: The simulated insertion loss results of the 4×4 Butler matrix when port-1 is excited.

Fig. 4.9 depicts the simulated insertion loss results of the 4×4 Butler matrix when port-2 is excited . It is seen from Fig. 4.9 that equal power division is achieved when port-2 of the Butler matrix is excited. Amplitude imbalance between the output ports again reaches its max value at the beginning of the frequency band. Maximum amplitude imbalance between the output ports is 3.2 dB.

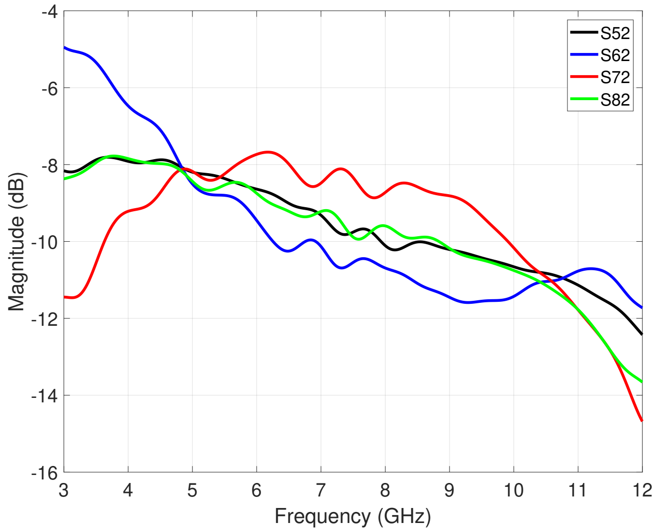

Figure 4.9: The simulated insertion loss results of the 4×4 Butler matrix when port-2 is excited.

Fig. 4.10 shows the simulated insertion loss results of the 4×4 Butler matrix when port-3 is excited. Fig. 4.10 shows that equal power division is acquired when port-3 of the Butler matrix is excited. Amplitude imbalance behavior of the Butler matrix when port-3 is excited is similar to the previous scenarios. Maximum amplitude imbalance between the output ports is 3.2 dB.

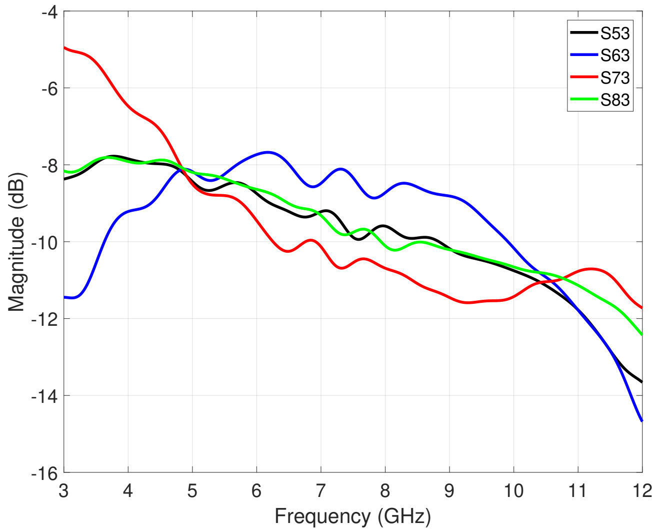

Figure 4.10: The simulated insertion loss results of the 4×4 Butler matrix when port-3 is excited.

In Fig. 4.11, the simulated insertion loss results of the 4×4 Butler matrix when port-4 is excited are provided. Fig. 4.11 shows that equal power division is also preserved when port-4 of the Butler matrix is excited. Amplitude imbalance behavior is similar to the amplitude imbalance when other ports are excited. Maximum amplitude imbalance between the output ports is 3.5 dB which is same as the scenario when port-1 is excited.

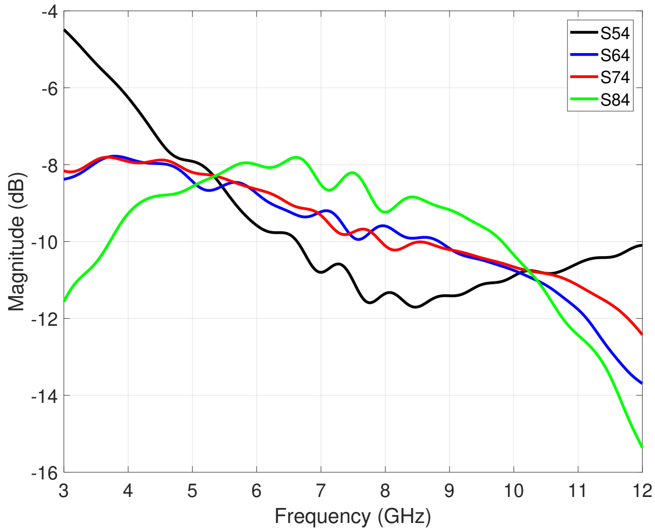

Figure 4.11: The simulated insertion loss results of the 4×4 Butler matrix when port-4 is excited.

Fig. 4.12 shows the simulated phase difference results of the 4×4 Butler matrix when port-1 is excited. Fig. 4.12 shows that an average of 45° consecutive phase difference between output port is acquired. However, results indicate that at the end of the frequency band phase imbalance increases up to 36°.

Fig. 4.13 shows the simulated phase difference results of the 4×4 Butler matrix when port-2 is excited. Fig. 4.13 shows that an average of 135° consecutive phase difference between output port is acquired. However, at the end of the frequency band, same phase difference degradation seen when port-1 is excited also had been experienced. When port-2 is excited, maximum phase imbalance is about 37.7°.

In Fig. 4.14, the simulated phase difference results of the 4×4 Butler matrix when port-3 is excited are shown. It is seen from Fig. 4.14 that aside from the negative phase difference of 135°, the phase difference behavior seen in Fig. 4.14 and Fig. 4.13 are very similar to each other as it was the case for insertion losses. The maximum phase imbalance acquired when port-3 is excited is about 37.7°.

Fig. 4.15 shows the simulated phase difference results of the 4×4 Butler matrix when port-4 is excited. Fig. 4.15 shows that an average of negative 45° consecutive phase difference between the output ports is acquired. Results of the 4.15 is also similar with 4.12 and the max phase imbalance is about 36° at the end of the frequency band.

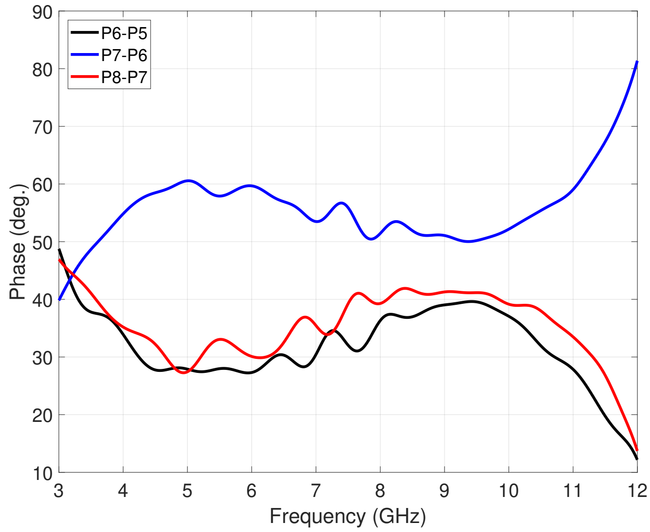

Figure 4.12: The simulated phase difference results of the 4×4 Butler matrix when port-1 is excited.

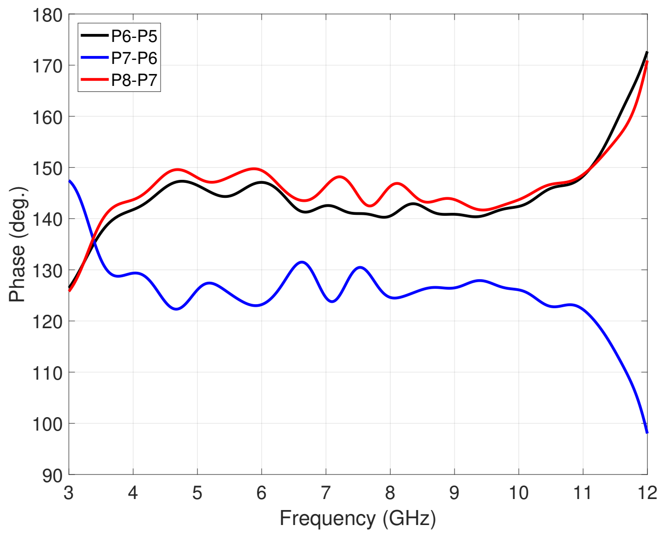

Figure 4.13: The simulated phase difference results of the 4×4 Butler matrix when port-2 is excited.

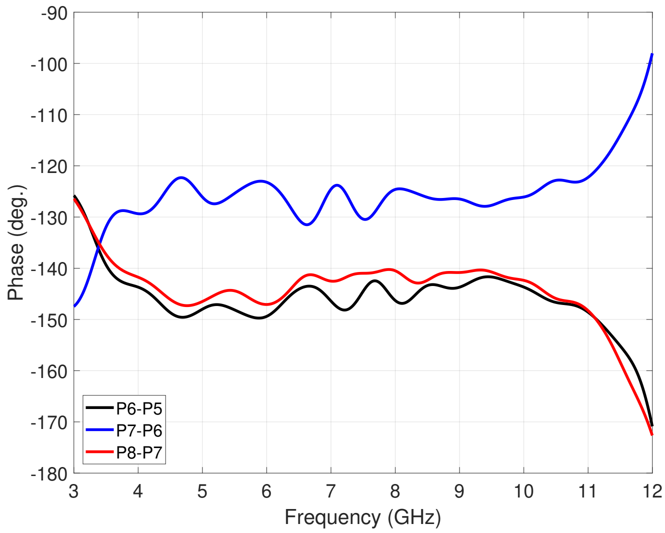

Figure 4.14: The simulated phase difference results of the 4×4 Butler matrix when port-3 is excited.

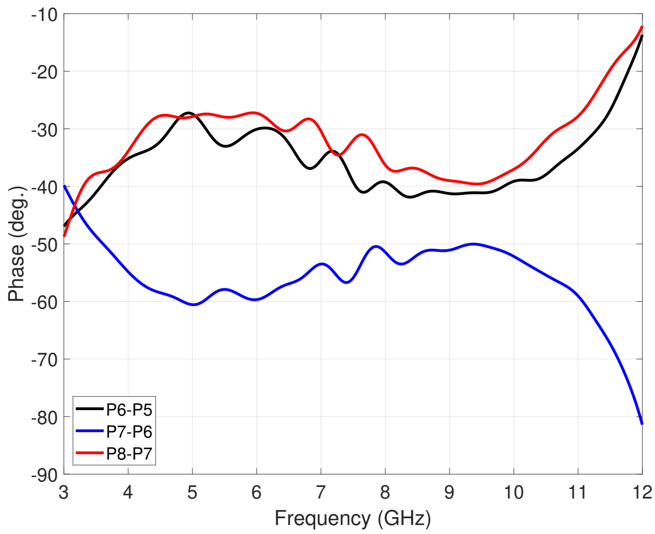

Figure 4.15: The simulated phase difference results of the 4×4 Butler matrix when port-4 is excited.

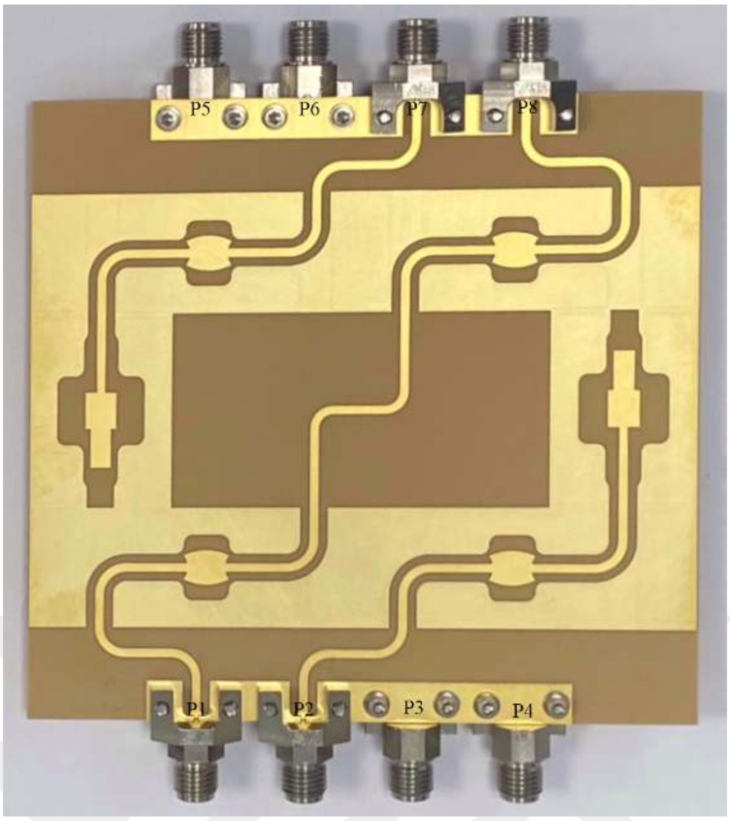

Figure 4.16: The manufactured 4×4 Butler matrix.

4.2 Measurement Results of the 4×4 Butler Matrix

In order to verify the simulated results, the 4×4 Butler matrix mentioned in the previous section has been manufactured. Size of the manufactured 4×4 Butler matrix is 92.4 mm x 82.9 mm. The port numbers for the measurement results are marked on the manufactured geometry shown in Fig. 4.16. In order to measure the whole performance of the coupler, two-port pna network analyzer was utilized. The connectors that are not used during the 2-port measurements were terminated with the 50 ohm terminations. The phase difference between the output ports of the 4×4 Butler matrix were calculated after multiple measurements. In these measurement, one of the inputs ports of the 4×4 Butler matrix was connected to the Port-1 of the PNA network analyzer while one of the output ports of the 4×4 Butler matrix was connected to the Port-2 of the pna network analyzer. For each input port, all of the output ports of the Butler matrix were measured one by one to calculate consecutive phase difference between the output ports. During the measurements, in order measure the phase behavior of the Butler matrix as accurately as possible, phase stable cables were used between the ports of the pna network analyzer and the ports of the Butler matrix.

In Fig. 4.17 the simulated and measured return loss results of the 4×4 Butler matrix are presented. It is seen from the 4.17 that measured return loss results agree well with the simulated results aside from the beginning and the end of the frequency band. Fig. 4.17 shows that the magnitude of the return loss is above 10dB within the whole the operating frequency band.

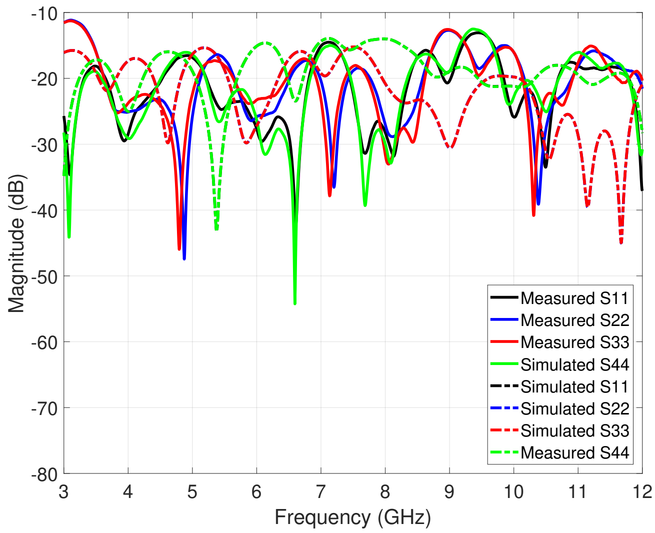

Figure 4.17: The simulated and measured return loss results of the 4×4 Butler matrix.

Fig. 4.18 indicates that the simulated and measured insertion loss of the 4×4 Butler matrix when port-1 is excited. The results presented in 4.18 shows that the measured phase differences are in good correlation with the simulated results. However, a slight disagreement which is about 2dB, is observed at the end of the frequency band.

Fig. 4.19 depicts the simulated and measured insertion loss of the 4×4 Butler matrix when port-2 is excited. The results presented in 4.19 shows that the measured phase difference correlates well with the simulated results. Similar to the results in 4.18, the degradation between the simulated and measured results at the end of the frequency is also seen in 4.19.

In Fig. 4.20, the simulated and measured insertion loss of the 4×4 Butler matrix when port-3 is excited are demonstrated. It is seen from the results in 4.20 that insertion losses of the Butler matrix when port-3 is excited are very similar to the insertion losses of the Butler matrix when port-2 is excited. These results were also expected from simulation results. Hence, same degradation between simulated and measured results are also seen in Fig. 4.20 at the end of the frequency band. This degradation is about 1.8 dB.

Fig. 4.21 indicates the simulated and measured insertion loss of the 4×4 Butler matrix when port-4 is excited. As it is expected from the simulated results, the measured insertion losses of the 4×4 Butler matrix when port-4 is excited are very similar with the measured

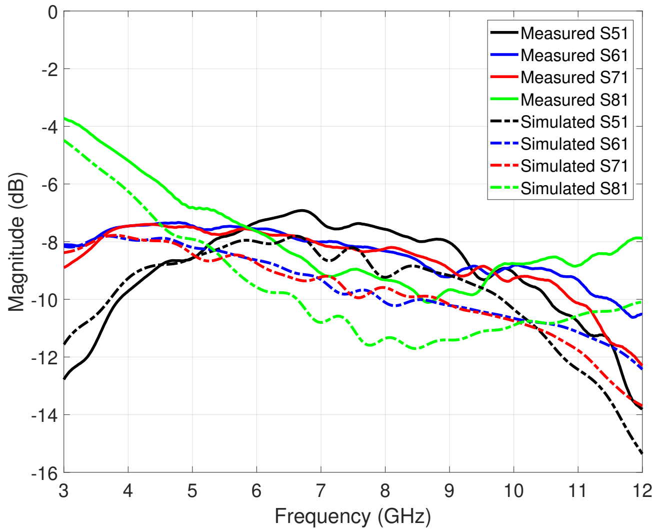

Figure 4.18: The simulated and measured insertion loss results of the 4×4 Butler matrix when port-1 is excited.

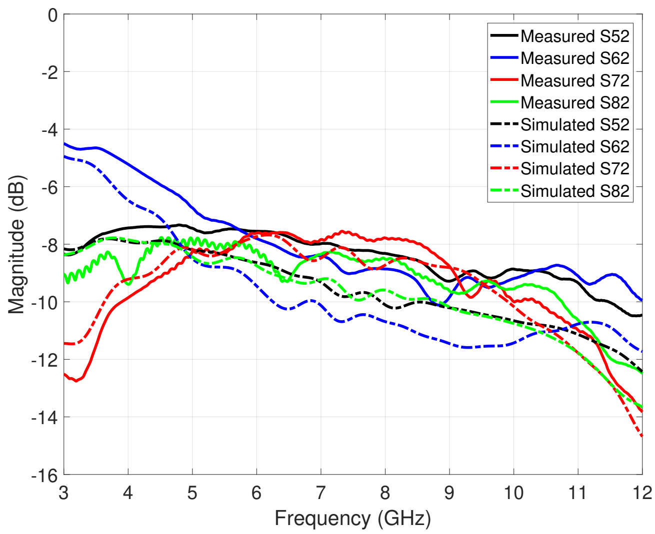

Figure 4.19: The simulated and measured insertion loss results of the 4×4 Butler matrix when port-2 is excited.

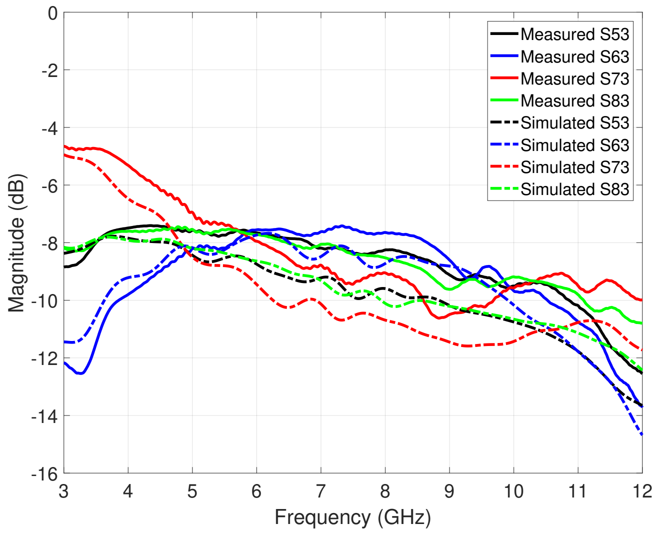

Figure 4.20: The simulated and measured insertion loss results of the 4×4 Butler matrix when port-3 is excited.

insertion losses of the 4×4 Butler matrix when port-1 is excited. Therefore, same 2 dB amplitude deviation seen in Fig. 4.18 is also observed in Fig. 4.21 between the simulated and measured results.

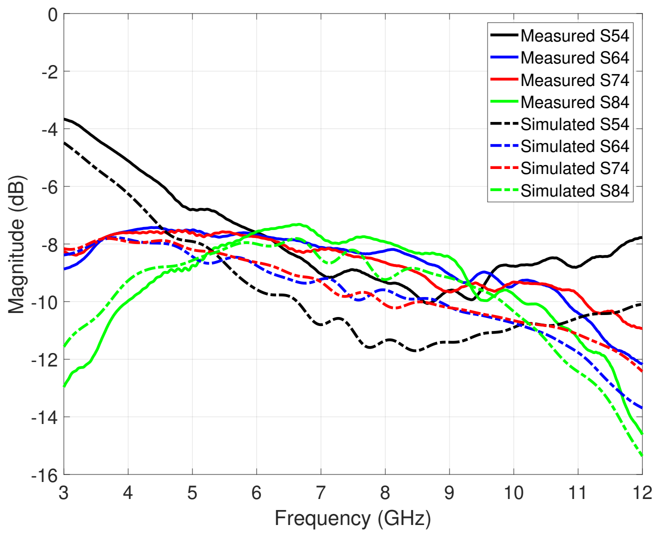

Figure 4.21: The simulated and measured insertion loss results of the 4×4 Butler matrix when port-4 is excited.

In Fig. 4.22, the simulated and measured phase difference results of the 4×4 Butler matrix when port-1 is excited, are provided. It is seen from Fig. 4.22 that the average consecutive phase difference between the output ports is about 45° along the whole band as expected. Moreover, the measured and the simulated results are in good agreement with each other. The maximum deviation between the simulated and measured results are observed after 11.5 GHz which increases up to approximately 10°.

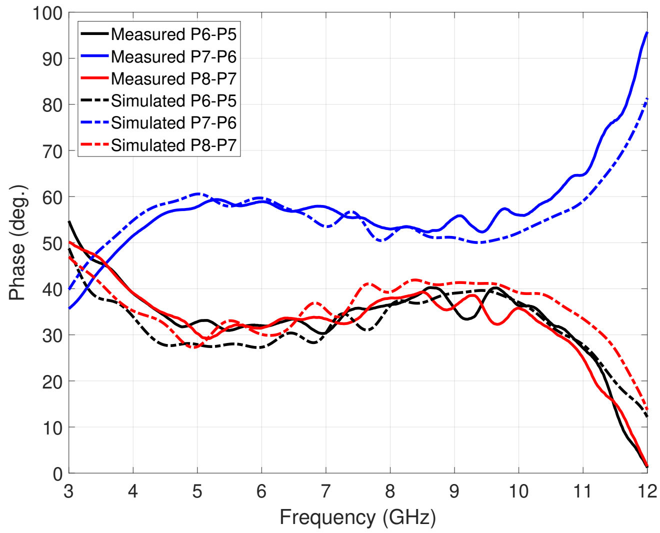

Figure 4.22: The simulated and measured phase difference results of the 4×4 Butler matrix when port-1 is excited.

Fig. 4.23 depicts the simulated and measured phase difference results of the 4×4 Butler matrix when port-2 is excited. The phase difference results presented in Fig. 4.23 demonstrates good correlation between the measured and the simulated results while an average of 135° consecutive phase difference between the output ports has been acquired. However, at the end of the frequency band, 8° of phase difference is observed between the simulated and measured results.

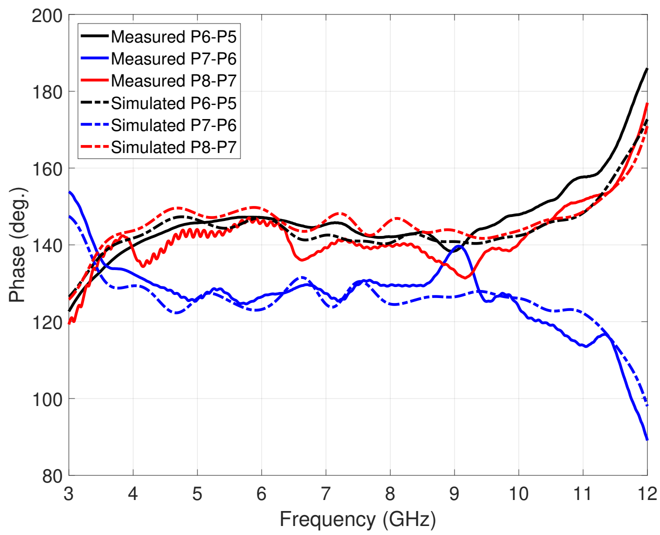

Figure 4.23: The simulated and measured phase difference results of the 4×4 Butler matrix when port-2 is excited.

In Fig. 4.24 the simulated and measured phase difference results of the 4×4 Butler matrix when port-3 is excited, are depicted. -135° of consecutive phase difference is seen in Fig. 4.24. When manufacturing results are examined, the deviation from the simulated results are also most visible at the end of the frequency band. This deviation is about 8° .

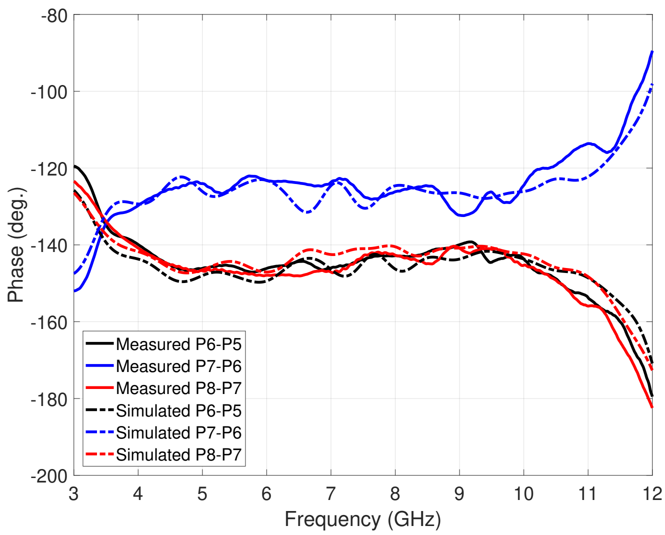

Figure 4.24: The simulated and measured phase difference results of the 4×4 Butler matrix when port-3 is excited.

Fig. 4.25 indicates the simulated and measured phase difference results of the 4×4 Butler matrix when port-4 is excited. The results in Fig. 4.25 are very similar to the ones in Fig. 4.22 except the phase values have negative sign. An average of -45° consecutive phase difference between the output ports has been acquired. At the end of the frequency band, 10° of phase deviation between the simulated and measured results are observed.

The results presented in Fig. 4.17 to Fig. 4.25 all shows that the manufactured results are in good correlation with the simulated results. However, in all of them, at the end of the frequency band, the deviation between the simulated and measured results are observed. The reason for these unwanted degradation is believed to be due to the performances of the rf connectors. As the frequency of operation increases, the rf connectors tends have worse return loss and insertion loss values. This loss of performance in rf connectors, effects the performance of the component that these connectors are used.

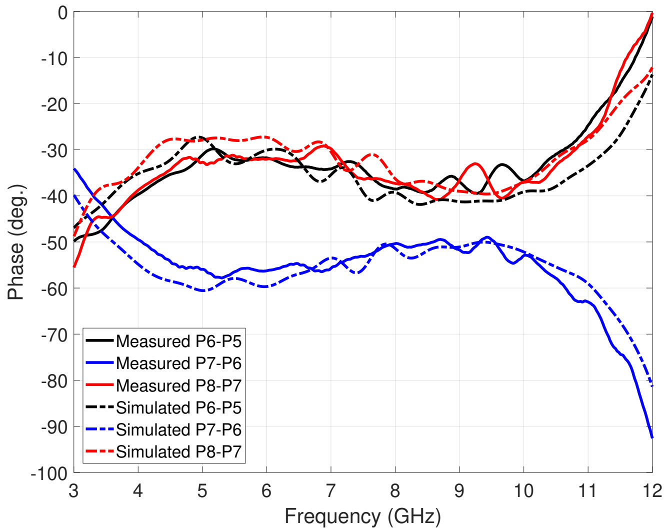

Figure 4.25: The simulated and measured phase difference results of the 4×4 Butler matrix when port-4 is excited.

4.3 4×4 Butler Matrix Combined with the 4×1 Antenna Array

The 4×4 Butler matrix has capability to excite an antenna array with 4 ports. Therefore, in order to observe how the designed Butler matrix operates when combined with an antenna array, a 4×1 antenna array has been designed to be used with the Butler matrix. The antenna element type of the antenna array has been chosen to be the patch antenna. Patch antennas are microstrip based antennas that can radiate the electromagnetic wave directionally either in a linearly polarized manner or circularly polarized manner. In this study, a simple linearly polarized pin-fed patch antenna with a rectangular resonator is designed at 10 GHz. This patch antenna is designed on a substrate material with $\varepsilon_r = 3.55$, $\tan\delta$=0.0027 and the thickness of 0.803mm. In Fig. 4.26 the geometry of the designed patch antenna element is provided.

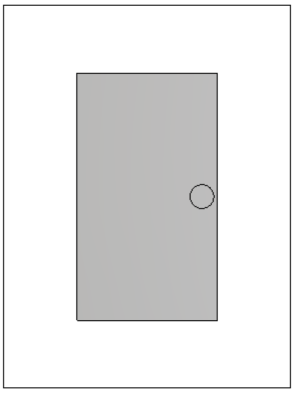

Figure 4.26: The geometry of the designed patch antenna element.

The dimensions of the resonator of the designed antenna are 7.32mm x 12.94mm. The feed offset given to the patch antenna is 2.86mm while the total substrate dimensions are 15mm x 20mm. In Fig. 4.27, the return loss of the designed patch antenna is provided. It is seen from Fig. 4.27 that designed patch antenna operates at 10 GHz.

The 4×1 antenna array is formed by bringing together 4 identical antenna elements such that distance between the antenna elements are same as the distance between the output ports of the Butler matrix. Therefore the distance between the antenna elements are chosen to be 15mm. As the unit antenna element, patch antenna shown in Fig. 4.26 is used. Since the last two ports of the Butler matrix resides in the other face of the Butler matrix card, 1.37mm vertical offset is given to the last two elements of the 4×1 antenna array. In Fig. 4.28, the

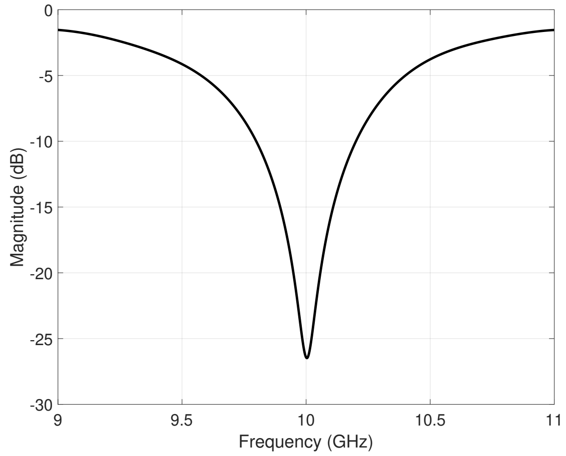

Figure 4.27: Return loss of the designed antenna element.

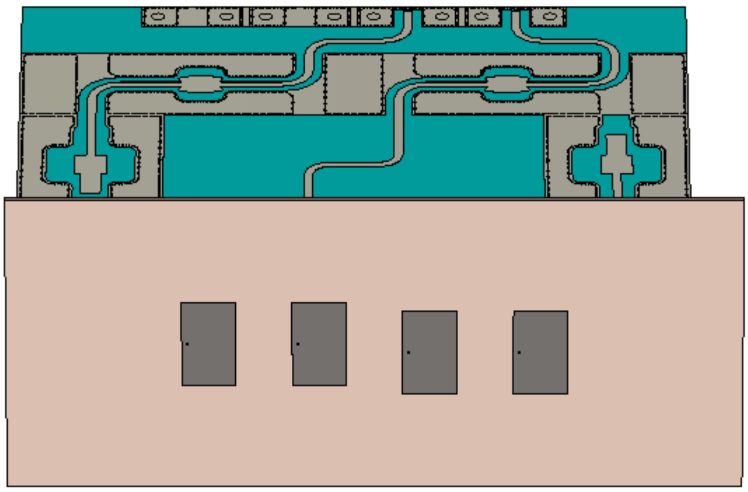

Figure 4.28: The geometry of the 4×4 Butler matrix combined with 4×1 antenna array.

geometry of the 4×4 Butler matrix combined with 4×1 antenna array is provided. Size of the 4×1 antenna array is 45mmx100mm.

In Fig. 4.29 to Fig. 4.32, the e-field distribution of the 4×4 Butler matrix when all input ports are excited one by one are presented. It is seen from the e-field distributions that none of the array antennas are illuminated at the same time due to the phase difference between the output ports of the 4×4 Butler matrix.

Fig. 4.33 to Fig. 4.36 to indicates the 3D antenna pattern of the 4×1 antenna array when all port are excited one by one. In order to have a better look at the antenna patterns, the antenna patterns at azimuth plane are needed to be examined.

Fig. 4.37 demonstrates the antenna patterns of the 4×1 antenna array at azimuth plane

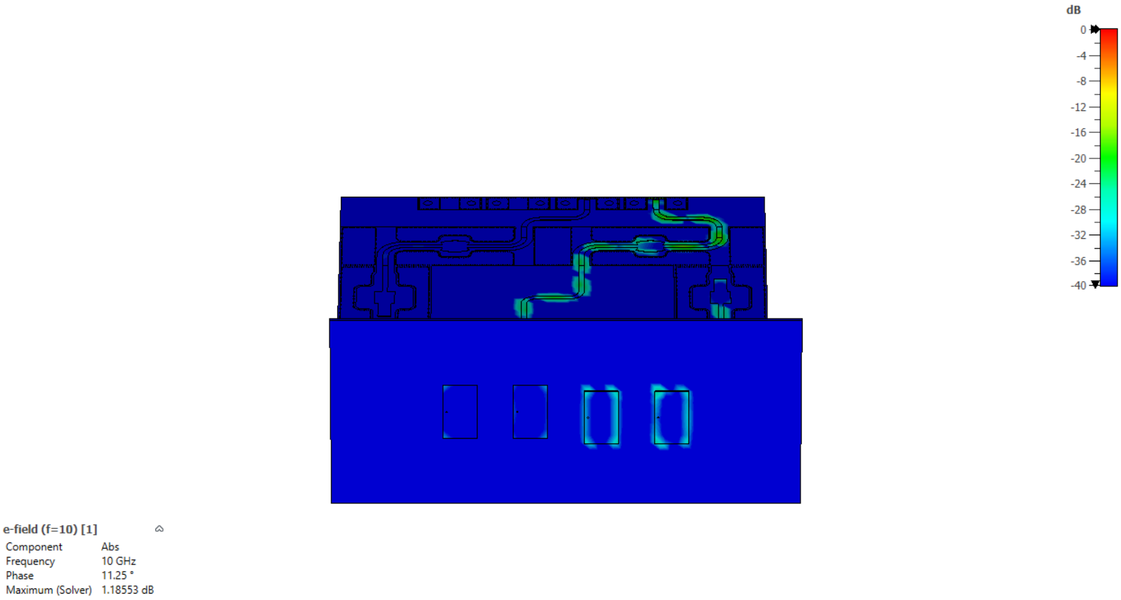

Figure 4.29: The e-field distribution of the 4×4 Butler matrix when port-1 is excited.

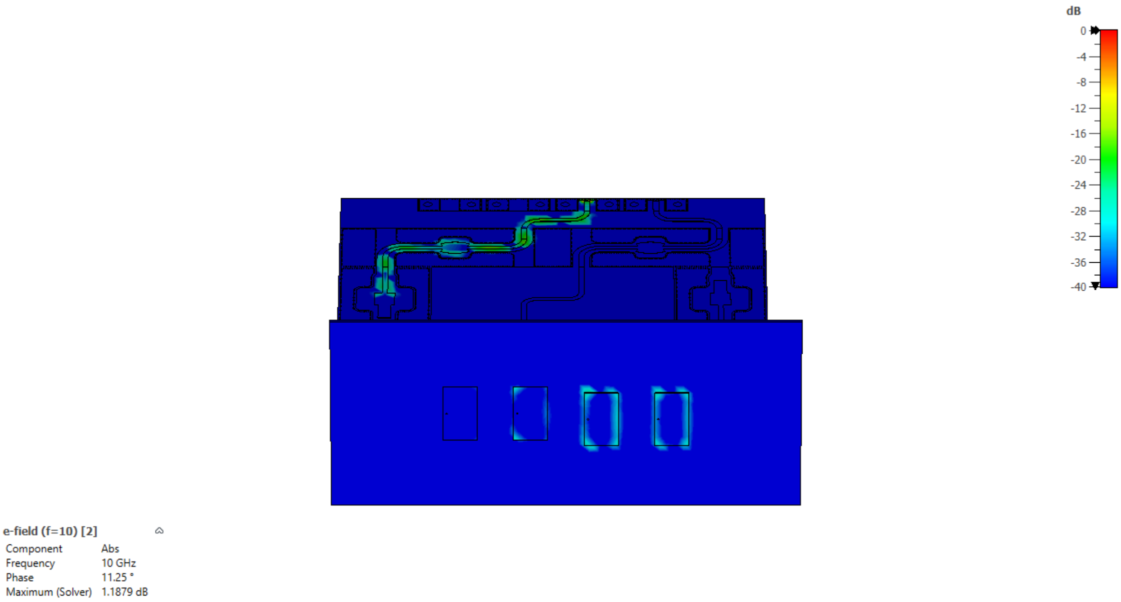

Figure 4.30: The e-field distribution of the 4×4 Butler matrix when port-2 is excited.

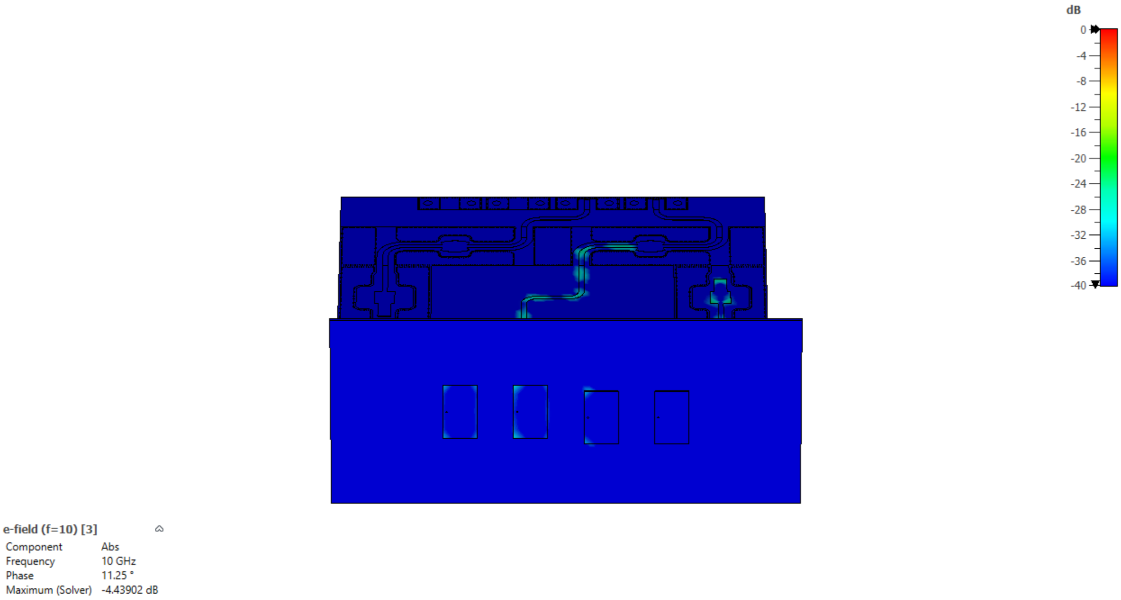

Figure 4.31: The e-field distribution of the 4×4 Butler matrix when port-3 is excited.

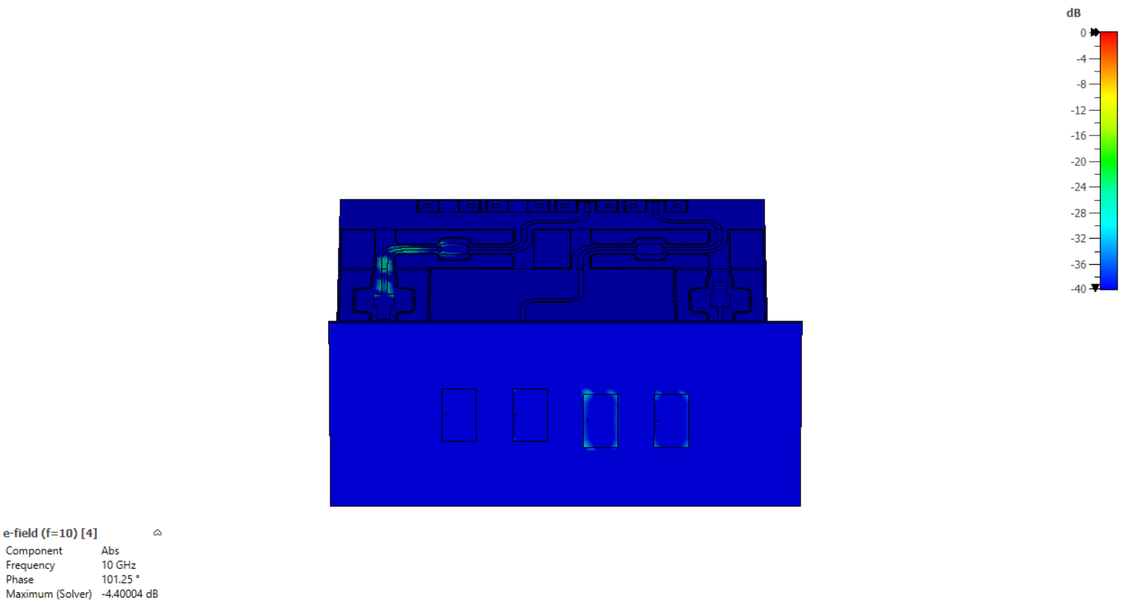

Figure 4.32: The e-field distribution of the 4×4 Butler matrix when port-4 is excited.

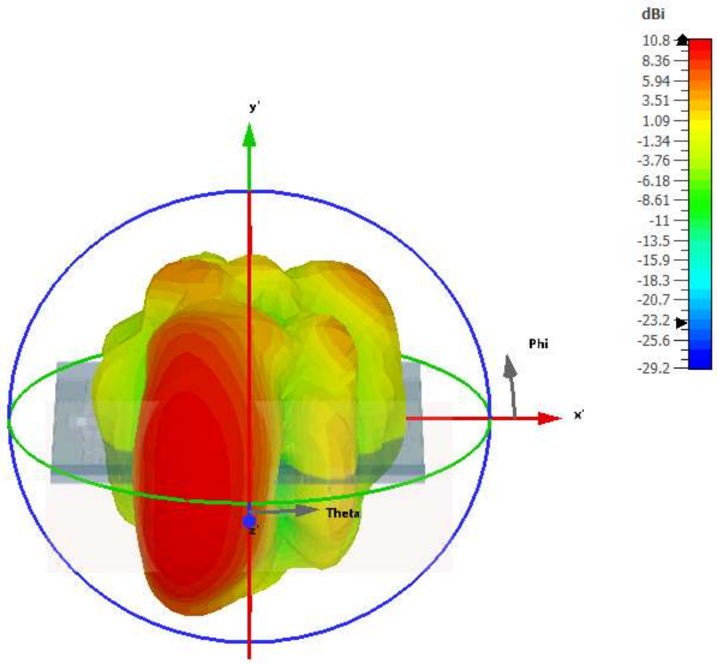

Figure 4.33: The 3D antenna pattern of the 4×1 antenna array when port-1 is excited.

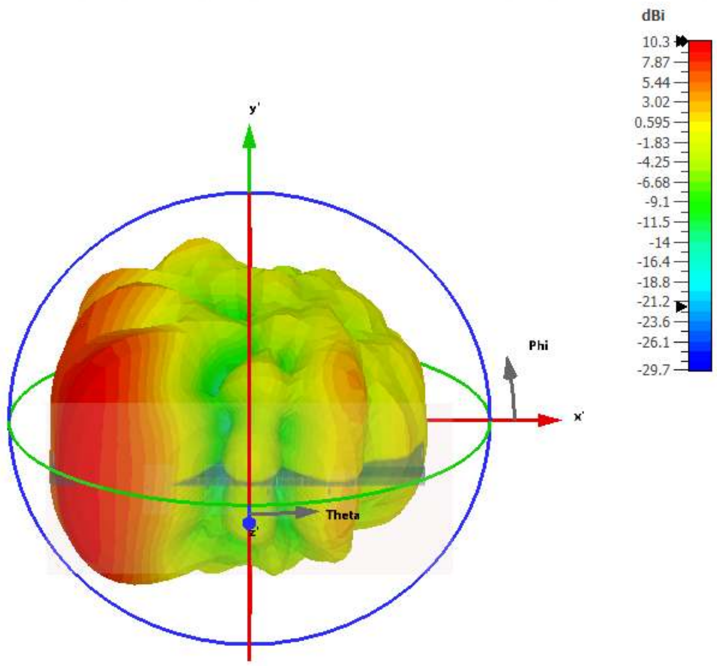

Figure 4.34: The 3D antenna pattern of the 4×1 antenna array when port-2 is excited.

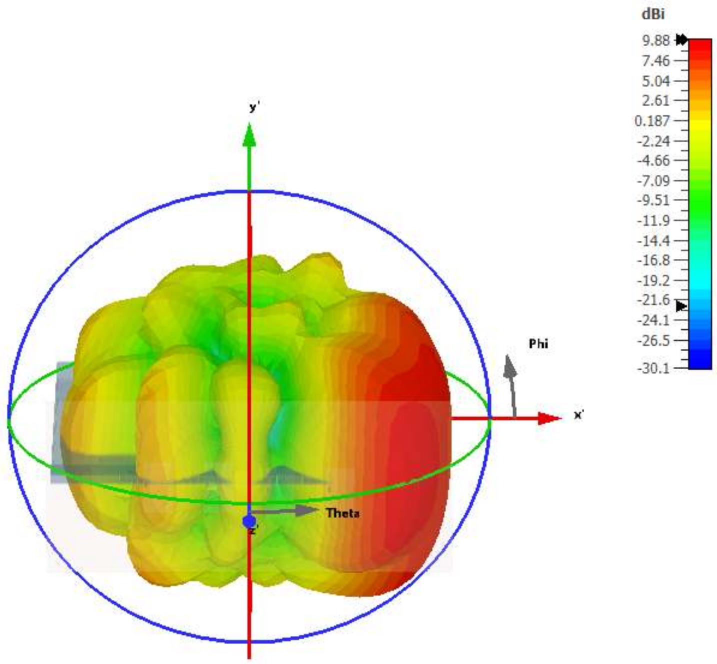

Figure 4.35: The 3D antenna pattern of the 4×1 antenna array when port-3 is excited.

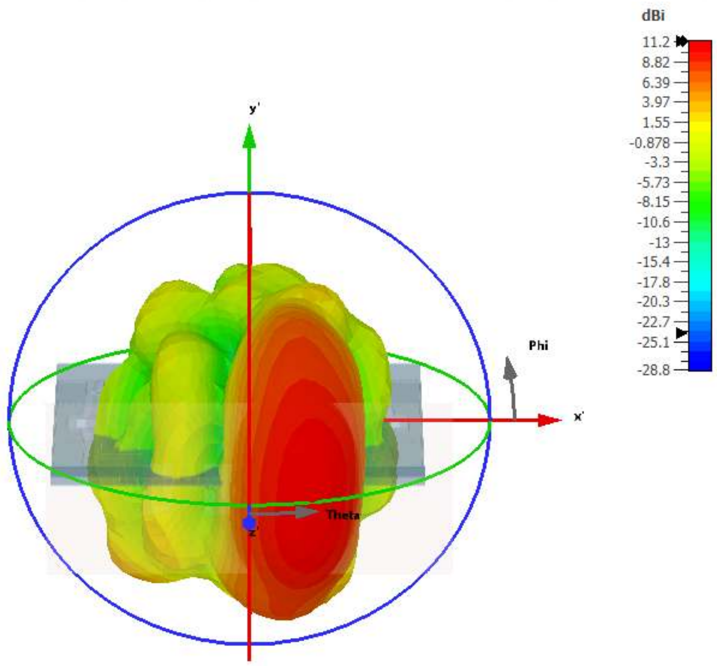

Figure 4.36: The 3D antenna pattern of the 4×1 antenna array when port-4 is excited.

when all ports are excited one by one. It is seen from the Fig. 4.37 that 4 different antenna beams directed at 4 different directions have been acquired. When port-1 and port-4 is excited, the beams are directed to approximately +/- 45° while when port-2 and port-3 are excited the beam directions are found to be approximately +/- 14°.

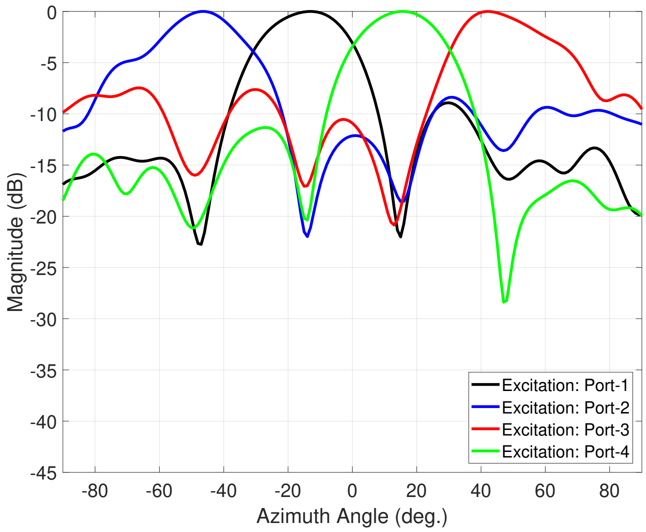

Figure 4.37: The antenna patterns of the 4×1 antenna array at azimuth plane when all ports are excited one by one.

4.4 Measurement Results of the 4×4 Butler Matrix Combined with the 4×1 Antenna Array

In order to verify the beamforming capabilities of the Butler matrix, the 4×1 patch antenna array mentioned in previous section has been manufactured. In Fig. 4.38 the geometry of the manufactured 4×1 patch antenna array is demonstrated. The dimensions of the manufactured patch antenna array is 45mm x 100mm.

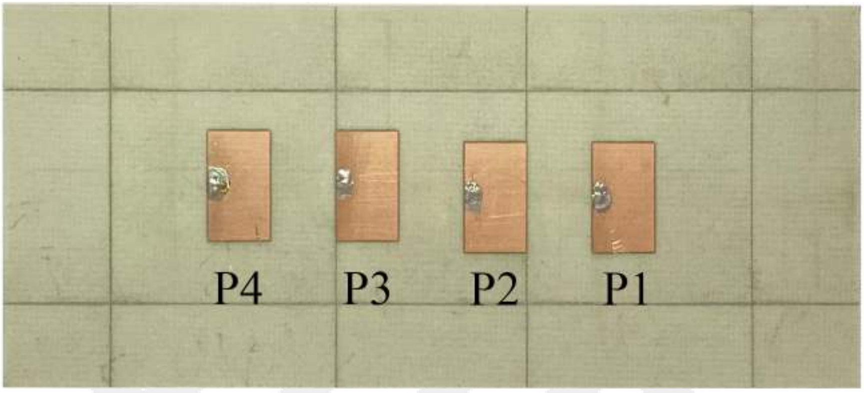

Figure 4.38: The geometry of the manufactured 4×1 patch antenna array.

Before combining the patch antenna array with the manufactured 4×4 Butler matrix, return loss of the each antenna element has been measured at PNA. During the measurement of each port of the antenna array, the ports that were not being measured were terminated with a 50 ohm termination. the simulated and measured return loss results of antenna elements of the 4×1 patch antenna array are presented in Fig. 4.39.

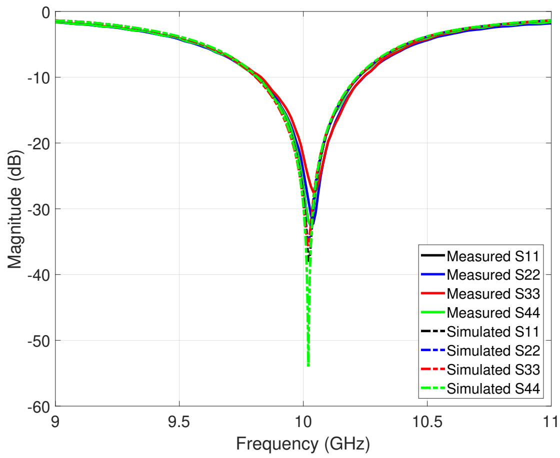

Figure 4.39: The simulated and measured return loss results of antenna elements of the 4×1 patch antenna array.

It is seen from Fig. 4.39 that return loss measurement results of patch antenna elements agree very well with simulation results. Return loss results of the all antennas are above 22dB at 10GHz where farfield pattern measurements are to be performed. These results indicate that the 4×1 patch antenna array and the 4×4 Butler matrix can be combined and measured at 10 GHz with a very low mismatch loss. In Fig. 4.40, the geometry of the manufactured 4×1 patch antenna array combined with the 4×4 Butler array is shown. The input ports of the 4×1 patch antenna array are connected to the output ports of the 4×4 Butler matrix via male to male sma adapters.

Figure 4.40: The geometry of the manufactured 4×1 patch antenna array combined with the 4×4 Butler matrix.

In order to verify the results of the 4×4 Butler matrix, the farfield patterns of the 4×1 patch antenna array have been measured while each port of the Butler matrix were excited one by one. The input ports of the Butler matrix that were not being measured were terminated by a 50 ohm load. The measurements are performed in a 6mx5mx4m anechoic nearfield chamber. The block diagram of the anechoic nearfield chamber is given in Fig. 4.41. The anechoic chamber is built with rf pyramidal absorbers to avoid unwanted reflections up to 40 GHz. A planar nearfield measurement is performed in order to measure the antenna array. An open ended waveguide is used as the TX antenna while the antenna under test is used as the RX antenna. The distance between the probe and the antenna array is set to 3λ at 10 GHz.

The measurement setup of the 4×1 patch antenna array combined with the 4×4 Butler matrix is provided in Fig. 4.42. The antenna array combined with the Butler matrix is connected to the mast by using an 3D-printed abs based plastic jig.

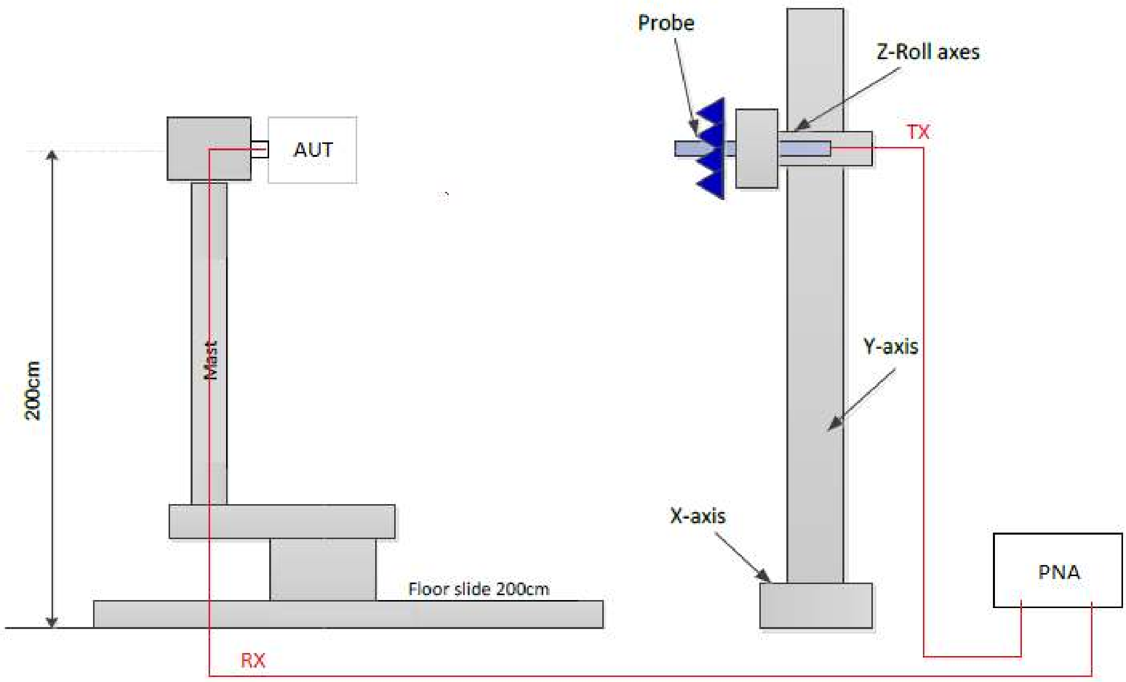

Figure 4.41: The block diagram of the anechoic nearfield chamber.

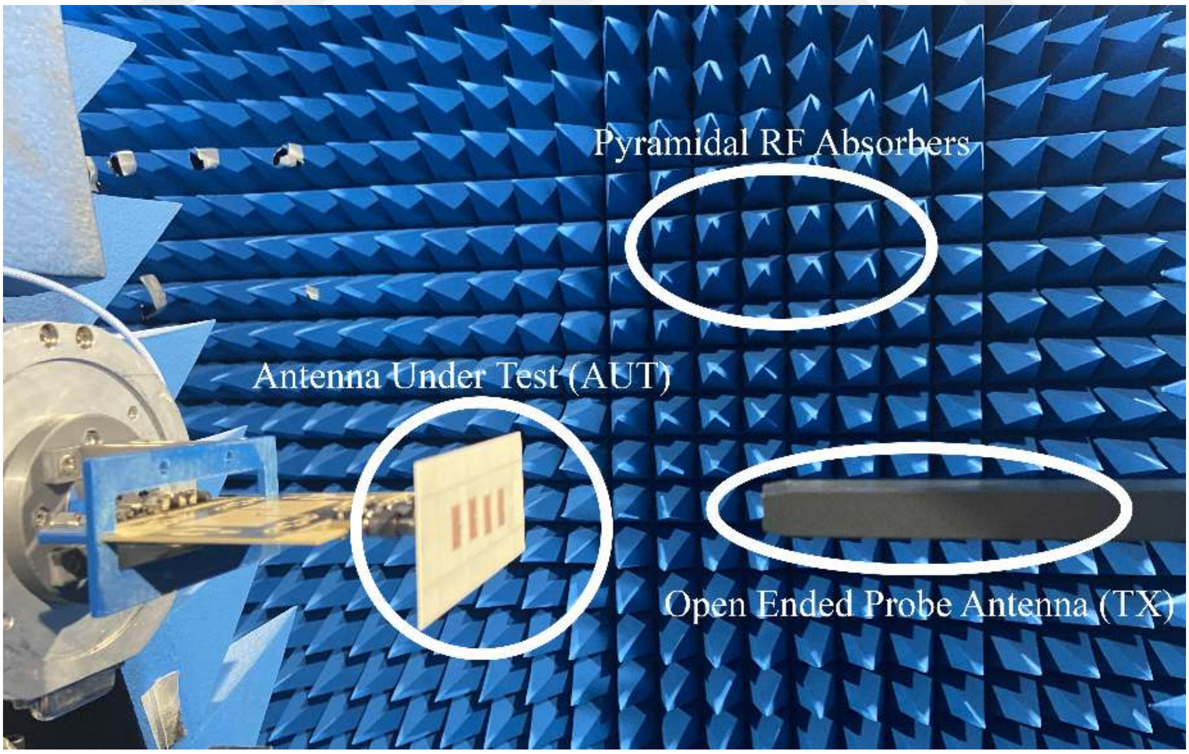

Figure 4.42: The measurement setup of the 4×1 patch antenna array combined with the 4×4 Butler matrix.

Fig. 4.43 shows the simulated and measured normalized antenna patterns of the 4×1 antenna array at the azimuth plane (el=0) when all ports are excited one by one. The planar nearfield measurement is taken within a 80° x 80° window due to the physical limitations of the chamber. In order to avoid any errors due to the interpolations, the simulated and measured results are compared within +/- 80° window. Results presented in Fig. 4.43 show that measurement results are in good agreement with the simulation results. A maximum main lobe direction deviation of 2.2° is observed between the measured and the simulated results when port-3 of the 4×4 Butler matrix is excited. The main lobe direction deviation between the measured and simulated results of the other excitations are observed to be less than 0.5°. These differences between the measured and the simulated patterns are considered to be due to the small reflection sources around the antenna array.

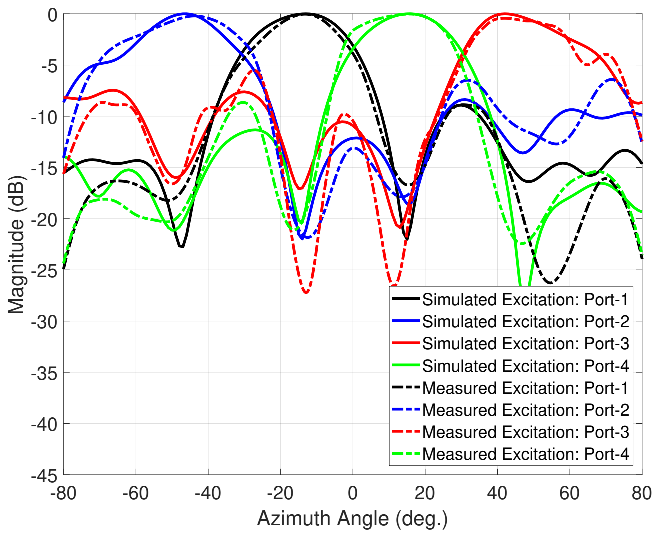

Figure 4.43: The simulated and measured normalized antenna patterns of the 4×1 antenna array at azimuth plane (el=0) when all ports are excited one by one.

Chapter 5

Conclusion

In this study, an ultra-wideband 4x4 Butler matrix is proposed. The studies related to the main components of the proposed Butler matrix which are the quadrature hybrid couplers and phase shifters, are presented in the second and third chapter. In the second chapter, the wideband hybrid couplers that can operate within the frequency band of 24GHz to 34GHz were designed. The coupler designs employed the both the elliptical and butterfly shaped resonators in order to achieve wideband performance. The simulated results of the designed structure has shown that the proposed structures not only has a minimal amplitude imbalance between its output ports but also has the minimal phase error along the whole operating band. Two different manufacturing topology is utilized during the production of these structures. The coupler with the elliptically shaped resonator is manufactured such that PCB cards of the coupler are combined to each other mechanically by the metal screws and nuts. It has been seen that weight of the connectors were too much for a 0.127mm thick PCB card and the planarity of the PCB cards had been severely affected by this issue. Hence the measurement results were not acceptable. The second structure which has the butterfly shaped resonators has been manufactured by another process. In order to combine PCB cards, a bonding material called prepreg has been used. It has been seen that the added thickness of the prepreg material and chemical nature of the bonding agent increased the stiffness of the coupler structure. However, the results of this structure was also unsatisfactory. This has been attributed to the unpredictable nature of the prepreg material during production process at high frequencies. Since the production tolerances at Ka-band are too tight and insertion loss of the materials have higher losses at this frequency band,it has been decided to continue on studies below Ka-band where the production and the material related errors would be more forgiving and have less effect on the results. Therefore, the design frequency band of the coupler has been shifted to the 3GHz - 12GHz. Initially, the quadrature hybrid coupler in [15] has been chosen to be benchmark to work below Ka-Band frequency. During the studies performed on the design stated in [15], it has been seen that the standing waves are formed when there is a gap between PCB cards of the multi-layer stackup. The degrading effects of this standing wave formation was also present in [15]. Therefore, in order solve this problem, a new method has been found. By inserting the shielding vias along the microstrip lines and the resonators, discontinuity crated due to an either air gap or a bonding material has been avoided. This solution has also been applied to the design stated in [15] and the measurement results were in good agreement with the simulated results. By using this newfound method, a novel quadrature hybrid coupler that employs butterfly shaped resonators and coupling aperture had been proposed. In terms of the operating bandwidth and phase imbalance, the proposed design outperformed other topologies mentioned in literature while keeping its dimensions fairly compact considering its wide operating frequency bandwidth.

In the third chapter, wideband phase shifter designs operating at Ka band are presented. Four wideband 45 degree phase shifters were proposed and compared. The presented structures were all consisted of multiple layers that shared the same ground plane. The phase shifting in all structures were accomplished by exploiting two coupled patch elements which were shaped elliptically, rectangularly and in a butterfly shaped manner through the elliptically or the rectangularly shaped slots etched to the ground plane. The slotted ground plane were shared by both patch elements placed on the different layers of the structures. The proposed designs achieved 45 degree phase shift with phase imbalance of 7 degrees within the frequency band of 24GHz to 34GHz and they exhibited different insertion loss results ranging from 0.65 dB to 1.65 dB while all of them have less than -10 dB return loss across the whole operating band. It has been seen that the phase shifter with elliptical patches and elliptical slot etched to the ground plane was the worst among them while the phase shifter with phase shifter with butterfly shaped patch resonators was the best of them. Although the simulation results indicated promising results, the manufacturing problems stated in the previous chapter has avoided the verification of the models. For this reason, in order to simplify manufacturing process and eliminate errors due to the high frequency operation, the operating frequency band is decreased to the below Ka frequency band. Since phase shifter with the butterfly shaped resonator outperformed all other structures at Ka band, phase shifter design with the both butterfly shaped resonator and coupling aperture had been thought to achieve best results below Ka-band. In order to avoid any unwanted standing wave formations, shielding vias were integrated to the models at the earlier stages of the design. However, the optimal results of this structure didn't yield any favorable results. Therefore, the phase shifter design with rectangular resonator and coupling slot has been chosen as the next design step. It has been seen that by also adding open ended rectangular stub to the rectangular resonators, phase shifter with satisfactory results were acquired.

In fourth chapter, a wideband 4×4 Butler matrix design operating below Ka band was presented. The proposed 4×4 Butler matrix, operates within the frequencies 3GHz to 12 GHz and it has been designed using the proposed quadrature hybrid coupler and the phase shifter. The designed Butler matrix has also been manufactured to verify its operation. It has been seen that the measured results especially the consecutive phase differences between the output ports of the Butler matrix were very close to the simulated results. In the simulation environment, the 4×4 Butler matrix was also connected to the 4×1 antenna array, in order to see if it would be able tilt the beam of the antenna array to the desired directions. The simulation results of the 4×4 Butler matrix combined with a 4×1 antenna array has shown that 4×4 Butler matrix was able tilt antenna beam successfully to the 4 different directions. So as to verify the beam tilting capabilities of the 4×4 Butler matrix, a 4×1 patch antenna array was manufactured and combined with the Butler matrix. The farfield patterns created by exciting each input port of the Butler matrix has been measured in the nearfield chamber. The measurement results yielded that the designed 4×4 Butler matrix was able to tilt antenna array pattern successfully to the desired directions.

This work indicates that an ultra-wideband performance can be achieved with a multi-layer slot coupled methodology. Use of the prepreg materials and the shielding vias makes ultra-wideband operation possible in the multi-layer topologies. However, it has been seen that especially at the end of the frequency band, the insertion loss and the phase errors of the multi-layer topology tends have higher values. This problem can be overcome by adjusting the frequency band according to the frequency of desired operation. As a future work, a 8x8 Butler matrix will be studied to be able increase the beam tilting capability of the Butler matrix and create more directive antenna beams directed towards 8 different angles on the azimuth plane.

References

[1] Balanis, Constantine A. Blanis, ”Antenna Theory Analysis and Design,” *Wiley*, 2016

[2] Merrill I. Skolnik, ”Radar Handbook,”*McGraw-Hill*, 2009.

[3] D. M. Pozar, ”Microwave Engineering,” *Wiley*, 2005

[4] B. M. Alqahtani, A. F. Sheta and M. A. Alkanhal, ”New compact wide-band branch-line couplers,”*2009 European Microwave Conference (EuMC), Rome, 2009* , pp. 1159-1162.

[5] Young-Hoon Chun and Jia-Sheng Hong, ”Compact wide-band branch-line hybrids,” in *IEEE Transactions on Microwave Theory and Techniques*, vol. 54, no. 2, pp. 704-709, Feb. 2006.

[6] R. D. Cerna and M. A. Yarleque, ”Design and implementation of a wideband 8x8 Butler Matrix for AWS and PCS 1900 MHz beamforming networks,”*IEEE International Wireless Symposium (IWS 2015)*, Shenzhen, 2015, pp. 1-4.

[7] H. Yoon and B. Min, ”Two Section Wideband 90° Hybrid Coupler Using Parallel-Coupled Three-Line,” in *IEEE Microwave and Wireless Components Letters*, vol. 27, no. 6, pp. 548-550, June 2017.

[8] T. Djerafi, N. J. G. Fonseca and K. Wu, ”Design and implementation of a planar 4x4 butler matrix in SIW technology for wideband applications,”*The 40th European Microwave Conference, Paris, 2010*, pp. 910-913.

[9] T. Djerafi and K. Wu, ”Super-Compact Substrate Integrated Waveguide Cruciform Directional Coupler,” in *IEEE Microwave and Wireless Components Letters*, vol. 17, no. 11, pp. 757-759, Nov. 2007.

[10] X. Jing, S. Sun, Q. S. Liu and Y. Li, ”Study of wideband patch-based Butler matrix and its high-frequency application,” *2014 IEEE Antennas and Propagation Society International Symposium (APSURSI)*, Memphis, TN, 2014, pp. 470-471.

[11] X. Jing, L. J. Jiang, S. Sun and L. Zhu, ”A patch-resonator-based Butler Matrix with new triangular phase shifters,” *2016 IEEE International Symposium on Antennas and Propagation (APSURSI), Fajardo, 2016* , pp. 61-62.

[12] T. Yang, M. Ettorre and R. Sauleau, ”Novel Phase Shifter Design Based on Substrate-Integrated-Waveguide Technology,” in *IEEE Microwave and Wireless Components Letters*, vol. 22, no. 10, pp. 518-520, Oct. 2012.

[13] L. Guo, H. Zhu and A. Abbosh, ”Wideband Phase Shifter With Wide Phase Range Using Parallel Coupled Lines and L-Shaped Networks,” in *IEEE Microwave and Wireless Components Letters*, vol. 26, no. 8, pp. 592-594, Aug. 2016.

[14] S. Sarkooyeh, M. Salimi, (2015). ”An Innovative Ultra Wideband Microstrip Phase Shifter Based on the LANGE Coupler,” in *International Journal of Science and Engineering Applications*,vol 4.,2015.

[15] A. M. Abbosh and M. E. Bialkowski, ”Design of Compact Directional Couplers for UWB Applications,” in*IEEE Transactions on Microwave Theory and Techniques*, vol. 55, no. 2, pp. 189-194, Feb. 2007.

[16] A. M. Abbosh, ”Ultra-Wideband Phase Shifters,” in *IEEE Transactions on Microwave Theory and Techniques*, vol. 55, no. 9, pp. 1935-1941, Sept. 2007.

[17] T. Djerafi, N. J. G. Fonseca and K. Wu, ”Design and implementation of a planar 4×4 butler matrix in SIW technology for wideband applications,” *The 40th European Microwave Conference*, 2010, pp. 910-913.

[18] J. Lian, Y. Ban, C. Xiao and Z. Yu, ”Compact Substrate-Integrated 4 × 8 Butler Matrix With Sidelobe Suppression for Millimeter-Wave Multibeam Application,” in *IEEE Antennas and Wireless Propagation Letters*, vol. 17, no. 5, pp. 928-932, May 2018.

[19] X. Jing, S. Sun, Q. S. Liu and Y. Li, ”Study of wideband patch-based Butler matrix and its high-frequency application,” *2014 IEEE Antennas and Propagation Society International Symposium (APSURSI)*, 2014, pp. 470-471.

[20] H. Nachouane, A. Najid, A. Tribak and F. Riouch, ”Broadband 4×4 Butler matrix using wideband 90° hybrid couplers and crossovers for beamforming networks,” *2014 International Conference on Multimedia Computing and Systems (ICMCS)*, 2014, pp. 1444-1448.

[21] N. V. Priyadarshan and A. Thenmozhi, ”Beam forming network using 4×4 narrowband butler matrix for tracking and localization applications,” *2017 International Conference on Intelligent Computing and Control Systems (ICICCS)*, 2017, pp. 1241-1246.

[22] M. Nedil, A. M. Habib and T. A. Denidni, ”Novel Ultra-Wideband CB-CBW Butler matrix,” *2008 IEEE Antennas and Propagation Society International Symposium*, 2008, pp. 1-4.

[23] O. Haraz, A. Sebak and S. Alshebeili, “Ultra-Wideband 4×4 Butler Matrix Employing Trapezoidal-Shaped Microstrip-Slot Technique. “, *Wireless Personal Communications 82*, 2014, pp. 709-721.

[24] M. Wong, V. F. Hanna, O. Picon and H. Baudrand, ”Analysis and design of slot-coupled directional couplers between double-sided substrate microstrip lines,” *in IEEE Transactions on Microwave Theory and Techniques*, vol. 39, no. 12, pp. 2123-2129, Dec. 1991.

[25] A. M. Abbosh, ”Ultra-Wideband Phase Shifters,” in *IEEE Transactions on Microwave Theory and Techniques*, vol. 55, no. 9, pp. 1935-1941, Sept. 2007.

[26] W. Hilberg, ”From Approximations to Exact Relations for Characteristic Impedances”, in *IEEE Transactions on Microwave Theory and Techniques*, May 1969.